

DYNAMIC BEHAVIOUR OF PILE FOUNDATIONS  
WITH SOIL-PILE INTERACTION

CENTRE FOR NEWFOUNDLAND STUDIES

**TOTAL OF 10 PAGES ONLY  
MAY BE XEROXED**

(Without Author's Permission)

YINGCAI HAN







DYNAMIC BEHAVIOUR OF PILE FOUNDATIONS  
WITH SOIL-PILE INTERACTION

by

Yingcai Han

A thesis submitted to the School of Graduate Studies  
in partial fulfillment of the requirements for  
the degree of Doctor Philosophy

Faculty of Engineering and Applied Science  
Memorial University of Newfoundland

April 1995

St. John's

Newfoundland

Canada



National Library  
of Canada

Acquisitions and  
Bibliographic Services Branch

395 Wellington Street  
Ottawa, Ontario  
K1A 0N4

Bibliothèque nationale  
du Canada

Direction des acquisitions et  
des services bibliographiques

395, rue Wellington  
Ottawa (Ontario)  
K1A 0N4

Your file Votre référence

Our file Notre référence

The author has granted an irrevocable non-exclusive licence allowing the National Library of Canada to reproduce, loan, distribute or sell copies of his/her thesis by any means and in any form or format, making this thesis available to interested persons.

The author retains ownership of the copyright in his/her thesis. Neither the thesis nor substantial extracts from it may be printed or otherwise reproduced without his/her permission.

L'auteur a accordé une licence irrévocable et non exclusive permettant à la Bibliothèque nationale du Canada de reproduire, prêter, distribuer ou vendre des copies de sa thèse de quelque manière et sous quelque forme que ce soit pour mettre des exemplaires de cette thèse à la disposition des personnes intéressées.

L'auteur conserve la propriété du droit d'auteur qui protège sa thèse. Ni la thèse ni des extraits substantiels de celle-ci ne doivent être imprimés ou autrement reproduits sans son autorisation.

ISBN 0-612-17597-9

Canada

## ABSTRACT

Pile foundations are often used in soft soils to support heavy structures, such as offshore towers, nuclear power plants, tall buildings, dams and bridges. There are many situations where these structures may undergo dynamic loading, for example, earthquake forces, wave forces, wind forces, blasting and unbalanced machines etc. There has been a remarkable increase in the study of pile dynamics in the last twenty years, although piles have been used for hundreds of years.

In this study, the dynamic behavior of single piles and pile groups are investigated theoretically and compared with experimental results performed earlier. Both theoretical and experimental studies have shown that the dynamic response of the piles is very sensitive to the properties of the soil in the vicinity of the piles. The impedances of the soil layer are formulated for different modes of vibration based on a new model of the boundary zone with non-reflective interface, which is more realistic and robust than the current leading models of Novak and Veletsos.

With the impedances of the soil media derived, the stiffness and damping for single piles and pile groups are presented. The validity of the boundary zone model for the soil-pile system is verified by comparison with the dynamic experiments which were conducted on single steel piles and on a concrete pile group in the field, respectively. The effects of non-linearity of the soil-pile system under strong excitation, the pile-soil-pile interaction (group effect) and the influence of frozen soil on the piles are investigated comprehensively. The results obtained from this study provide a guideline for engineering design, to increase the safety of the piles and the structures.

## ACKNOWLEDGEMENTS

I would like to thank my supervisor, Dr. Gary Sabin, for his guidance and encouragement. With his help, especially in mathematics, some important problems in this area have been solved. Special thanks are due to Dr. Jack Clark, Dr. Arisi Swamidas and Associate Dean, Dr. J. Sharp, Faculty of Engineering and Applied Science, Memorial University of Newfoundland. With their help and support I completed my Ph.D. program. Also, I would like to thank my former supervisor, Professor M. Novak, University of Western Ontario, for his valuable guidance and suggestions. I have learned much of the advanced knowledge on dynamics of soil and foundation from him.

Thanks are also due to the Institute of Engineering Mechanics, Harbin, China and The National Science Foundation of China. With their help and research grant, I conducted a series of experiments on pile foundations in China.

I am especially thankful to my wife Han Zailing and two daughters, Han Zhi and Han Yu, whose understandings and sacrifices made it possible for me to complete this dissertation.

Finally, I express my thanks to God for His guidance in my work and in my life.

# Contents

Table of Contents	i
List of Figures	iv
List of Tables	xi
List of Symbols	xii
<b>1 Introduction</b>	<b>1</b>
<b>2 Review of Previous Work</b>	<b>3</b>
2.1 Single Pile . . . . .	4
2.2 Pile Group . . . . .	9
2.3 Soil - Structure Interaction (SSI) . . . . .	12
<b>3 Impedances of Soil Layer</b>	<b>15</b>
3.1 Introduction . . . . .	15
3.2 Model of Soil Layer with Non-reflective Interface . . . . .	17
3.3 Differential Equations in Cylindrical Coordinates . . . . .	20
3.4 Impedance Functions of Soil Layer . . . . .	21

3.4.1	Vertical Excitation . . . . .	21
3.4.2	Torsional Excitation . . . . .	31
3.4.3	Radial Excitation . . . . .	40
3.4.4	Rocking Excitation . . . . .	49
3.4.5	Horizontal Excitation . . . . .	57
<b>4</b>	<b>Stiffness and Damping of Single Piles in Layered Media</b>	<b>72</b>
4.1.	Introduction . . . . .	72
4.2	Element Stiffness Matrices . . . . .	73
4.3	Complex Stiffnesses of Pile . . . . .	79
<b>5</b>	<b>Dynamic Experiments of Single Pile</b>	<b>87</b>
5.1	Experimental Setup . . . . .	88
5.2	Pile Response under Horizontal Excitation . . . . .	94
5.3	Pile Response under Vertical Excitation . . . . .	112
<b>6</b>	<b>Stiffness and Damping of Pile Group</b>	<b>127</b>
6.1	Pile-Soil-Pile Interaction . . . . .	127
6.2	Stiffness and Damping of Pile Group . . . . .	131
<b>7</b>	<b>Dynamic Experiments of Pile Group</b>	<b>137</b>
7.1	Experimental Setup . . . . .	138
7.2	Linear Vibration of Pile Group . . . . .	147
7.3	Nonlinear Vibration of Pile Group . . . . .	150
7.4	Summary and Conclusions . . . . .	161

<b>8 Influence of Frozen Soil on Piles</b>	<b>171</b>
3.1 Pile Group . . . . .	171
3.2 Single Piles . . . . .	178
<b>9 Summary, Conclusions and Recommendations</b>	<b>191</b>
<b>References</b>	<b>196</b>
<b>A Impedance Functions of Viscoelastic Halfspace</b>	<b>204</b>
<b>B Interaction Factor of Two-Pile Group</b>	<b>207</b>
<b>Appendices</b>	<b>204</b>

## List of Figures

- 3.1 Model of boundary zone with non-reflective interface, (A) composition of the zones, and (B) variation of shear modulus with radial distance. . . . . 19
- 3.2 Comparison of impedance functions for vertical vibration by different solutions,  $t_m/r_o = 1.0$ ,  $G_i/G_o = 0.25$ ,  $\beta_i = 0.1$ ,  $\beta_o = 0.05$ ; (A) stiffness factor  $S_{v1}$ , and (B) damping factor  $S_{v2}$ . . . . . 27
- 3.3 Vertical impedances for a composite layer with material damping  $\beta_i = 0.1$ ,  $\beta_o = 0.05$  and different parameters: (A) for  $t_m/r_o = 0.1$ ; (B) for  $t_m/r_o = 0.2$ . . . . . 28
- 3.4 Vertical impedances for a composite layer with material damping  $\beta_i = 0.1$ ,  $\beta_o = 0.05$  and different parameters: (A) for  $t_m/r_o = 0.5$ ; (B) for  $t_m/r_o = 1.0$ . . . . . 29
- 3.5 Effects of material damping on vertical impedances of soil layer, (A) stiffness factor  $S_{v1}$ , and (B) damping factor  $S_{v2}$ . . . . . 30
- 3.6 Comparison of torsional impedance functions by different solutions,  $t_m/r_o = 1.0$ ,  $G_i/G_o = 0.25$ ,  $\beta_i = \beta_o = 0.0$ ; (A) stiffness factor  $S_{\theta 1}$ , and (B) damping factor  $S_{\theta 2}$ . . . . . 36

3.7	Torsional impedances for a composite layer with material damping $\beta_i = 0.1$ , $\beta_o = 0.05$ and different parameters: (A) for $t_m/r_o = 0.25$ ; (B) for $t_m/r_o = 0.5$ . . . . .	37
3.8	Torsional impedances for a composite layer with material damping $\beta_i = 0.1$ , $\beta_o = 0.05$ and different parameters: (A) for $t_m/r_o = 1.0$ ; (B) for $t_m/r_o = 2.0$ . . . . .	38
3.9	Effects of material damping on torsional impedances of soil layer, (A) stiffness factor $S_{\theta 1}$ , and (B) damping factor $S_{\theta 2}$ . . . . .	39
3.10	Comparison of radial impedance functions by different solutions, $t_m/r_o = 2.0$ , $G_i/G_o = 0.5$ , $\nu = 0.25$ , $\beta_i = 0.1$ and $\beta_o = 0.05$ ; (A) stiffness factor $S_1$ , and (B) damping factor $S_{\delta 2}$ . . . . .	46
3.11	Radial impedances for a composite layer with material damping $\beta_i = 0.1$ , $\beta_o = 0.05$ and different parameters: (A) for $t_m/r_o = 0.5$ ; (B) for $t_m/r_o = 1.0$ . . . . .	47
3.12	Effects of Poisson's ratio on radial impedances of soil layer, (A) stiffness factor $S_{\delta 1}$ , and (B) damping factor $S_{\delta 2}$ . . . . .	48
3.13	Rocking impedances for a composite layer with material damping $\beta_i = 0.1$ , $\beta_o = 0.05$ and different parameters: (A) for $t_m/r_o = 0.25$ ; (B) for $t_m/r_o = 0.5$ . . . . .	54
3.14	Rocking impedances for a composite layer with material damping $\beta_i = 0.1$ , $\beta_o = 0.05$ and different parameters: (A) for $t_m/r_o = 1.0$ ; (B) for $t_m/r_o = 2.0$ . . . . .	55
3.15	Effects of material damping on rocking impedances of soil layer, (A) stiffness factor $S_{\phi 1}$ , and (B) damping factor $S_{\phi 2}$ . . . . .	56

3.16	Comparison of horizontal impedance functions by different solutions, $t_m/r_o = 0.5, G_i/G_o = 0.25, \beta_i = 0.1, \beta_o = 0.05, \nu = 0.25$ : (A) stiffness factor $S_{u1}$ , and (B) damping factor $S_{u2}$ . . . . .	66
3.17	Horizontal impedances for a composite layer with material damping $\beta_i = 0.1, \beta_o = 0.05, \nu = 0.25$ and different parameters: (A) for $t_m/r_o = 0.1$ ; (B) for $t_m/r_o = 0.25$ . . . . .	67
3.18	Horizontal impedances for a composite layer with material damping $\beta_i = 0.1, \beta_o = 0.05, \nu = 0.25$ and different parameters: (A) for $t_m/r_o = 0.5$ ; (B) for $t_m/r_o = 1.0$ . . . . .	68
3.19	Effects of material damping on horizontal impedances of soil layer, (A) stiffness factor $S_{u1}$ , and (B) damping factor $S_{u2}$ . . . . .	69
3.20	Effects of Poisson's ratio on horizontal impedances of soil layer, (A) stiffness factor $S_{u1}$ , and (B) damping factor $S_{u2}$ . . . . .	70
3.21	High-frequency behavior of horizontal impedances of a composite layer with $t_m/r_o = 1.0, \nu = 0.25, \beta_i = 0.1, \beta_o = 0.05$ ; (A) stiffness factor $S_{u1}$ , and (B) damping factor $S_{u2}$ . . . . .	71
4.1	Pile embedded in layered media and node numbering . . . . .	74
4.2	Frequency variations of vertical parameters for the steel pile in loose sand with boundary zone of $t_m/r_o = 0.5, G_i/G_o = 0.25, \beta_i = 0.1, \beta_o = 0.05, \nu = 0.4$ . . . . .	85
4.3	Frequency variations of horizontal parameters for the steel pile in loose sand with boundary zone of $t_m/r_o = 0.5, G_i/G_o = 0.25, \beta_i = 0.1, \beta_o = 0.05, \nu = 0.4$ . . . . .	86

5.1	Inverse value of sand Young's modulus vs strain . . . . .	91
5.2	Properties of pile and soil used in analysis . . . . .	92
5.3	Theoretical and experimental horizontal response of pile cap for different excitation intensities (pile cap separated from soil) . . . . .	97
5.4	Theoretical response curves of a system with nonlinear restoring force and nonlinear damping ( $n < 1$ ) for increasing excitation intensity ( $\rho =$ excitation moment/mass = $m_e e/m$ ) . . . . .	98
5.5	Theoretical and experimental response curves with different excitation intensity and contact between cap and soil . . . . .	99
5.6	Pile horizontal stiffness and damping coefficient . . . . .	102
5.7	Pile rocking stiffness and damping coefficient . . . . .	103
5.8	Pile horizontal damping ratio . . . . .	104
5.9	Pile rocking damping ratio . . . . .	104
5.10	Comparison of theoretical curves and measured deflections along pile shaft (excitation $\theta = 14$ ) . . . . .	105
5.11	Comparison of theoretical curves and measured deflections along pile shaft (excitation $\theta = 8$ ) . . . . .	105
5.12	Theoretical and experimental response curves for repeated loading ( $\theta = 5$ , cap separated) . . . . .	107
5.13	Theoretical and experimental response curves for repeated loading ( $\theta = 5_e$ , cap in contact with soil) . . . . .	108
5.14	Theoretical pile separation vs dimensionless amplitude . . . . .	109
5.15	Vertical pile response measured and back-calculated for three levels of excitation intensity ( $\omega = 2\pi f$ ) . . . . .	116

5.16	Pile restoring force characteristics vs. pile head displacement corresponding to response curves from Fig. 5.15. . . . .	117
5.17	Experimental pile response in vertical direction vs. theoretical prediction ( $\theta = 28$ ) . . . . .	120
5.18	Notations and geometry for pile in test pit. . . . .	122
5.19	Pile stiffness parameter $f_{v1}$ for different test pit dimensions ( $G_i/G_o = 0.25, \beta_i = \beta_o = 0.10, \rho_i = \rho_o, \nu = 0.4$ ). . . . .	123
5.20	Pile damping parameter $f_{v1}$ for different test pit dimensions ( $G_i/G_o = 0.25, \beta_i = \beta_o = 0.10, \rho_i = \rho_o, \nu = 0.4$ ). . . . .	124
6.1	Interaction curve for horizontal and vertical displacement of pile 2 due to horizontal and vertical force on pile 1 (Kaynia and Kausel, 1982)130	
7.1	Plan view of piles and cross-hole test . . . . .	142
7.2	Triaxial test measured data for the soil in the test site at several different depth . . . . .	143
7.3	Laboratory-measured properties of the soil in the test site . . . . .	144
7.4	(a) Layout of the pile group and (b) the measured shear wave velocity and mass density of the soil. . . . .	145
7.5	Test setup for the lateral vibration of the pile cap . . . . .	146
7.6	Measured on the cap (a) for horizontal response; (b) for rocking response151	
7.7	Comparison of theoretical predictions with experimental results . . . . .	152
7.8	Influence of pile-soil-pile interaction on dynamic response of group . . . . .	153
7.9	Stiffness and damping of pile group . . . . .	154
7.10	GER (group efficiency ratio) for horizontal vibration of group . . . . .	155

7.11 Measured displacement response of the pile group in X-direction.(a) horizontal vibration, (b) rocking vibration. . . . .	164
7.12 Measured displacement response of the pile group in Y-direction.(a) horizontal vibration, (b) rocking vibration. . . . .	165
7.13 Theoretical-deduced relationships between pile separation and maxi- mum vibration amplitude . . . . .	166
7.14 Comparison of theoretical and measured response of the group in X-direction,(a) horizontal vibration, (b) rocking vibration. . . . .	167
7.15 Comparison of theoretical and measured response of the group in Y-direction,(a) horizontal vibration, (b) rocking vibration. . . . .	168
7.16 Stiffness of the pile group under different excitation intensities (a) horizontal vibration, (b) rocking vibration. . . . .	169
7.17 Comparison of measured response for $\theta = 8$ with theoretical predic- tion in different parameters of boundary zone. . . . .	170
8.1 Measured displacement response of pile group with frozen layer (a) horizontal vibration, (b) rocking vibration . . . . .	174
8.2 Comparison of theoretical predictions with measured response of pile group with frozen layer (a) horizontal vibration, (b) rocking vibration	175
8.3 Effect of frozen soil on dynamic response of pile group (a) horizontal vibration, (b) rocking vibration . . . . .	176
8.4 Effect of frozen soil on stiffness and damping of pile group (a) hori- zontal vibration, (b) rocking vibration . . . . .	177

8.5	Measured horizontal displacement response of the pile with no frozen soil . . . . .	183
8.6	Measured horizontal displacement response of the pile with frozen soil layer : . . . . .	184
8.7	Measured and theoretical response of the pile with bounday zone in the case without frozen soil . . . . .	185
8.8	Measured and theoretical response of the pile with no bounday zone in the case without frozen soil . . . . .	186
8.9	Measured and theoretical response of the pile in the case with a frozen soil layer . . . . .	187
8.10	Relative influence of a frozen soil layer on the pile response at $\theta = 8$ .	188
8.11	Relative influence of a frozen soil layer on the pile response at $\theta = 28$	189
8.12	Influence of a frozen soil layer on the stiffness and damping of a single pile . . . . .	190
B.1	Group of two floating piles . . . . .	208
B.2	Single pile-basic geometry . . . . .	210
B.3	Geometry for integration over circular area . . . . .	212

## List of Tables

5.1	Pile Properties . . . . .	88
5.2	Properties of Backfill Soil . . . . .	90
5.3	Properties of Natural Deposite . . . . .	90
5.4	Magnitude of Horizontal Exciting Force . . . . .	93
5.5	Damping Parameters of the Pile . . . . .	105
5.6	Dynamic parameters of pile under Repeated Loading . . . . .	111
5.7	Nonlinear vibration parameters of pile in vertical direction . . . . .	115
7.1	Soil properties . . . . .	139
7.2	Pile properties . . . . .	140
7.3	Excitation scheme adopted for linear vibration . . . . .	148
7.4	Excitation scheme adopted for nonlinear vibration . . . . .	156
7.5	Boundary zone parameters for nonlinear vibration in X-direction . . . . .	158
7.6	Boundary zone parameters for nonlinear vibration in Y-direction . . . . .	158
7.7	Theoretical dynamic behaviour of the pile group in X-direction . . . . .	160
7.8	Theoretical dynamic behaviour of the pile group in Y-direction . . . . .	160
8.1	Theoretical dynamic behaviour of the pile with and without the frozen soil layer . . . . .	181

# List of Symbols

$A$	amplitude, or cross section area of pile
$A_n$	coefficient in the power series
$a, B, b$	constants
$\tilde{a}, \tilde{b}, \tilde{n}$	complex frequency parameter
$a_0, a_i$	dimensionless frequency
$B_{1,2,3,4}, C_{1,2,3,4}$	complex-value integration constants
$C_{j1,2}(a_0, \nu, D)$	dimensionless parameter of viscoelastic half-space
$C_j$	coefficient of equivalent viscous damping
$c_{\psi}^1, c_{uu}^1, c_{\psi\psi}^1$	vertical, horizontal and rocking damping constant of single pile
$c_{u\psi}^1, c_{\psi u}^1$	cross-damping constant of single pile
$d, S$	diameter of pile, and spacing between piles
$E_p, E_s$	Young's modulus of pile and soil
$E_p I, E_p I_1$	bending stiffness of the pile and the topmost element of pile
$f_{\psi 1}, f_{\psi 2}$	vertical dimensionless stiffness and damping parameter of pile
$f_{u 1}, f_{u 2}$	horizontal dimensionless stiffness and damping parameter of pile
$f_{\psi 1}, f_{\psi 2}$	rocking dimensionless stiffness and damping parameter of pile
$f_{\psi 1}, f_{\psi 2}$	cross dimensionless stiffness and damping parameter of pile
$\tilde{f}_v, \tilde{f}_u$	static vertical and horizontal flexibility of single pile
$G_1^*, G_2^*$	complex shear modulus of the inner zone and the outer zone
$G_1, G_2, G_3$	shear modulus of the inner zone, the outer zone, and soil below pile tip
$H, M$	horizontal transverse force, and moment
$h$	height of element of pile
$I$	mass moment of inertia
$I_0, I_1$	modified Bessel function of zero order and order one of the first kind
$K_0, K_1$	modified Bessel function of zero order and order one of the second kind
$K_t(A)$	equivalent linear stiffness
$K_{\psi}^1, K_{uu}^1, K_{\psi\psi}^1$	vertical, horizontal and rocking complex stiffness of single pile
$K_{\psi}^G, K_{uu}^G, K_{\psi\psi}^G$	vertical, horizontal and rocking group stiffness
$K_{u\psi}^G, K_{\psi u}^G$	group cross stiffness
$K_{u\psi}^1, K_{\psi u}^1$	cross-stiffness of single pile
$k_v^1, k_{uu}^1, k_{\psi\psi}^1$	vertical, horizontal and rocking real stiffness of single pile
$k_v, k_s, k_{\psi}, k_r$	vertical, torsional, rocking and radial impedance of composite layer
$k_{u1}, k_{u2}, k_u$	horizontal impedance of the inner zone, the outer zone, and the composite layer

$k_{vt}, k_{ht}, k_{\theta t}$	vertical, horizontal and rocking stiffness of soil below pile tip
$m$	constant, or mass of pile per unit length
$m, e$	excitation intensity
$N, N_{st}$	axial force, and static axial force
$\{P\}, \{P\}_H$	vector of vertical and horizontal forces
$r_0, r_1, r_n$	radius of pile, pile radius at the topmost element and the tip
$r, \theta, z$	radial, tangential, and vertical variable
$S_{s1}, S_{s2}$	radial stiffness and damping factor of composite layer
$S_{u1}, S_{u2}$	horizontal stiffness and damping factor of composite layer
$S_{v1}, S_{v2}$	vertical stiffness and damping factor of composite layer
$S_{\theta 1}, S_{\theta 2}$	torsional stiffness and damping factor of composite layer
$S_{\omega 1}, S_{\omega}$	rocking stiffness and damping factor of composite layer
$t$	time
$R, t_m$	radius and thickness of boundary zone
$w, u, v$	vertical, radial and tangential displacement
$V_s, V_n, V_b$	shear wave velocity of soil, soil in the lowest layer and soil below pile tip
$\{v\}, \{\delta\}$	vectors of displacement at pile head
$\alpha_r, \alpha_{ij}$	interaction factor and dynamic interaction factor of piles
$[\alpha]_v, [\alpha]_H$	interaction coefficient matrix of vertical, horizontal and rotational displacement
$\beta_i, \beta_o$	damping ratio of the inner zone, and the outer zone
$\gamma_{ij}, \epsilon_i$	shear strain, and normal strain
$\Delta$	vector of unknown displacement
$\delta_{dij}, \delta_{sij}$	dynamic and static displacement
$\epsilon_{ij}^v, \epsilon_{2i-1, 2j-1}^H, \epsilon_{2i, 2j}^H$	elements of $[\alpha]_v^{-1}$ and $[\alpha]_H^{-1}$
$\eta, \eta_1$	constants
$\lambda_i^*, \lambda_o^*$	complex Lamé constant in inner zone and the outer zone
$\lambda_o, \lambda_{o1}, \lambda_i, \lambda_{i1}, sr_o$	constants
$\nu, \rho$	Poisson's ratio, and mass density
$\xi$	variable
$\xi_m$	coefficient of additional mass
$\sigma_i, \sigma_r, \sigma_\theta$	normal stress, radial and tangent normal stress
$\tau_{ij}, \tau_i, \tau_o$	shear stress, shear stress in the inner zone and the outer zone
$\Phi, \Psi$	displacement functions
$\phi, \psi$	potential function; $\psi$ also rocking amplitude
$\Omega$	backbone curve of natural frequency
$\omega$	circular frequency

# Chapter 1

## Introduction

Pile foundations are often used in soft soils to support heavy structures, such as offshore towers, nuclear powerplants, tall buildings, dams and bridges. There are many situations where these structures may undergo dynamic loading, for example, earthquake forces, wave forces, wind forces, blasting and unbalanced machines etc.

Modal characteristics of a pile-supported structure and its response to dynamic loads depend to a high degree on foundation flexibility. For pile-supported structures, the flexibility of individual piles is routinely taken into account, but the interaction of piles in a group, referred to as pile-soil-pile interaction or group effect, is often neglected. The group effect has been considered in offshore engineering by only a few researchers ( O'Neill, 1983; Mitwally and Novak, 1987; Novak and Mitwally, 1990 ).

The studies undertaken here are concentrated on the dynamics of pile foundations, involved with the impedances of a single pile and the behaviour of a typical pile group. The linear and nonlinear vibration and the seismic response are investigated

experimentally and theoretically with the consideration of pile-soil-pile interaction. Once the properties of the pile foundation are established, they can be incorporated into the examination of pile-structure interaction using the substructure approach just as with other types of foundation.

#### Organization of the thesis:

In Chapter 2, a comprehensive review of the literature is presented. In Chapter 3, the impedances of soil medium are formulated as a plane strain problem by means of an analytical solution. Chapter 4 deals with stiffness and damping of single pile using the finite element method. Chapter 5 describes tests on single pile performed by the author prior to this thesis and comparison of computed and the measured response using the theory in Chapters 3 and 4. Chapter 6 deals with stiffness and damping for pile group using pile-soil-pile interaction factors of Poulos (1980) for static condition and Kaynia and Kausel (1982) for dynamic condition. Chapter 7 describes full scale tests on pile group again performed by the author prior to this thesis and comparison of the measured response with computed results. Chapter 8 deals with effect of frozen soil layer on the response of single pile as well as the group. Chapter 9 lists summary, conclusion and recommendations.

## Chapter 2

# Review of Previous Work

Piles have been used for hundreds of years but in the last twenty years or so there has been a remarkable increase in the study of pile dynamics. The dynamic behaviour of piles is, of course, very complex and this might have lead Terzaghi and Peck ( 1967 ) to state that "... theoretical refinements in dealing with pile problems... are completely out of place and can be safely ignored".

Fortunately, not everybody became discouraged by this pessimistic evaluation, and a number of analytical and numerical approaches to the analysis of pile dynamic behaviour have been developed. These approaches have provided a much sounder theoretical basis for pile design than the equivalent cantilever concept or other purely empirical methods which dominated the field for decades. Nevertheless, some differences between the various theoretical approaches exist and the experiments reported are sometimes inconclusive; also, some uncertainties are inevitable when applying an idealized theory to field conditions. Thus, further studies of pile dynamics in theory, or from experiments and field observations, are needed for engineering applications.

The subject of pile dynamics received a comprehensive treatment in the state-of-the-art report by Tajimi (1977), covering developments up to 1977, and in a few special volumes, i.e., De Beer et al. (1977), O'Neill and Dobry (1980), Nogami (1987), Prakash and Sharma (1990) and Novak (1991).

## 2.1 Single Pile

The earliest systematic, theoretical studies of dynamic soil-pile interaction are due to Parmelee et al. (1964), Tajimi (1969), Penzien (1970), Novak (1974) and a few others. Parmelee and Penzien employed a non-linear discrete model and a static theory to describe the dynamic elastic stress and displacement fields. Tajimi used a linear viscoelastic stratum of the Kelvin-Voigt type to model the soil, but in his analysis of the horizontal response neglected the vertical component of the soil motion. Novak assumed linearity and an elastic soil medium composed of independent infinitesimally thin horizontal layers extending to infinity.

The problem of the interaction between the pile and the soil is very difficult to solve, even for the idealized assumptions of linear elastic or viscoelastic homogeneous soil and the pile being bonded to the soil. Thus, approximate procedures were formulated first. In 1974, Novak formulated a very simple approach for the horizontal response of an end bearing pile in a homogeneous soil based on plane strain soil reactions, which can be interpreted as a dynamic Winkler medium or a plane strain assumption. This solution identified dimensionless parameters of the problem, yielding a number of design charts and tables for dynamic stiffness and

damping of piles. Material damping was later included in a closed form expression for the soil reactions in Novak et al. (1978). The application of the same approach to vertical response of floating piles was made by Novak (1977). Torsional response was also examined in this way (Novak and Howell, 1977, 1978) and the importance of material damping for this vibration mode was demonstrated.

A somewhat more rigorous solution was formulated by Nogami and Novak (1976) and Novak and Nogami (1977). These approximate solutions offered a basic insight into the behaviour of the soil-pile system.

Much of the attention was focussed on the complex dynamic stiffnesses of the pile (impedance functions) because they have a strong influence on the response of pile supported buildings and structures. The impedance functions were also used in the dynamic analysis of embedded foundations (Han, 1989).

More recent analysis based on the solution of governing equations of a three dimensional continuum were formulated by Sen et al. (1985) and Pak and Jennings (1987). All vibration modes were investigated by Rajapakse and Shah (1987a, b, 1989). The latter authors evaluated the accuracy of some of the existing solutions and generated an extensive set of charts for impedances of floating piles.

Finite element solutions were formulated by Kuhlemeyer (1979a, b), Blaney et al. (1976), Wolf and Von Arx (1978), Waas and Hartmann (1981), Sanchez-Salineró (1982) and others. Boundary element approaches were developed by Banerjee

(1973), Banerjee and Sen (1987) and a few others. Ready to use charts and formulae were produced for homogeneous soil by Roesset (1980), Dobry et al. (1982), Novak and El-Sharnouby (1983) and a few others.

Comparing the results of experiments with theoretical predictions repeatedly showed that if the soil was assumed to be homogeneous, both pile stiffness and damping can be grossly overestimated. In fact, the soil is not homogeneous since the soil shear modulus varies with depth. In particular it reduces toward the ground surface which results from the diminishing confining pressure. In this situation the pile may be separated from the soil, even producing gaps.

Observations of this kind lead to the development of approaches better suited for nonhomogeneous soils. Significant progress was made by Kaynia (1982) and Kaynia and Kausel (1982, 1990) who based their solution of piles, in layered media, on the formulation of displacement fields due to uniformly distributed forces on cylindrical surfaces. Banerjee and Sen (1987) presented a boundary element solution for piles embedded in a semi-infinite nonhomogeneous soil in which the shear modulus varied linearly with depth. A few other methods suitable for linear layered media use a semi-analytical finite element approach. Solutions of this type were formulated by Waas and Hartmann (1981, 1984) and Mizuhata and Kusakabe (1984).

A much simpler and very versatile solution was formulated by Novak and Aboul-Ella (1978a, b) who extended the plane strain approach to include layered media. Roesset et al. (1986) also found the plane strain approach to work very well for

high frequencies. For very low frequencies, an adjustment to the plane strain soil reaction was made by Novak and El-Sharnouby (1983).

The sensitivity of the response to pile separation and free length shows when evaluating most experiments. The prediction of the separation length is difficult and only empirical suggestions can be made (Han and Novak, 1988a).

While the consideration of a free separation length in the analysis may produce the reduction in both pile stiffness and damping often observed in experiments, a better measure to this effect, or a complementary one, may be to account for soil nonhomogeneity in radial direction. A simple way of doing this is to assume a weak, cylindrical boundary zone around the pile. The purpose of such a zone is to account in a very approximate way for soil nonlinearity in the region of the highest stresses, pile separation, slippage and other deficiencies of the pile-soil interface. Such a zone was proposed by Novak and Sheta (1980). In their plane strain solution, the mass of the boundary zone was neglected in order to prevent wave reflections from the fictitious interface between the cylindrical zone and the outer region. The omission of the mass of the boundary zone in the original solution lead Lakshmanan and Minai (1981) and Veletsos and Dotson (1986, 1988) and Dotson and Veletsos (1990) to further develop the concept and to include the mass of the boundary zone in the analysis. Some of the effects of the boundary mass were investigated by Novak and Han (1990) who found that a homogeneous boundary with a non-zero mass yielded undulating impedances due to wave reflections from the fictitious interface between the two media. The ideal boundary zone should have properties smoothly approach-

ing those of the outer zone to alleviate wave reflections from the interface. With the consideration of the separation effect and weakened soil in the boundary zone, a reasonable agreement between the theoretical results and experiment data were obtained (Woods, 1984; Han and Novak, 1988b; Han and Vaziri, 1991; El-Marsafawi, Han and Novak, 1992).

At large displacements, piles behave in a nonlinear fashion because of soil nonlinearity at high strain, pile separation (gapping), slippage and friction. The incorporation of these factors into a continuum theory is extremely difficult, and therefore lumped mass models are most often used when nonlinear analysis is required. Such models feature nonlinear springs, nonlinear dampers, gaps and Coulomb friction blocks, as proposed by Penzien (1970), Matlock et al. (1978, 1980) and a number of others. The combination of these elements makes it possible to generate a variety of nonlinear force-displacement relationships. Models of this type are very versatile but it is difficult to relate the characteristics of the discrete elements to standard geotechnical parameters of soil. To help overcome this difficulty, various nonlinear soil resistance-deflection relationships known as P - Y curves have been recommended in the literature. For applications in offshore structures, the American Petroleum Institute (1986) specifies the P - Y curves for clay as well as sand making a difference between static and cyclic loadings.

With the boundary zone model, the nonlinear vibration of piles under steady-state excitation was investigated by Han and Novak (1988a, b), and Han (1989a, b; 1992). If a nonlinear transient response rather than the steady-state response is to

be investigated, then a time-domain analysis is called for. A time-domain analysis which extended the dynamic Winkler model to allow for nonlinearities, was formulated by Nogami and Konagai (1987, 1988), Nogami et al. (1988), and Mitwally and Novak (1988).

## 2.2 Pile Group

Piles are usually used in groups, and if they are not very widely spaced they interact with each other generating the phenomenon known as pile-soil-pile interaction or group effect.

Under static loads, pile interaction increases group settlement, redistributes the loads on individual piles and reduces the bearing capacity, unless this reduction is counteracted by densification of the soil within the group due to pile driving. The investigation of static group effects was put on a rational basis, relying on continuum mechanics, by Poulos (1968, 1971, 1979) and Butterfield and Banerjee (1971). Extensive data on static group effects are available in Poulos and Davis (1980), El-Sharnouby and Novak (1985, 1986, 1991).

Dynamic investigations of pile groups are more recent. The techniques employed are extensions of the approaches used for single piles and most of them are limited to linear interaction with no allowance for gapping. The first theoretical analysis of pile-soil-pile interaction was carried out by Wolf and Von Arx (1978) who employed an axisymmetric finite element formulation to establish the dynamic displacement

field due to ring loads. Waas and Hartmann (1981, 1984) formulated an efficient semi-analytical method which used ring loads and is well suited for layered media, properly accounting for the far field. Kaynia (1982) and Kaynia and Kausel (1982, 1990) further improved the accuracy by combining the cylindrical loads, actually a boundary element formulation, with the consistent stiffness matrix of layered media to account for the far field. A very simple approach was employed by Kobori et al. (1991) who used the cylindrical loads for the pile and disk loads for the base. Baba (1991) formulated a three-dimensional analysis of end bearing piles.

The thin layer method was used by Shimizu et al. (1977), Masuda et al. (1986) and a few others. Boundary element solutions, employing Green's functions of generally layered media, were formulated by Banerjee and Sen (1987), Mamoon et al. (1990). Simpler solutions based on the dynamic Winkler medium were developed by Nogami (1985), Sheta and Novak (1982) and Otani et al. (1991).

With the pile-soil-pile interaction theories being so complex, it is of importance to examine how the theories perform when compared with experiments. Dynamic experiments with a group of 102 model piles, each 1.06 m in length, were done by Novak and El-Sharnouby (1984). Successful experiments conducted on a group of 56 full scale piles were reported by Masuda et al. (1986). Six full scale piles were tested and very good results were obtained but the weak zone and separation had to be included in analysis for a satisfactory match with experimental results (Han, 1992; Han and Vaziri, 1991, 1992; El-Marsafawi, Han and Novak, 1992). Kobori et al. (1991) also found the theory to be of sufficient applicability. Thus, it may be

concluded that the linear theory works quite well as long as the experiments do not deviate too much from the theoretical assumptions, as might be expected. Often, a correction for separation, gapping and nonlinearity is needed, however, at least in the form of a weak zone and a pile free length.

The dynamic interaction factors were formulated by Kaynia and Kausel (1982), which is an extension of the widely used static interaction factor approach. It was observed that the accuracy, of the interaction factor approach, was quite sufficient for a homogeneous medium but less accurate for a nonhomogeneous one. A remarkably simple approximate method for dynamic interaction factor evaluation was proposed by Dobry and Gazetas (1988) and extended for nonhomogeneous soil by Makris, Gazetas and Fan (1989) and Gazetas and Makris (1991).

Nonlinear dynamic analysis of a pile group is very difficult and this may be the main reason why it has received very little attention than the linear analysis. Nogami and Konagai (1987) developed a group analysis assuming that in the vertical vibration, response nonlinearity stems mainly from slippage at the soil-pile interface; they represented the soil using the dynamic Winkler model. Nogami et al. (1988) and Otani et al. (1991) extended the concept of the dynamic Winkler medium further to include horizontal response, slippage, gapping and inelastic soil behaviour and were able to generate a variety of degrading hysteresis loops. The dynamic experiments of nonlinear vibration of pile groups under lateral loading were conducted by Han (1992) and compared with theoretical results that incorporated a boundary zone, which included weakened soil and gapping in the interface between the pile and the

soil.

### **2.3 Soil - Structure Interaction (SSI)**

It is well-recognized now that the foundation material on which a building is constructed may interact dynamically with the structure during its response to earthquake excitation or other excitation - to the extent that the maximum stresses and deflections in the system are modified significantly from values that would have been developed if it were on a rigid foundation. However, forty years ago when the methods of analysis of structure response to earthquake motions were just beginning to be developed, such interaction effects were considered to be of little consequence, and hence were ignored. It was concluded that the base shear force due to earthquake excitation in a typical tall building is hardly affected by foundation flexibility even for the most flexible foundation that might be considered suitable for such a building ( Merritt and Housner, 1954). Interest in SSI effects on the response of structures to earthquakes was expanded dramatically during the next two decades owing to developments in the nuclear power industry and offshore engineering. The effects of SSI on seismic response of structures were outlined by Clough (1992).

The analysis of the soil-structure interaction problem may be carried out on the basis of a direct finite element or boundary element approach and by use of a substructure or subsystem procedure. In the first approach, a finite element model of the entire system is made and the response of the model is evaluated in one step. The direct approach is more time consuming and costly than the substructure ap-

proach which will be employed in this study.

In the substructure approach the problem is solved in two stages: in the first stage, elements of the response of superstructures, foundations and soil are obtained independently; in the second stage, the individual responses are combined so as to satisfy the interaction conditions and the response of the complete system is obtained (Sarrazin et al., 1972; Roesset et al., 1973, 1982).

The subject of linear soil-structure-interaction analysis was reviewed by Luco (1982), and a thorough treatment of the substructure method, including all derivations and a discussion of the assumptions and limitations, as well as illustrative examples from actual practice, was included in textbooks (Wolf, 1985, 1988).

However, most of the studies on soil-structure interaction were done with respect to shallow foundations or on an elastic half space. Relatively few studies were devoted to deep foundations and considered pile-soil-pile interaction. Seismic response analysis of a pile supported structure was carried out by Nogami et al. (1991), Hadjian et al. (1990), El-Hifnawy and Novak (1986, 1987). Random response analysis of an offshore tower, considering pile-soil-pile interaction, was studied by Novak and Mitwally (1990).

The latest developments in dynamics of pile foundation and soil-structure interaction are included in this literature survey. From the review above, it can be seen that further research must be done in both theory and experiment, in order to apply

the advanced theory of pile dynamics to engineering practice. The contact situation between the pile and soil is very sensitive to the dynamic response of piles. Thus the boundary zone model should be improved to better account for this phenomenon. Soil-structure interaction depends on the real confining pressure of soil deposits and on the contact situation, so the dynamic experiments of full scale piles and other model pile tests should be studied further. The research project proposed in the following section will attempt to answer these questions.

## Chapter 3

# Impedances of Soil Layer

### 3.1 Introduction

One of the more important problem in soil-structure interaction is how to model the soil. A number of approaches are available to account for dynamic soil-structure interaction but they are usually based on the assumptions that the soil behaviour is governed by the laws of linear elasticity or viscoelasticity and the soil is perfectly bonded to an embedded foundation or a pile. In practice, however, the bonding between the soil and the footing is rarely perfect and slippage or even separation often occurs in the contact area. Furthermore, the soil region immediately adjacent to the footing can undergo a large degree of straining which would cause the soil-structure system to behave in a nonlinear manner. Both theoretical and experimental studies have shown that the properties of the soil in the vicinity of the footing are very sensitive to the dynamic response of the footing ( Han and Novak, 1988; Han, 1989; Han and Vaziri, 1992, and El-Marsafawi et al, 1992).

To account for the nonlinearities resulting from loss of contact between the soil

and the footing. Novak and Sheta (1980) proposed including a cylindrical annulus of weakened soil (an inner weakened zone or so-called boundary zone) around the footing in their plane strain analysis. Although their analysis allowed for different properties in the weakened boundary zone and the outer zone, each zone is assumed to be homogeneous. One of the simplifications involved in the original boundary zone concept was that the mass of the inner zone was neglected to avoid the wave reflection from the interface between the inner zone and the outer zone. To overcome this problem Lakshmanan and Mirai (1981), Veletsos and Dotson (1986, 1988) and Dotson and Veletsos (1990) proposed schemes that could account for the mass of the boundary zone. Some of the effects of the boundary zone mass were investigated by Novak and Han (1990) who found that a homogeneous boundary zone with a non-zero mass yields undulating impedances due to wave reflections from the interface between the two media. Since in reality the interface between the two media is only fictitious ( actually nonexistent ), the undulating impedances may be not suitable for practical applications. The ideal boundary zone should have properties smoothly approaching those of the outer zone. to alleviate wave reflections from the interface.

In this study the impedances for a composite soil layer are formulated based on a new model of the boundary zone with non-reflective interface. A parabolic variation of the medium properties is assumed, so that the boundary zone has properties smoothly approaching those of the outer zone to alleviate wave reflections from the interface. The impedances of the soil layer are presented for different modes of vibration . The results are evaluated over wide range of the parameters involved and

compared with those obtained for a homogeneous layer, as well as compared with Novak's and Veletsos's results. Since the boundary zone mass is accounted in this model and the non-reflective interface is formed, the impedances ( soil stiffness and damping ) are considered to be more suitable to practical applications than previous ones.

### 3.2 Model of Soil Layer with Non-reflective Interface

The system examined is a linear viscoelastic layer of unit depth and infinite extent with a circular hole of radius  $r_o$ , as shown in Fig. 3.1 (a). The impedances of the composite layer are derived based on the following assumptions : the outer zone medium is homogeneous, isotropic and viscoelastic with frequency independent material damping; within the boundary zone, the complex shear modulus,  $G^*(r)$ , varies parabolically, as expressed by the function  $f(r)$ , shown in Fig. 3.1 (b). The variation of  $G^*(r)$  is continuous within the boundary zone both in the function itself and its derivatives, so that no reflective wave can be produced at the interface (this is referred to as non-reflection interface):

The properties of the soil medium for each region are defined by the complex-valued modulus

$$G^*(r) = \begin{cases} G_1^* & r = r_o \\ G_o^* f(r) & r_o < r < R \\ G_o^* & r \geq R \end{cases} \quad (3.1)$$

and

$$\begin{cases} G_i^* = G_i(1 + i2\beta_i) \\ G_o^* = G_o(1 + i2\beta_o) \end{cases} \quad (3.2)$$

in which  $G_i$  and  $G_o$  = shear moduli of the inner and outer zones;  $r_o$  = radius of the cylindrical cavity in the medium;  $R$  = radius of boundary zone;  $r$  = radial distance to an arbitrary point;  $\beta_i$  and  $\beta_o$  = damping ratio for the two zones; and  $i = \sqrt{-1}$ .

The parabolic function,  $f(r)$ , can be expressed as :

$$f(r) = 1 - m^2 \left( \frac{r - R}{r_o} \right)^2 \quad (3.3)$$

and

$$m^2 = \frac{1 - G_i^*/G_o^*}{(t_m/r_o)^2} \quad (3.4)$$

where  $t_m$  = thickness of boundary zone;  $m$  = a constant whose value depends on  $G_i^*/G_o^*$  and  $t_m/r_o$ , as shown in eq.(3.4). It should be explained that the soil in the boundary zone may be weakened, as well as may be strengthened in some cases, such as pile driving. When the soil is weakened,  $G_i/G_o < 1$ ; when the soil is strengthened,  $G_i/G_o > 1$ .

Denoting

$$\xi = r/r_o \quad (3.5)$$

then

$$f(\xi) = 1 - m^2(\xi - R/r_o)^2 \quad (3.6)$$

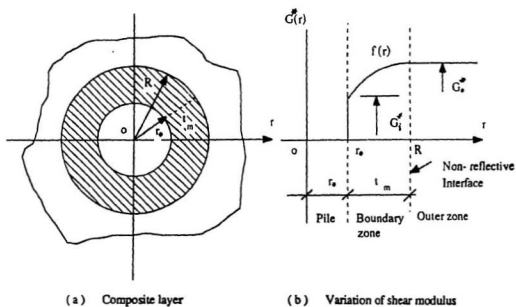


Figure 3.1: Model of boundary zone with non-reflective interface, (A) composition of the zones, and (B) variation of shear modulus with radial distance.

### 3.3 Differential Equations in Cylindrical Coordinates

For a homogeneous isotropic medium, the differential equations can be derived from the standard form, written in cylindrical coordinates, ( Sokolnikoff, 1956 )

$$\begin{cases} \frac{\partial \sigma_r}{\partial r} + \frac{1}{r} \frac{\partial \tau_{r\theta}}{\partial \theta} + \frac{\partial \tau_{rz}}{\partial z} + \frac{\sigma_r - \sigma_\theta}{r} = \rho \frac{\partial^2 u}{\partial t^2} \\ \frac{\partial \tau_{r\theta}}{\partial r} + \frac{1}{r} \frac{\partial \sigma_\theta}{\partial \theta} + \frac{\partial \tau_{\theta z}}{\partial z} + \frac{2}{r} \tau_{r\theta} = \rho \frac{\partial^2 v}{\partial t^2} \\ \frac{\partial \tau_{rz}}{\partial r} + \frac{1}{r} \frac{\partial \tau_{\theta z}}{\partial \theta} + \frac{\partial \sigma_z}{\partial z} + \frac{1}{r} \tau_{rz} = \rho \frac{\partial^2 w}{\partial t^2} \end{cases} \quad (3.7)$$

in which  $u, v$  and  $w$  = radial, tangential and vertical displacement, respectively;  $r, \theta$  and  $z$  = radial, angular and vertical variables;  $\sigma_i$  = normal stress;  $\tau_{ij}$  = shear stress;  $\rho$  = mass density and  $t$  = time.

Hooke's law for the medium assumes the form

$$\begin{cases} \sigma_i = \lambda^* (\epsilon_r + \epsilon_\theta + \epsilon_z) + 2G^* \epsilon_i \\ \tau_{ij} = 2G^* \gamma_{ij} \end{cases} \quad (3.8)$$

where  $\lambda^*$  = complex Lamé constant of the medium and the strains,  $\epsilon_i$  and  $\gamma_{ij}$ , can be expressed as

$$\begin{aligned} \epsilon_r &= \frac{\partial u}{\partial r} \\ \epsilon_\theta &= \frac{1}{r} \frac{\partial v}{\partial \theta} + \frac{u}{r} \\ \epsilon_z &= \frac{\partial w}{\partial z} \\ \gamma_{r\theta} &= \frac{1}{2} \left( \frac{1}{r} \frac{\partial u}{\partial \theta} + \frac{\partial v}{\partial r} - \frac{v}{r} \right) \end{aligned} \quad (3.9)$$

$$\begin{aligned}\gamma_{rz} &= \frac{1}{2} \left( \frac{\partial w}{\partial r} + \frac{\partial u}{\partial z} \right) \\ \gamma_{\theta z} &= \frac{1}{2} \left( \frac{\partial v}{\partial z} + \frac{1}{r} \frac{\partial w}{\partial \theta} \right)\end{aligned}$$

### 3.4 Impedance Functions of Soil Layer

#### 3.4.1 Vertical Excitation

##### Within the Boundary Zone

The radial and tangential displacements are assumed to be very small in comparison to the vertical displacement and hence can be neglected. That is  $u = v = 0$ , and also the variation of vertical displacement with depth is not considered. The governing equation can be derived from eq.(3.7) for the composite layer excited vertically,

$$G^*(r) \frac{\partial^2 w}{\partial r^2} + \left( \frac{dG^*(r)}{dr} + \frac{G^*(r)}{r} \right) \frac{\partial w}{\partial r} = \rho \frac{\partial^2 w}{\partial t^2} \quad (3.10)$$

The mass density for the inner zone is assumed to be equal to that of the outer zone.

Under harmonic excitation

$$w = w(r)e^{i\omega t} \quad (3.11)$$

eq.(3.10) can be written as

$$f(\xi) \frac{d^2 w}{d\xi^2} + \left( \frac{df(\xi)}{d\xi} + \frac{f(\xi)}{\xi} \right) \frac{dw}{d\xi} - \lambda_0^2 w = 0 \quad (3.12)$$

in which

$$\lambda_0 = \frac{ia_0}{\sqrt{1+i2\beta_0}} \quad (3.13)$$

where dimensionless frequency,  $a_0 = \omega r_0/V_s$ ,  $\omega$  is circular frequency, and  $V_s$  is shear wave velocity of soil.

Let

$$x = m(R/r_0 - \xi) \quad (3.14)$$

then

$$f(\xi) = 1 - x^2 \quad (3.15)$$

Substituting eq.(3.14) and (3.15) into eq.(3.12), yields

$$(x^2 - 1) \frac{d^2 w}{dx^2} + \left[ 2x + \frac{x^2 - 1}{x - mR/r_0} \right] \frac{dw}{dx} + \left( \frac{\lambda_0}{m} \right)^2 w = 0 \quad (3.16)$$

Denoting

$$a = mR/r_0$$

$$b = \left( \frac{\lambda_0}{m} \right)^2$$

Eq.(3.16) can be rewritten as

$$(x^2 - 1) \frac{d^2 w}{dx^2} + \left[ 2x + \frac{x^2 - 1}{x - a} \right] \frac{dw}{dx} + bw = 0 \quad (3.17)$$

The displacement,  $w$ , can be expressed by a power series as

$$w = \sum_{n=0}^{\infty} A_n x^n \quad (3.18)$$

Substituting eq.(3.18) into eq.(3.17), the coefficients in the power series can be determined as

$$A_0 = C_1$$

$$A_1 = C_2 \quad (3.19)$$

$$A_2 = \frac{abA_n + A_1}{2a}$$

$$A_n = \frac{(n-1)^2 A_{n-1} + a[b + (n-2)(n-1)]A_{n-2} - [b + (n-3)(n-1)]A_{n-3}}{n(n-1)a}$$

where  $C_1$  and  $C_2$  are complex-valued constants which can be determined by considering the boundary conditions.

Finally, the shear stress is

$$\tau_r = G^*(r) \frac{dw}{dr} = -\frac{m}{r_0} G^*(r) \frac{dw}{dx} \quad (3.20)$$

### Outer Medium

The governing equation for the vertical vibration of the homogeneous medium can be derived from eq.(3.7), but  $G^*$  is taken as constant in the outer zone. The equation is derived as

$$\xi^2 \frac{d^2 w}{d\xi^2} + \xi \frac{dw}{d\xi} - \lambda_0^2 \xi^2 w(\xi) = 0 \quad (3.21)$$

This is a Bessel equation for which its solution is

$$w(\xi) = C_3 I_0(\lambda_0 \xi) + C_4 K_0(\lambda_0 \xi) \quad (3.22)$$

where  $I_0$  and  $K_0$  are modified Bessel functions of zero order of the first and second kind, respectively;  $C_3$  and  $C_4$  are complex-valued constants of integration which can be determined from the boundary conditions.

The boundary conditions are :

$$\begin{cases} w_i = 1 & \text{at } \xi = 1 \\ w_o = 0 & \text{at } \xi = \infty \\ w_i = w_o & \text{at } \xi = R/r_o \\ \tau_i = \tau_o & \text{at } \xi = R/r_o \end{cases} \quad (3.23)$$

To satisfy these boundary conditions,  $C_4 = 0$  must hold.

Eq.(3.22) can now be written as

$$w(\xi) = C_3 K_o(\lambda_o \xi) \quad (3.24)$$

At the boundary of the hole,  $r = r_o$ , so  $\xi = 1$ . Thus, eq.(3.14) reduces to

$$x_1 = \sqrt{1 - G_i/G_o^*} \quad (3.25)$$

and likewise eq.(3.18) becomes

$$C_1 + C_2 x_1 + A_2 x_1^2 + \dots + A_n x_1^n = 1 \quad (3.26)$$

At the interface of the two zones,  $\xi = R/r_o$ , so  $x = 0$ . From eq.s(3.18) and (3.24), it follows that

$$C_1 = C_3 K_o(\lambda_o \frac{R}{r_o}) \quad (3.27)$$

and the shear stresses is

$$\tau_i = C_2 (-\frac{m}{r_o}) G_o^* \quad (3.28)$$

$$\tau_o = -C_3 \frac{\lambda_o}{r_o} K_1(\lambda_o \frac{R}{r_o}) G_o^* \quad (3.29)$$

where  $K_1$  is modified Bessel function of first order and the second kind. Using  $\tau_i = \tau_o$  at the interface it follows that

$$C_2 = C_3 \frac{\lambda_o}{m} K_1(\lambda_o \frac{R}{r_o}) \quad (3.30)$$

From eq.s(3.26),(3.27) and (3.30).  $C_1, C_2$  and  $C_3$  can be calculated.

The impedances of the composite layer for vertical vibration is defined as

$$k_v = -2\pi r_o r_i(r=r_o) \quad (3.31)$$

then,  $k_v$  can now be determined from

$$k_v = \pi G_i 2m(1 + i2\beta_i) \frac{dw}{dx} \Big|_{x=x_i} \quad (3.32)$$

It is desirable to express  $k_v$  in the following form

$$k_v = \pi G_i (S_{v1} + ia_i S_{v2}) \quad (3.33)$$

in which

$$a_i = \frac{\omega r_o}{V_{si}} \quad (3.34)$$

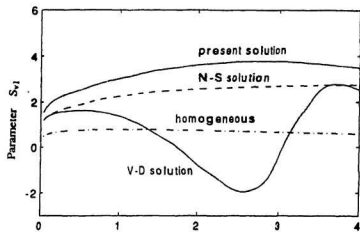
where  $V_{si} = \sqrt{G_i/\rho}$  is the shear wave velocity for the boundary zone;  $S_{v1}$  and  $S_{v2}$  are dimensionless factors that depend on  $\alpha_o, t_m/r_o, G_i/G_o, \beta_i$  and  $\beta_o$ . The factors  $S_{v1}$  and  $S_{v2}$  are referred to as the vertical stiffness and damping of soil, respectively.

In this study, the impedances of the soil layer was expressed in terms of the shear modulus of the inner region,  $G_i$ , following the format employed in Veletsos and Dotson(1988). The stiffness and damping factors,  $S_{v1}$  and  $S_{v2}$ , obtained from the present analysis are compared with those obtained for the Novak-Sheta (N-S) and Veletsos-Dotson (V-D) idealizations, as shown in Fig. 3.2. These solutions are for a soil layer with  $t_m/r_o = 1.0, G_i/G_o = 0.25, \beta_i = 0.1$ , and  $\beta_o = 0.05$ . The mass density for the inner zone is taken to be the equal to that for the outer region in

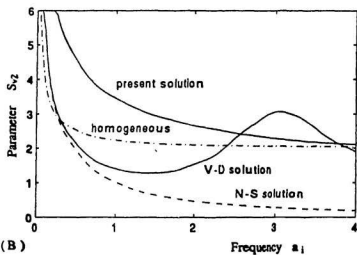
the present solution and V-D solution. for the N-S solution the mass density for the inner zone is assumed to be zero. It can be observed that the three sets of results are significantly different; the V-D solution results in pronounced oscillations ( undulations) caused by wave reflections from the interface between the two media. It is a defect in theory to assume zero-mass in the inner zone for N-S solution. The results from the present analysis are smooth curves over a wide range, the value of  $\alpha_i$  from 0.0 to 4.0, which indicates that the wave reflections from the interface are alleviated because it embodies a continuous variation in soil properties in the boundary zone with smooth (continuous derivatives) transition into the outer zone. For comparison, the results for a homogeneous layer are also included in Fig. 3.2.

To illustrate the influence of parameters involved, the stiffness and damping factors for a vertically excited layer are plotted in Fig. 3.3 and Fig. 3.4 as a function of  $\alpha_i$  for several different combinations of  $t_m/r_o$  and  $G_o/G_i$ , with material damping,  $\beta_i = 0.1$  and  $\beta_o = 0.05$ . It should be noticed that the undulations caused by wave reflection vanish as expected in all of the cases presented, owing to the model of non-reflective interface. The influence of the material properties in the boundary zone is sensitive to the stiffness and damping of the soil layer. The stiffness factor,  $S_{v1}$ , increases with the level of  $G_o/G_i$  and is smallest for the homogeneous case ( $G_o/G_i = 1$ ). The damping factor,  $S_{v2}$ , at lower frequency levels becomes larger as the magnitude of  $G_o/G_i$  increases; however, at higher frequencies this tendency diminished.

The effects of material damping on the impedances of the soil layer are shown



(A)



(B)

Figure 3.2: Comparison of impedance functions for vertical vibration by different solutions,  $t_m/r_o = 1.0$ ,  $G_i/G_o = 0.25$ ,  $\beta_i = 0.1$ ,  $\beta_o = 0.05$ ; (A) stiffness factor  $S_{v1}$ , and (B) damping factor  $S_{v2}$ .

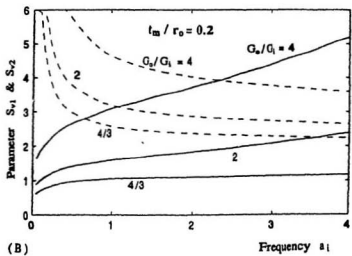
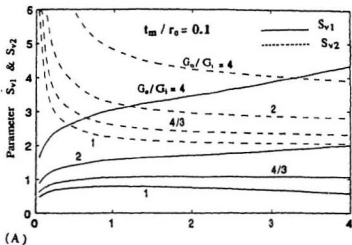


Figure 3.3: Vertical impedances for a composite layer with material damping  $\beta_1 = 0.1$ ,  $\beta_0 = 0.05$  and different parameters: (A) for  $t_m/r_0 = 0.1$ ; (B) for  $t_m/r_0 = 0.2$ .

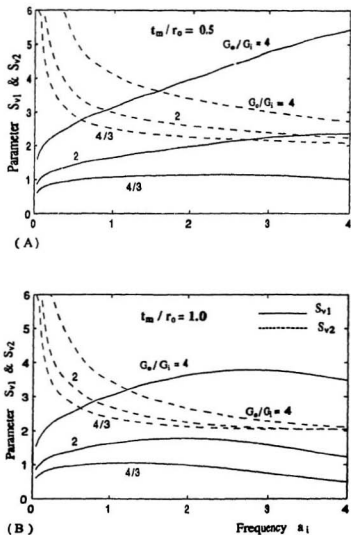
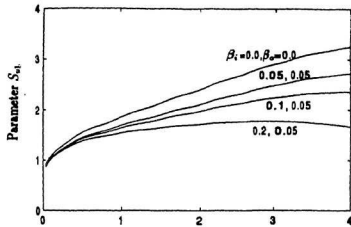
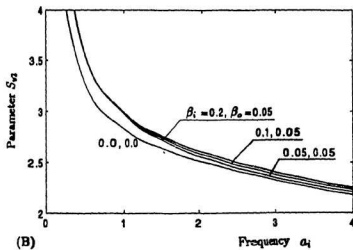


Figure 3.4: Vertical impedances for a composite layer with material damping  $\beta_1 = 0.1$ ,  $\beta_2 = 0.05$  and different parameters: (A) for  $t_m/r_0 = 0.5$ ; (B) for  $t_m/r_0 = 1.0$ .



(A)



(B)

Figure 3.5: Effects of material damping on vertical impedances of soil layer, (A) stiffness factor  $S_{v1}$ , and (B) damping factor  $S_{v2}$ .

in Fig. 3.5. Several values of damping ratio are selected, in one case both  $\beta_1$  and  $\beta_2$  are zero and in other cases  $\beta_1 = 0.05$  and  $\beta_2 = 0.05, 0.1$  and  $0.2$ , respectively. It can be seen that the stiffness factor,  $S_{v1}$ , reduces with material damping increasing, but the effect to damping factor,  $S_{v2}$ , are small. This trend in damping response can be explained by reference to the fact that the radiation damping becomes more dominant (relative to the material damping) at higher frequency levels.

### 3.4.2 Torsional Excitation

#### Within the Boundary Zone

The assumptions that are made for the case of torsional vibration of the medium around the vertical axis of the cylinder are that the radial and vertical displacements are infinitesimally small and hence can be neglected. That is  $u = w = 0$ . Variation of tangential displacement with depth is not considered. The governing equation can be derived from eq.(3.7) for the layer excited torsionally,

$$G^*(r)\left(\frac{\partial^2 v}{\partial r^2} + \frac{1}{r} \frac{\partial v}{\partial r} - \frac{1}{r^2} v\right) + \frac{dG^*(r)}{dr} \left(\frac{\partial v}{\partial r} - \frac{v}{r}\right) = \rho \frac{\partial^2 v}{\partial t^2} \quad (3.35)$$

The mass density for the inner zone is assumed to be equal to that of the outer zone.

Under harmonic excitation

$$v = v(r)e^{i\omega t} \quad (3.36)$$

eq.(3.35) can be written as

$$f(\xi) \frac{d^2 v}{d\xi^2} + \left[ \frac{df(\xi)}{d\xi} + \frac{f(\xi)}{\xi} \right] \frac{dv}{d\xi} - \left[ \frac{1}{\xi} \frac{df(\xi)}{d\xi} + \frac{f(\xi)}{\xi^2} + \lambda_0^2 \right] v = 0 \quad (3.37)$$

Substituting eq.(3.14) and (3.15) into eq.(3.37), yields

$$(x^2 - 1) \frac{d^2 v}{dx^2} + \left[ 2x + \frac{x^2 - 1}{x - a} \right] \frac{dv}{dx} + \left[ \frac{2x}{a - x} + \frac{1 - x^2}{(x - a)^2} + b \right] v = 0 \quad (3.38)$$

The displacement,  $v$ , can be expressed by a power series as

$$v = \sum_{n=0}^{\infty} A_n x^n \quad (3.39)$$

Substituting eq.(3.39) into eq.(3.38), the coefficients in the power series can be determined as

$$\begin{aligned} A_0 &= C_1 \\ A_1 &= C_2 \\ A_2 &= \frac{(a^2 b + 1)A_0 + aA_1}{2a^2} \\ A_3 &= \frac{2a(1 - b)A_0 + a^2(b + 2)A_1 + 6aA_2}{6a^2} \end{aligned} \quad (3.40)$$

with denoting

$$\begin{cases} \delta_1 = (n - 1)(2n - 3)a \\ \delta_2 = (n - 1)(n - 2)a^2 - (n - 2)^2 + ba^2 + 1 \\ \delta_3 = -a[(n - 3)(2n - 3) + 2(b - 1)] \\ \delta_4 = (n - 2)(n - 4) + b - 3 \end{cases} \quad (3.41)$$

the general term can be expressed as

$$A_n = \frac{\delta_1 A_{n-1} + \delta_2 A_{n-2} + \delta_3 A_{n-3} + \delta_4 A_{n-4}}{n(n - 1)a^2} \quad (3.42)$$

where  $C_1$  and  $C_2$  are complex-valued constants which can be determined by considering the boundary conditions.

Finally, the shear stress is

$$\tau_1 = G^*(r) \left( \frac{dv}{dr} - \frac{v}{r} \right) = -G^*(r) \left( \frac{m}{r_0} \frac{dv}{dx} + \frac{v}{r} \right) \quad (3.43)$$

### Outer Medium

The governing equation for the torsional vibration of the homogeneous medium can be derived from eq.(3.7), but  $G^*$  is taken as constant in the outer zone. The equation is derived as

$$\xi^2 \frac{d^2 v}{d\xi^2} + \xi \frac{dv}{d\xi} - (\lambda_0^2 \xi^2 + 1)v(\xi) = 0 \quad (3.44)$$

This is a Bessel equation for which its solution is

$$v(\xi) = C_3 K_1(\lambda_0 \xi) + C_4 I_1(\lambda_0 \xi) \quad (3.45)$$

where  $I_1$  and  $K_1$  are modified Bessel functions of order one of the first and second kind, respectively;  $C_3$  and  $C_4$  are complex-valued constants of integration which can be determined from the boundary conditions.

The boundary conditions are :

$$\begin{cases} v_1/r_0 = 1 & \text{at } \xi = 1 \\ v_0 = 0 & \text{at } \xi = \infty \\ v_i = v_0 & \text{at } \xi = R/r_0 \\ \tau_1 = \tau_0 & \text{at } \xi = R/r_0 \end{cases} \quad (3.46)$$

From these boundary conditions,  $C_1, C_2, C_3$  and  $C_4$  can be calculated.

The impedances of the composite layer for torsional vibration is defined as the moment of the shear stresses around the cylinder axis with respect to unit torsional angle (  $v_i/r_o = 1$  ),

$$k_\theta = -2\pi r_o^2 \tau_i(r=r_o) \quad (3.47)$$

then,  $k_\theta$  can now be determined from

$$k_\theta = 2\pi r_o^2 G_i \left( 1 + i2\beta_i \right) \left( \frac{m}{r_o} \frac{dv}{dx} + 1 \right) \Big|_{x=x_1} \quad (3.48)$$

It is desirable to express  $k_\theta$  in the following form

$$k_\theta = 2\pi r_o^2 G_i (S_{\theta 1} + ia_i S_{\theta 2}) \quad (3.49)$$

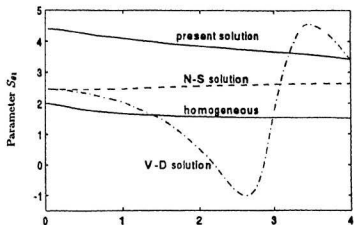
where  $S_{\theta 1}$  and  $S_{\theta 2}$  are dimensionless factors that depend on  $a_o, t_m/r_o, G_i/G_o, \beta_i$  and  $\beta_o$ . The factors  $S_{\theta 1}$  and  $S_{\theta 2}$  are referred to as the torsional stiffness and damping of soil, respectively.

The stiffness and damping factors,  $S_{\theta 1}$  and  $S_{\theta 2}$ , obtained from the present analysis are compared with those obtained for the Novak-Sheta (N-S) and Veletsos-Dotson (V-D) idealizations, as shown in Fig. 3.6. These solutions are for a soil layer with  $t_m/r_o = 1.0, G_i/G_o = 0.25, \beta_i = \beta_o = 0.0$ . The mass density for the inner zone is taken to be the equal to that for the outer region in the present solution and V-D solution, for the N-S solution the mass density for the inner zone is assumed to be zero. It can be observed that similar to the case of vertical vibration the V-D solution results in pronounced oscillations ( undulations ) caused by wave reflections

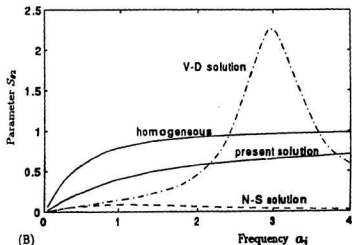
from the interface between the two media. The results from the present analysis are smooth curves over a wide range, indicated that the wave reflections from the interface are alleviated because it embodies a continuous variation in soil properties in the boundary zone with smooth (continuous derivatives) transition into the outer zone. For comparison, the results for a homogeneous layer are also included in Fig. 3.6.

To illustrate the influence of parameters involved, the stiffness and damping factors for a torsionally excited layer are plotted in Fig. 3.7 and Fig. 3.8 as a function of  $a_i$  for several different combinations of  $t_m/r_o$  and  $G_o/G_i$ , with material damping,  $\beta_i = 0.1$  and  $\beta_o = 0.05$ . It should be noticed that the undulations caused by wave reflection vanish as expected in all of the cases presented. The torsional stiffness factor,  $S_{\theta 1}$ , increases with the level of  $G_o/G_i$  and is smallest for the homogeneous case ( $G_o/G_i = 1$ ).

The effects of material damping on the torsional impedances of the soil layer are shown in Fig. 3.9. Several values of damping ratio are selected, in one case both  $\beta_i$  and  $\beta_o$  are zero and in other cases  $\beta_o = 0.05$  and  $\beta_i = 0.05, 0.1$  and  $0.2$ , respectively. It can be seen that the stiffness factor,  $S_{\theta 1}$ , reduces with material damping increasing, but the effect to damping factor,  $S_{\theta 2}$ , are small. This trend in damping response can be explained by reference to the fact that the radiation damping becomes more dominant (relative to the material damping) at higher frequency levels.

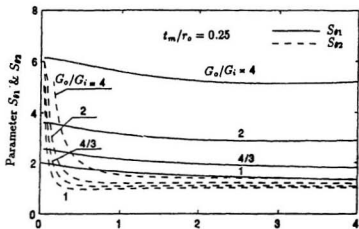


(A)

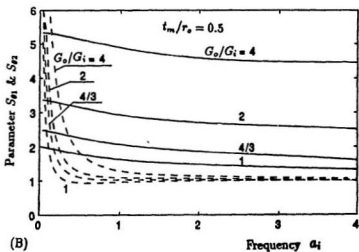


(B)

Figure 3.6: Comparison of torsional impedance functions by different solutions,  $t_m/r_o = 1.0$ ,  $G_i/G_o = 0.25$ ,  $\beta_i = \beta_o = 0.0$ ; (A) stiffness factor  $S_{H1}$ , and (B) damping factor  $S_{H2}$ .



(A)



(B)

Figure 3.7: Torsional impedances for a composite layer with material damping  $\beta_i = 0.1$ ,  $\beta_o = 0.05$  and different parameters: (A) for  $t_m/r_o = 0.25$ ; (B) for  $t_m/r_o = 0.5$ .

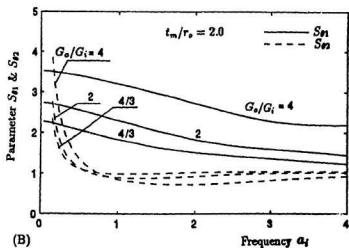
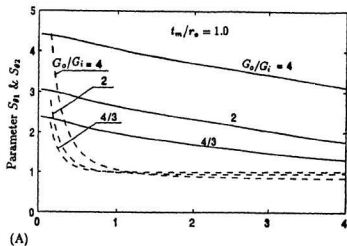
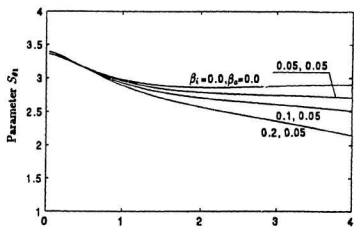
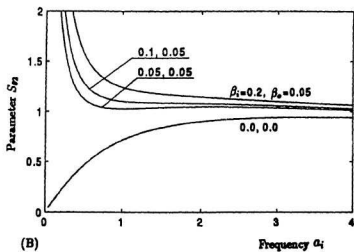


Figure 3.8: Torsional impedances for a composite layer with material damping  $\beta_i = 0.1$ ,  $\beta_o = 0.05$  and different parameters: (A) for  $t_m/r_o = 1.0$ ; (B) for  $t_m/r_o = 2.0$ .



(A)



(B)

Figure 3.9: Effects of material damping on torsional impedances of soil layer, (A) stiffness factor  $S_{\theta 1}$ , and (B) damping factor  $S_{\theta 2}$ .

### 3.4.3 Radial Excitation

#### Within Boundary Zone

The composite layer is subjected to an axisymmetrical, volumetrical deformation associated with the propagation of P-wave in the radial direction, or say breathing vibration, such as in the cases of cavity expansion, pile vibration and driving. In this case,  $v = w = 0$ , the governing equations can be derived from eq.(3.7) as

$$\frac{\partial \sigma_r}{\partial r} + \frac{\sigma_r - \sigma_\theta}{r} = \rho \frac{\partial^2 u(r, t)}{\partial t^2} \quad (3.50)$$

where,  $\sigma_r$  = normal stress,  $\sigma_\theta$  = tangent stress, and  $u(r, t)$  = radial displacement.

The stresses,  $\sigma_r$  and  $\sigma_\theta$ , can be expressed as

$$\begin{cases} \sigma_r = (\lambda^* + 2G^*) \frac{\partial u(r, t)}{\partial r} + \lambda^* \frac{u(r, t)}{r} \\ \sigma_\theta = \lambda^* \frac{\partial u(r, t)}{\partial r} + (\lambda^* + 2G^*) \frac{u(r, t)}{r} \end{cases} \quad (3.51)$$

where  $\lambda^*$  = complex Lamé constant of medium in boundary zone, and expressed as

$$\lambda^* = \frac{2\nu}{1 - 2\nu} G^* \quad (3.52)$$

where  $\nu$  = Poisson's ratio, to be assumed a constant in the boundary zone and the same as that in the outer medium.

Substituting eq.(3.51) into eq.(3.50), yields

$$\frac{\partial}{\partial r} \left[ (\lambda^* + 2G^*) \frac{\partial u(r, t)}{\partial r} + \lambda^* \frac{u(r, t)}{r} \right] + \frac{2G^*}{r} \left( \frac{\partial u(r, t)}{\partial r} - \frac{u(r, t)}{r} \right) = \rho \frac{\partial^2 u(r, t)}{\partial t^2} \quad (3.53)$$

Within the boundary zone,  $\lambda^*$  and  $G^*$  are variable, eq.(3.53) can be written as

$$(\lambda^* + 2G^*) \left[ \frac{\partial^2 u(r, t)}{\partial r^2} + \frac{1}{r} \frac{\partial u(r, t)}{\partial r} - \frac{1}{r^2} u(r, t) \right] + \frac{d(\lambda^* + 2G^*)}{dr} \frac{\partial u(r, t)}{\partial r} + \frac{d\lambda^*}{dr} \frac{u(r, t)}{r} = \rho \frac{\partial^2 u(r, t)}{\partial t^2} \quad (3.54)$$

Under harmonic excitation

$$u(r, t) = u(r)e^{i\omega t} \quad (3.55)$$

eq.(3.54) becomes

$$f(\xi) \frac{d^2 u}{d\xi^2} + \left[ \frac{df(\xi)}{d\xi} + \frac{f(\xi)}{\xi} \right] \frac{du}{d\xi} - \left[ \frac{f(\xi)}{\xi^2} - \frac{df(\xi)}{d\xi} \frac{\eta_1^2}{\xi} + (sr_o)^2 \right] u = 0 \quad (3.56)$$

in which

$$\begin{cases} sr_o = \frac{ia_o}{\eta\sqrt{1+i2\beta_o}} \\ \eta = \sqrt{2(1-\nu)/(1-2\nu)} \\ \eta_1 = \sqrt{\nu/(1-\nu)} \end{cases} \quad (3.57)$$

and denoting

$$B = \left( \frac{sr_o}{m} \right)^2 \quad (3.58)$$

With reference to eq.(3.14) and (3.15), eq.(3.56) can be written as

$$(x^2 - 1) \frac{d^2 u}{dx^2} + \left[ 2x + \frac{x^2 - 1}{x - a} \right] \frac{du}{dx} + \left[ \frac{1 - x^2}{(x - a)^2} + \eta_1^2 \frac{2x}{x - a} + B \right] u = 0 \quad (3.59)$$

The displacement,  $u$ , can be expressed by a power series as

$$u = \sum_{n=0}^{\infty} A_n x^n \quad (3.60)$$

Substituting eq.(3.60) into eq.(3.59), the coefficients in the power series can be determined as

$$\begin{aligned} A_0 &= C_1 \\ A_1 &= C_2 \end{aligned} \quad (3.61)$$

$$A_2 = \frac{(a^2B + 1)A_0 + aA_1}{2a^2}$$

$$A_3 = \frac{-2a(B + \eta_1^2)A_0 + a^2(B + 2)A_1 + 6aA_2}{6a^2}$$

with denoting

$$\begin{cases} \delta 1 = (n-1)(2n-3)a \\ \delta 2 = (n-2)(n-3)(a^2-1) + (n-2)(2a^2-1) + Ba^2 + 1 \\ \delta 3 = -a[(n-3)(2n-3) + 2(B + \eta_1^2)] \\ \delta 4 = (n-2)(n-4) + B + 2\eta_1^2 - 1 \end{cases} \quad (3.62)$$

the general term can be expressed as

$$A_n = \frac{\delta 1 A_{n-1} + \delta 2 A_{n-2} + \delta 3 A_{n-3} + \delta 4 A_{n-4}}{n(n-1)a^2} \quad (3.63)$$

where  $C_1$  and  $C_2$  are complex-valued constants which can be determined by considering the boundary conditions. Finally, the normal stress is

$$\sigma_r = -\frac{m}{r_0}(\lambda^* + 2G^*)\frac{du}{dx} + \lambda^*\frac{u}{r} \quad (3.64)$$

### Outer Medium

The governing equations of the homogeneous medium can be derived from eq.(3.53), but  $\lambda^*$  and  $G^*$  are taken as constants. For the axisymmetric, volumetric deformation associated with the propagation of P-wave in the radial direction, breathing vibration, the equation is

$$(\lambda_0^* + 2G_0^*)\left[\frac{\partial^2 u(r,t)}{\partial r^2} + \frac{1}{r}\frac{\partial u(r,t)}{\partial r} - \frac{1}{r^2}u(r,t)\right] = \rho\frac{\partial^2 u(r,t)}{\partial t^2} \quad (3.65)$$

where  $\lambda_0^*$  = complex Lamé constant of medium in outer zone. For harmonic excitation, eq.(3.65) becomes

$$\frac{d^2 u(r)}{dr^2} + \frac{1}{r}\frac{du(r)}{dr} - (s^2 + \frac{1}{r^2})u(r) = 0 \quad (3.66)$$

This is a modified Bessel equation, for which its solution is

$$u(r) = C_3 K_1(sr) + C_4 I_1(sr) \quad (3.67)$$

where  $I_1$  and  $K_1$  are the modified Bessel function of order one, the first and second kind, respectively;  $C_3$  and  $C_4$  are complex-valued constants of integration which can be determined from the boundary conditions.

The boundary conditions are : the displacement amplitude is unity at the boundary of the hole and displacements vanish as  $r \rightarrow \infty$ ; displacements and stresses are equal at the interface between the two zones. To satisfy these boundary conditions,  $C_4 = 0$  must hold. Eq.(3.67) can now be written as

$$u(r) = C_3 K_1(sr) \quad (3.68)$$

At the boundary of the hole,  $r = r_0$ , and  $\xi = 1$

$$x_1 = \sqrt{1 - G_i^*/G_o^*} \quad (3.69)$$

and likewise eq.(3.60) becomes

$$C_1 + C_2 x_1 + A_2 x_1^2 + \dots + A_n x_1^n = 1 \quad (3.70)$$

At the interface of the two zones,  $r = R$  and  $x = 0$ , from eqs. (60) and (68), it follows that

$$C_1 = C_3 K_1(sR) \quad (3.71)$$

From eq.(3.1) and eq.(3.52) one knows that  $\lambda^* = \lambda_o^*$  and  $G^* = G_o^*$  at the interface ( $r = R$ ), and the normal stresses  $\sigma_i = \sigma_o$ , then

$$C_2 = C_3 \left[ \frac{r_0}{mR} K_1(sR) + \frac{sr_0}{m} K_0(sR) \right] \quad (3.72)$$

From eq.s(3.70), (3.71) and (3.72),  $C_1, C_2$  and  $C_3$  can be obtained. Since the displacement amplitude is unity at  $r = r_o$ , the radial stiffness is defined as

$$k_r = -\sigma_r(r=r_o) \quad (3.73)$$

then,  $k_r$  can now be determined from

$$k_r = \frac{2(1-\nu)}{1-2\nu} \frac{m}{r_o} G_i^* \left. \frac{du}{dx} \right|_{x=x_1} - \frac{2\nu}{1-2\nu} \frac{1}{r_o} G_i^* \quad (3.74)$$

Separating the real and imaginary parts of eq.(3.74), the complex-valued radial stiffness can be written as

$$k_r = \frac{G_i}{r_o} [S_{b1} + ia_i S_{b2}] \quad (3.75)$$

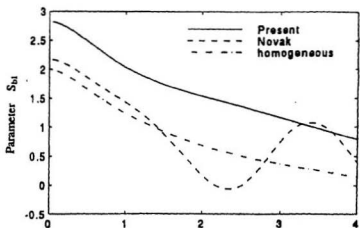
The real part  $S_{b1}$  is a dimensionless stiffness factor and  $S_{b2}$  is a damping factor. The values of  $S_{b1}$  and  $S_{b2}$  depend on frequency  $a_o$ , damping ratio  $\beta_o$  and Poisson's ratio  $\nu$ ; also on the boundary zone parameters, such as, modulus ratio  $G_i/G_o$ , thickness ratio  $t_m/r_o$  and damping ratio  $\beta_i$ .

The stiffness and damping factors,  $S_{b1}$  and  $S_{b2}$ , obtained from the present analysis are compared with those obtained for the Novak and Mitwally idealizations (1988), as shown in Fig. 3.10. These solutions are for a soil layer with  $t_m/r_o = 2.0$ ,  $G_i/G_o = 0.5$ ,  $\beta_i = 0.1$ ,  $\beta_o = 0.05$  and Poisson's ratio,  $\nu = 0.25$ . The mass for the inner zone is accounted in both Novak's solution and the present solution, however, the properties of soil for the inner zone were assumed to be constant in the former so that resulting in pronounced oscillations ( undulations) caused by wave reflections from the interface between the two media. The results from the present analysis are smooth curves over a wide range, indicated that the wave reflections from the

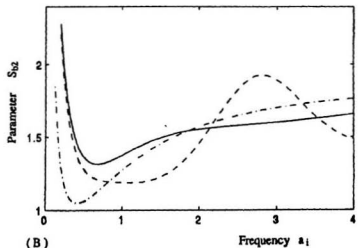
interface are alleviated because it embodies a continuous variation in soil properties in the boundary zone with smooth (continuous derivatives) transition into the outer zone. For comparison, the results for a homogeneous layer are also included in Fig. 3.10.

To illustrate the influence of parameters involved, the stiffness and damping factors for a radially excited layer are plotted in Fig. 3.11 as a function of  $a_i$  for several different combinations of  $t_m/r_o$  and  $G_o/G_i$ , with material damping,  $\beta_i = 0.1$  and  $\beta_o = 0.05$ . It should be noticed that the undulations caused by wave reflection vanish as expected in all of the cases presented. The radial stiffness factor,  $S_{b1}$ , increases with the level of  $G_o/G_i$  and is smallest for the homogeneous case ( $G_o/G_i = 1$ ).

The effects of Poisson's ratio on the radial impedances of the soil layer are shown in Fig. 3.12. Several values of Poisson's ratio are selected,  $\nu = 0.0, 0.2, 0.3$  and  $0.4$ , respectively. It can be seen that the stiffness factor,  $S_{b1}$ , reduces with Poisson's ratio increasing, but the damping factor,  $S_{b2}$ , increased with  $\nu$  increasing for higher frequency range.

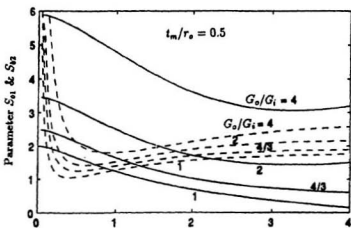


(A)

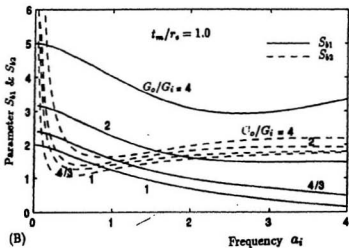


(B)

Figure 3.10: Comparison of radial impedance functions by different solutions,  $t_m/r_o = 2.0$ ,  $G_i/G_o = 0.5$ ,  $\nu = 0.25$ ,  $\beta_i = 0.1$  and  $\beta_o = 0.05$ ; (A) stiffness factor  $S_{1_1}$ , and (B) damping factor  $S_{2_2}$ .

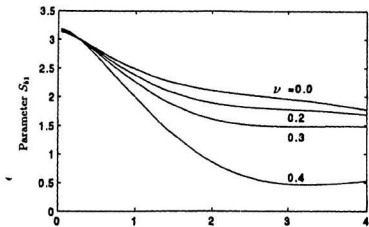


(A)

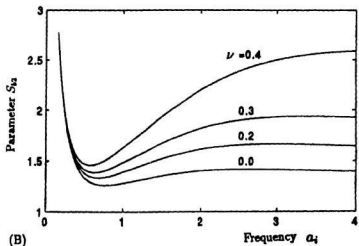


(B)

Figure 3.11: Radial impedances for a composite layer with material damping  $\beta_1 = 0.1$ ,  $\beta_o = 0.05$  and different parameters: (A) for  $t_m/r_o = 0.5$ ; (B) for  $t_m/r_o = 1.0$ .



(A)



(B)

Figure 3.12: Effects of Poisson's ratio on radial impedances of soil layer; (A) stiffness factor  $S_{11}$ , and (B) damping factor  $S_{12}$ .

### 3.4.4 Rocking Excitation

#### Within the Boundary Zone

In this case it is assumed that the particles of soil move vertically up and down along the cylinder axis. This case is very similar to the vertical case. The assumptions are  $u = v = \frac{\partial w}{\partial x} = 0$ . The governing equation can be derived from eq.(3.7) for the rocking vibration of the composite layer

$$G^*(r) \frac{\partial^2 w}{\partial r^2} + \left[ \frac{dG^*(r)}{dr} + \frac{G^*(r)}{r} \right] \frac{\partial w}{\partial r} + \frac{G^*(r)}{r^2} \frac{\partial^2 w}{\partial \theta^2} = \rho \frac{\partial^2 w}{\partial t^2} \quad (3.76)$$

The mass density for the inner zone is assumed to be equal to that of the outer zone.

Assuming

$$w = w(r) \cos \theta e^{i\omega t} \quad (3.77)$$

eq.(3.76) can be written as

$$f(\xi) \frac{d^2 w}{d\xi^2} + \left[ \frac{df(\xi)}{d\xi} + \frac{f(\xi)}{\xi} \right] \frac{dw}{d\xi} - \left[ \frac{f(\xi)}{\xi^2} + \lambda_o^2 \right] w = 0 \quad (3.78)$$

in which

$$\lambda_o = \frac{ia_o}{\sqrt{1 + i2\beta_o}} \quad (3.79)$$

Substituting eq.(3.14) and (3.15) into eq.(3.78), yields

$$(x^2 - 1) \frac{d^2 w}{dx^2} + \left[ 2x + \frac{x^2 - 1}{x - mR/r_o} \right] \frac{dw}{dx} + \left[ \frac{1 - x^2}{(x - mR/r_o)^2} + \left( \frac{\lambda_o}{m} \right)^2 \right] w = 0 \quad (3.80)$$

Denoting

$$a = mR/r_o$$

$$b = \left(\frac{1-a}{m}\right)^2$$

Eq.(3.80) can be rewritten as

$$(x^2 - 1) \frac{d^2 w}{dx^2} + \left[2x + \frac{x^2 - 1}{x - a}\right] \frac{dw}{dx} + \left\{\frac{1 - x^2}{(x - a)^2} + b\right\} w = 0 \quad (3.81)$$

The displacement,  $w$ , can be expressed by a power series as

$$w = \sum_{n=0}^{\infty} A_n x^n \quad (3.82)$$

Substituting eq.(3.82) into eq.(3.81), the coefficients in the power series can be determined as

$$\begin{aligned} A_0 &= C_1 \\ A_1 &= C_2 \\ A_2 &= \frac{(a^2 b + 1)A_0 + aA_1}{2a^2} \\ A_3 &= \frac{-2abA_0 + a^2(b + 2)A_1 + 6aA_2}{6a^2} \end{aligned} \quad (3.83)$$

with denoting

$$\begin{cases} \delta 1 = (n - 1)(2n - 3)a \\ \delta 2 = (n - 1)(n - 2)a^2 - (n - 2)^2 + ba^2 + 1 \\ \delta 3 = -a[(n - 3)(2i - 3) + 2b] \\ \delta 4 = (n - 2)(n - 4) + b - 1 \end{cases} \quad (3.84)$$

the general term can be expressed as

$$A_n = \frac{\delta 1 A_{n-1} + \delta 2 A_{n-2} + \delta 3 A_{n-3} + \delta 4 A_{n-4}}{(n - 1)a^2} \quad (3.85)$$

where  $C_1$  and  $C_2$  are complex-valued constants which can be determined by considering the boundary conditions.

Finally, the shear stress is

$$\tau_r = G^*(r) \frac{dw}{dr} \cos \theta = -\frac{m}{r_o} G^*(r) \frac{dw}{dx} \cos \theta \quad (3.86)$$

### Outer Medium

The governing equation for the rocking vibration of the homogeneous medium can be derived from eq.(3.7), but  $G^*$  is taken as constant in the outer zone. The equation is derived as

$$\xi^2 \frac{d^2 w}{d\xi^2} + \xi \frac{dw}{d\xi} - (\lambda_o^2 \xi^2 + 1)w(\xi) = 0 \quad (3.87)$$

This is a Bessel equation for which its solution is

$$w(\xi) = C_3 K_1(\lambda_o \xi) + C_4 I_1(\lambda_o \xi) \quad (3.88)$$

where  $I_1$  and  $K_1$  are modified Bessel functions of order one of the first and second kind, respectively;  $C_3$  and  $C_4$  are complex-valued constants of integration which can be determined from the boundary conditions.

The boundary conditions are :

$$\begin{cases} w_i = 1 & \text{at } \xi = 1 \text{ and } \theta = 0 \\ w_o = 0 & \text{at } \xi = \infty \\ w_i = w_o & \text{at } \xi = R/r_o \\ \tau_i = \tau_o & \text{at } \xi = R/r_o \end{cases} \quad (3.89)$$

To satisfy these boundary conditions,  $C_4 = 0$  must hold.

Eq.(3.88) can now be written as

$$w(\xi) = C_3 K_1(\lambda_o \xi) \quad (3.90)$$

At the boundary of the hole, yields

$$C_1 + C_2 x_1 + A_2 x_1^2 + \dots + A_n x_1^n = 1 \quad (3.91)$$

At the interface of the two zones,  $\xi = R/r_o$ , so  $x = 0$ . From eq.s(3.82) and (3.90), it follows that

$$C_1 = C_3 K_1(\lambda_o \frac{R}{r_o}) \quad (3.92)$$

Using  $\tau_i = \tau_o$  at the interface it follows that

$$C_2 = C_3 [\frac{\lambda_2}{m} K_0(\lambda_2 \frac{R}{r_o}) + \frac{r_o}{mR} K_1(\lambda_o \frac{R}{r_o})] \quad (3.93)$$

From eq.s(3.91),(3.92) and (3.93),  $C_1, C_2$  and  $C_3$  can be calculated.

The impedances of the composite layer for rocking vibration is defined as

$$k_\psi = \frac{M_\psi}{\psi} \quad (3.94)$$

where  $M_\psi$  is the soil reaction moment to the motion of the cylinder, expressed as

$$M_\psi = - \int_0^{2\pi} r_o^2 \tau_i \cos \theta d\theta \quad (3.95)$$

and the rocking amplitude of the cylinder is  $\psi = w(r = r_o)/(r_o \cos \theta)$ . then,  $k_\psi$  can now be determined from

$$k_\psi = \pi r_o^2 G_1 m (1 + i2\beta_1) \frac{dw}{dx} |_{x=r_1} \quad (3.96)$$

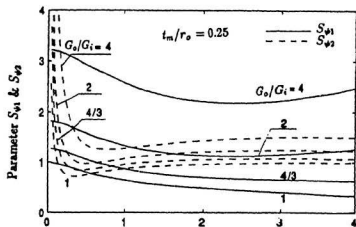
It is desirable to express  $k_\psi$  in the following form

$$k_\psi = \pi r_o^2 G_1 (S_{\psi 1} + ia, S_{\psi 2}) \quad (3.97)$$

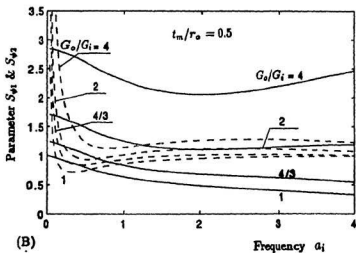
where  $S_{\psi 1}$  and  $S_{\psi 2}$  are dimensionless factors that depend on  $a_0, t_m/r_0, G_i/G_0, \beta_i$  and  $\beta_0$ . The factors  $S_{\psi 1}$  and  $S_{\psi 2}$  are referred to as the rocking stiffness and damping of soil, respectively.

To illustrate the influence of parameters involved, the stiffness and damping factors for the layer in rocking vibration are plotted in Fig. 3.13 and Fig. 3.14 as a function of  $a$ , for several different combinations of  $t_m/r_0$  and  $G_0/G_i$ , with material damping,  $\beta_i = 0.1$  and  $\beta_0 = 0.05$ . It should be noticed that the undulations caused by wave reflection vanish as expected in all of the cases presented, owing to the model of non-reflective interface. The influence of the material properties in the boundary zone is sensitive to the stiffness of the soil layer. The stiffness factor,  $S_{\psi 1}$ , increases with the level of  $G_0/G_i$  and is smallest for the homogeneous case ( $G_0/G_i = 1$ ).

The effects of material damping on the impedances of the soil layer are shown in Fig. 3.15. Several values of damping ratio are selected, in one case both  $\beta_i$  and  $\beta_0$  are zero and in other cases  $\beta_0 = 0.05$  and  $\beta_i = 0.05, 0.1$  and  $0.2$ , respectively. It can be seen that the stiffness factor,  $S_{\psi 1}$ , reduces with material damping increasing, but the effect to damping factor,  $S_{\psi 2}$ , is small in this case.

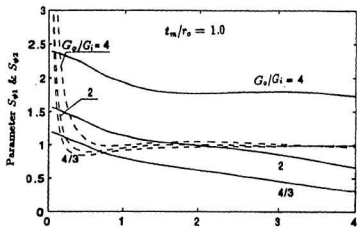


(A)

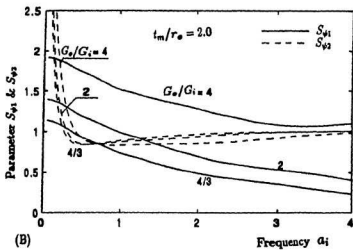


(B)

Figure 3.13: Rocking impedances for a composite layer with material damping  $\beta_i = 0.1$ ,  $\beta_o = 0.05$  and different parameters: (A) for  $t_m/r_o = 0.25$ ; (B) for  $t_m/r_o = 0.5$ .

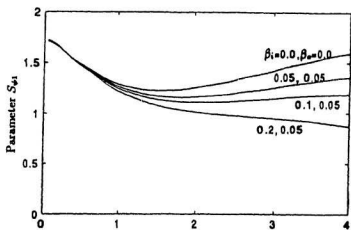


(A)

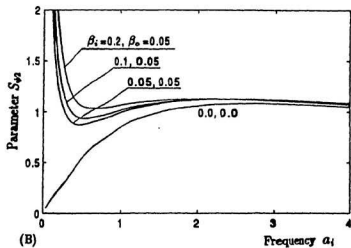


(B)

Figure 3.14: Rocking impedances for a composite layer with material damping  $\beta_1 = 0.1$ ,  $\beta_o = 0.05$  and different parameters: (A) for  $t_m/r_o = 1.0$ ; (B) for  $t_m/r_o = 2.0$ .



(A)



(B)

Figure 3.15: Effects of material damping on rocking impedances of soil layer, (A) stiffness factor  $S_{\psi_1}$ , and (B) damping factor  $S_{\psi_2}$ .

### 3.4.5 Horizontal Excitation

#### Within Boundary Zone

With the assumption that the vertical displacement are negligibly small in comparison to the radial and tangential displacements, that is  $w = 0$ , the equilibrium equation under horizontal excitation can be written as

$$\begin{cases} \frac{\partial \sigma_r}{\partial r} + \frac{1}{r} \frac{\partial \tau_{r\theta}}{\partial \theta} + \frac{\sigma_r - \sigma_\theta}{r} = \rho \frac{\partial^2 u}{\partial t^2} \\ \frac{\partial \tau_{\theta r}}{\partial r} + \frac{1}{r} \frac{\partial \sigma_\theta}{\partial \theta} + \frac{2\tau_{\theta r}}{r} = \rho \frac{\partial^2 v}{\partial t^2} \end{cases} \quad (3.98)$$

A general solution involving variations of soil properties in the boundary zone proves to be extremely difficult because of cross coupling between the radial and tangential displacements, and higher order differential equations that result from above equations. Hence, in this study it is assumed that  $\lambda_i^*$  and  $G_i^*$  are constants in the boundary zone under horizontal excitation.

For uncoupling of eq.s (3.98), the potential functions,  $\phi$  and  $\psi$ , are introduced, such that

$$\begin{cases} u = \frac{\partial \phi}{\partial r} + \frac{1}{r} \frac{\partial \psi}{\partial \theta} \\ v = \frac{1}{r} \frac{\partial \phi}{\partial \theta} - \frac{\partial \psi}{\partial r} \end{cases} \quad (3.99)$$

Assuming

$$\begin{cases} \phi = \Phi \cos \theta e^{i\omega t} \\ \psi = -\Psi \sin \theta e^{i\omega t} \end{cases} \quad (3.100)$$

the governing equation may be derived as

$$\begin{cases} \frac{d^2\Phi}{d\xi^2} + \frac{1}{\xi} \frac{d\Phi}{d\xi} - \left(\lambda_{11}^2 + \frac{1}{\xi^2}\right)\Phi = 0 \\ \frac{d^2\Psi}{d\xi^2} + \frac{1}{\xi} \frac{d\Psi}{d\xi} - \left(\lambda_1^2 + \frac{1}{\xi^2}\right)\Psi = 0 \end{cases} \quad (3.101)$$

in which

$$\begin{cases} \lambda_1 = \frac{ia_i}{\sqrt{1+i^2\beta_i}} \\ \lambda_{11} = \frac{\lambda_i}{\sqrt{2(1-\nu)/(1-2\nu)}} \end{cases} \quad (3.102)$$

Eq.(3.101) is modified Bessel equations, and the solutions are

$$\begin{cases} \Phi = C_1 I_1(\lambda_{11}\xi) + C_2 K_1(\lambda_{11}\xi) \\ \Psi = C_3 I_1(\lambda_1\xi) + C_4 K_1(\lambda_1\xi) \end{cases} \quad (3.103)$$

where  $C_1, C_2, C_3$  and  $C_4$  are complex-valued constants which can be determined by considering the boundary conditions. The boundary conditions are:

$$\begin{cases} u(\xi) = 1 & \text{at } \xi = 1 \text{ and } \theta = 0 \\ v(\xi) = -1 & \text{at } \xi = 1 \text{ and } \theta = \frac{\pi}{2} \\ u(\xi) = 0 & \text{at } \xi = R/r_o \\ v(\xi) = 0 & \text{at } \xi = R/r_o \end{cases} \quad (3.104)$$

From eq.(3.99), yields

$$\begin{aligned} u(\xi) = & C_1[\lambda_{11} I_0(\lambda_{11}\xi) - \frac{1}{\xi} I_1(\lambda_{11}\xi)] - C_2[\lambda_{11} K_0(\lambda_{11}\xi) + \frac{1}{\xi} K_1(\lambda_{11}\xi)] \\ & - C_3 \frac{1}{\xi} I_1(\lambda_1\xi) - C_4 \frac{1}{\xi} K_1(\lambda_1\xi) \end{aligned} \quad (3.105)$$

and

$$\begin{aligned} v(\xi) = & -C_1 \frac{1}{\xi} I_1(\lambda_{11}\xi) - C_2 \frac{1}{\xi} K_1(\lambda_{11}\xi) + C_3[\lambda_1 I_0(\lambda_1\xi) - \frac{1}{\xi} I_1(\lambda_1\xi)] \\ & - C_4[\lambda_1 K_0(\lambda_1\xi) + \frac{1}{\xi} K_1(\lambda_1\xi)] \end{aligned} \quad (3.106)$$

denoting

$$\begin{aligned}
 a_{11} &= \lambda_{i1} I_0(\lambda_{i1}) - I_1(\lambda_{i1}) \\
 a_{12} &= -[\lambda_{i1} K_0(\lambda_{i1}) + K_1(\lambda_{i1})] \\
 a_{13} &= -I_1(\lambda_i) \\
 a_{14} &= -K_1(\lambda_i) \\
 a_{21} &= -I_1(\lambda_{i1}) \\
 a_{22} &= -K_1(\lambda_{i1}) \\
 a_{23} &= \lambda_i I_0(\lambda_i) - I_1(\lambda_i) \\
 a_{24} &= -[\lambda_i K_0(\lambda_i) + K_1(\lambda_i)] \\
 a_{31} &= -\lambda_{i1} I_0(\lambda_{i1} \frac{R}{r_o}) + \frac{r_o}{R} I_1(\lambda_{i1} \frac{R}{r_o}) \\
 a_{32} &= \lambda_{i1} K_0(\lambda_{i1} \frac{R}{r_o}) + \frac{r_o}{R} K_1(\lambda_{i1} \frac{R}{r_o}) \\
 a_{33} &= \frac{r_o}{R} I_1(\lambda_i \frac{R}{r_o}) \\
 a_{34} &= \frac{r_o}{R} K_1(\lambda_i \frac{R}{r_o}) \\
 a_{41} &= \frac{r_o}{R} I_1(\lambda_{i1} \frac{R}{r_o}) \\
 a_{42} &= \frac{r_o}{R} K_1(\lambda_{i1} \frac{R}{r_o}) \\
 a_{43} &= -\lambda_i I_0(\lambda_i \frac{R}{r_o}) + \frac{r_o}{R} I_1(\lambda_i \frac{R}{r_o}) \\
 a_{44} &= \lambda_i K_0(\lambda_i \frac{R}{r_o}) + \frac{r_o}{R} K_1(\lambda_i \frac{R}{r_o})
 \end{aligned} \tag{3.107}$$

Satisfaction of these boundary conditions shown in eq.(3.104) leads to the following systems of algebraic equations for the determination of the remaining constants:

$$\begin{bmatrix} a_{11} & a_{12} & a_{13} & a_{14} \\ a_{21} & a_{22} & a_{23} & a_{24} \\ a_{31} & a_{32} & a_{33} & a_{34} \\ a_{41} & a_{42} & a_{43} & a_{44} \end{bmatrix} \begin{Bmatrix} C_1 \\ C_2 \\ C_3 \\ C_4 \end{Bmatrix} = \begin{Bmatrix} 1 \\ -1 \\ 0 \\ 0 \end{Bmatrix} \quad (3.108)$$

The following expressions for the stress amplitudes can be obtained from equations (3.8) and (3.9) by making use of eq.s (3.99) and (3.100):

$$\begin{cases} \sigma_r = \left[ \frac{\lambda_1^*}{r_o} \left( \frac{du}{d\xi} + \frac{u+v}{\xi} \right) + \frac{2G_1^*}{r_o} \frac{dv}{d\xi} \right] \cos \theta \\ \tau_{r\theta} = \frac{G_1^*}{r_o} \left( \frac{dv}{d\xi} - \frac{u+v}{\xi} \right) \sin \theta \end{cases} \quad (3.109)$$

in which the expressions for the derivatives of displacement can be derived from eq.s (3.105) and (3.106):

$$\begin{aligned} \frac{du}{d\xi} = & C_1 \left[ (\lambda_{11}^2 + \frac{2}{\xi^2}) I_1(\lambda_{11}\xi) - \frac{\lambda_{11}}{\xi} I_0(\lambda_{11}\xi) \right] + C_2 \left[ (\lambda_1^2 + \frac{2}{\xi^2}) K_1(\lambda_1\xi) + \frac{\lambda_1}{\xi} K_0(\lambda_1\xi) \right] \\ & + C_3 \left[ \frac{2}{\xi^2} I_1(\lambda_1\xi) - \frac{\lambda_1}{\xi} I_0(\lambda_1\xi) \right] + C_4 \left[ \frac{2}{\xi^2} K_1(\lambda_1\xi) + \frac{\lambda_1}{\xi} K_0(\lambda_1\xi) \right] \end{aligned} \quad (3.110)$$

$$\begin{aligned} \frac{dv}{d\xi} = & C_1 \left[ \frac{2}{\xi^2} I_1(\lambda_{11}\xi) - \frac{\lambda_{11}}{\xi} I_0(\lambda_{11}\xi) \right] + C_2 \left[ \frac{2}{\xi^2} K_1(\lambda_{11}\xi) + \frac{\lambda_{11}}{\xi} K_0(\lambda_{11}\xi) \right] + C_3 \left[ (\lambda_1^2 + \frac{2}{\xi^2}) I_1(\lambda_1\xi) \right. \\ & \left. - \frac{\lambda_1}{\xi} I_0(\lambda_1\xi) \right] + C_4 \left[ (\lambda_1^2 + \frac{2}{\xi^2}) K_1(\lambda_1\xi) + \frac{\lambda_1}{\xi} K_0(\lambda_1\xi) \right] \end{aligned} \quad (3.111)$$

The impedance function of the inner medium is defined as

$$\begin{aligned} K_{ul} &= - \int_0^{2\pi} (\sigma_r \cos \theta - \tau_{r\theta} \sin \theta) r_o d\theta \\ &= \pi G_1^* \left[ \frac{dv}{d\xi} - \eta^2 \frac{du}{d\xi} - (1 + \eta_1^2) \frac{u+v}{\xi} \right] \Big|_{\xi=1} \end{aligned} \quad (3.112)$$

where  $\eta$  and  $\eta_1$  are the same as those defined in eq.(3.57).

### Outer Medium

For the outer medium eq.s (3.98) to (3.101) again hold with the changes of parameters from inner zone to outer zone. Then, the governing equations shown in eq. (3.101) should be rewritten as

$$\begin{cases} \frac{d^2\Phi}{d\xi^2} + \frac{1}{\xi} \frac{d\Phi}{d\xi} - [\lambda_{o1}^2 + \frac{1}{\xi^2}] \Phi = 0 \\ \frac{d^2\Psi}{d\xi^2} + \frac{1}{\xi} \frac{d\Psi}{d\xi} - (\lambda_o^2 + \frac{1}{\xi^2}) \Psi = 0 \end{cases} \quad (3.113)$$

in which

$$\begin{cases} \lambda_o = \frac{ia_o}{\sqrt{1+i2\beta_o}} \\ \lambda_{o1} = \frac{\lambda_o}{\sqrt{2(1-\nu)/(1-2\nu)}} \end{cases} \quad (3.114)$$

The solutions for eq. (3.113) are

$$\begin{cases} \Phi = C_1 I_1(\lambda_{o1}\xi) + C_2 K_1(\lambda_{o1}\xi) \\ \Psi = C_3 I_1(\lambda_o\xi) + C_4 K_1(\lambda_o\xi) \end{cases} \quad (3.115)$$

where  $C_1, C_2, C_3$  and  $C_4$  are complex-valued constants which can be determined by considering the boundary conditions. The boundary conditions are:

$$\begin{cases} u(\xi) = 1 & \text{at } \xi = R/r_o \text{ and } \theta = 0 \\ v(\xi) = -1 & \text{at } \xi = R/r_o \text{ and } \theta = \frac{\pi}{2} \\ u(\xi) = 0 & \text{at } \xi = \infty \\ v(\xi) = 0 & \text{at } \xi = \infty \end{cases} \quad (3.116)$$

Since the displacements and stresses decay with horizontal distance  $\xi$ , the constants  $C_1$  and  $C_3$  must be zero. The solutions shown in eq. (3.115) can now be rewritten

as

$$\begin{cases} \Phi = C_2 K_1(\lambda_{o1} \xi) \\ \Psi = C_4 K_1(\lambda_o \xi) \end{cases} \quad (3.117)$$

From eq.s (3.99) and (3.117) the displacement amplitudes can be derived as

$$\begin{cases} u(\xi) = -C_2 [\lambda_{o1} K_o(\lambda_{o1} \xi) + \frac{1}{\xi} K_1(\lambda_{o1} \xi)] - C_4 \frac{1}{\xi} K_1(\lambda_o \xi) \\ v(\xi) = -C_2 \frac{1}{\xi} K_1(\lambda_{o1} \xi) - C_4 [\lambda_o K_o(\lambda_o \xi) + \frac{1}{\xi} K_1(\lambda_o \xi)] \end{cases} \quad (3.118)$$

The constants  $C_2$  and  $C_4$  can now be solved from the boundary conditions shown in eq. (3.116).

Similar to eq. (3.109), the expressions of the stress amplitudes for the outer don can be written as

$$\begin{cases} \sigma_r = \left[ \frac{\lambda_o^*}{r_o} \left( \frac{du}{d\xi} + \frac{u+v}{\xi} \right) + \frac{2G_o^*}{r_o} \frac{dv}{d\xi} \right] \cos \theta \\ \tau_{r,\theta} = \frac{G_o^*}{r_o} \left( \frac{dv}{d\xi} - \frac{u+v}{\xi} \right) \sin \theta \end{cases} \quad (3.119)$$

in which the expressions for the derivatives of displacement can be derived from eq.s (3.118):

$$\begin{cases} \frac{du}{d\xi} = C_2 \left[ (\lambda_{o1}^2 + \frac{2}{\xi^2}) K_1(\lambda_{o1} \xi) + \frac{\lambda_{o1}}{\xi} K_o(\lambda_{o1} \xi) \right] + C_4 \left[ \frac{2}{\xi^2} K_1(\lambda_o \xi) + \frac{\lambda_o}{\xi} K_o(\lambda_o \xi) \right] \\ \frac{dv}{d\xi} = C_2 \left[ \frac{2}{\xi^2} K_1(\lambda_{o1} \xi) + \frac{\lambda_{o1}}{\xi} K_o(\lambda_{o1} \xi) \right] + C_4 \left[ (\lambda_o^2 + \frac{2}{\xi^2}) K_1(\lambda_o \xi) + \frac{\lambda_o}{\xi} K_o(\lambda_o \xi) \right] \end{cases} \quad (3.120)$$

The impedance function of the outer medium is defined as

$$\begin{aligned} K_{u2} &= - \int_0^{2\pi} (\sigma_r \cos \theta - \tau_{r,\theta} \sin \theta) R d\theta \\ &= \pi G_o^* \left( \frac{G_o^*}{G_1} \right) \left( \frac{dv}{d\xi} - \eta^2 \frac{du}{d\xi} - (1 + \eta_1^2) \frac{u+v}{\xi} \right) \Big|_{\xi=R/r_o} \end{aligned} \quad (3.121)$$

where  $\eta$  and  $\eta_1$  are the same as those defined in eq.(3.57).

Using the separate impedances of the inner and outer media given by eq.s (3.112) and (3.121), the joint impedance of the combined medium in the horizontal vibration is

$$k_u = \frac{K_{u1}K_{u2}}{K_{u1} + K_{u2}} \quad (3.122)$$

It is desirable to express  $k_u$  in the following form

$$k_u = 2\pi G_i(S_{u1} + i a_i S_{u2}) \quad (3.123)$$

where  $S_{u1}$  and  $S_{u2}$  are dimensionless factors that depend on  $a_o, t_m/r_o, G_i/G_o, \beta_i$  and  $\beta_o$ . The factors  $S_{u1}$  and  $S_{u2}$  are referred to as the horizontal stiffness and damping of soil, respectively.

The stiffness and damping factors,  $S_{u1}$  and  $S_{u2}$ , obtained from the present analysis are compared with those obtained for the Novak's idealizations, as shown in Fig. 3.16. These solutions are for a soil layer with  $t_m/r_o = 0.5, G_i/G_o = 0.25, \beta_i = 0.1, \beta_o = 0.05$ , and  $\nu = 0.25$ . The mass density for the inner zone is taken to be equal to that for the outer region in the present solution, while for the Novak's solution the mass density for the inner zone is assumed to be zero. It can be observed that the difference between the two solutions appears with increasing of frequency  $a_i$ , although the difference is small. It can also be noticed that undulations caused by wave reflections from the interface between the media can not be observed in the lower frequency region ( maximum frequency  $a_i = 2.0$  ). For comparison, the results for a homogeneous layer are also included in Fig. 3.16.

To illustrate the influence of parameters involved, the stiffness and damping factors for a horizontally excited layer are plotted in Fig. 3.17 and Fig. 3.18 as a function of  $a_i$ , maximum frequency  $a_i = 2.0$ , for several different combinations of  $t_m/r_o$  and  $G_o/G_i$ , with material damping,  $\beta_i = 0.1, \beta_o = 0.05$  and Poisson's ratio  $\nu = 0.25$ . It should be noticed that the undulations caused by wave reflection are not obvious in the lower frequency region, except for the case with larger thickness ( $t_m/r_o = 1.0$ ). The influence of the material properties in the boundary zone is sensitive to the stiffness and damping of the soil layer. The stiffness factor,  $S_{u1}$ , increases with the level of  $G_o/G_i$  and is smallest for the homogeneous case ( $G_o/G_i = 1$ ). The damping factor,  $S_{u2}$ , at lower frequency levels becomes larger as the magnitude of  $G_o/G_i$  increases; however, at higher frequencies this tendency diminished. This trend in damping response can be explained by reference to the fact that the radiation damping becomes more dominant (relative to the material damping) at higher frequency levels.

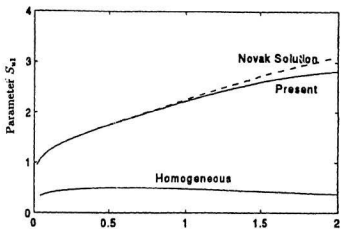
The effects of material damping on the impedances of the soil layer are shown in Fig. 3.19. These solutions are for a soil layer with  $t_m/r_o = 0.5, G_i/G_o = 0.5$ , and  $\nu = 0.25$ . Several values of damping ratio are selected, in one case both  $\beta_i$  and  $\beta_o$  are zero and in other cases  $\beta_o = 0.05$  and  $\beta_i = 0.05, 0.1$  and  $0.2$ , respectively. It can be seen that the stiffness factor,  $S_{u1}$ , reduces with material damping increasing, but the damping factor,  $S_{u2}$ , increases with material damping increasing.

The effects of Poisson's ratio on the horizontal impedances of the soil layer are

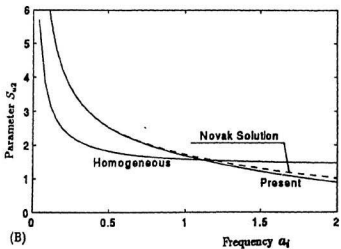
shown in Fig. 3.20. These solutions are for a soil layer with  $t_m/r_o = 0.5$ ,  $G_i/G_o = 0.5$ ,  $\beta_i = 0.1$ , and  $\beta_o = 0.05$ . Several values of Poisson's ratio are selected,  $\nu = 0.0, 0.15, 0.3$  and  $0.45$ , respectively. It can be seen that the stiffness factor,  $S_{u1}$ , increases with Poisson's ratio increasing, and the damping factor,  $S_{u2}$ , also increases with  $\nu$  increasing.

Although values of layer impedances for  $a_i > 2$  are needed infrequently in practice, it is nevertheless desirable to examine their behavior for this frequency range. In Fig. 3.21 are given representative plots of  $S_{u1}$  and  $S_{u2}$  for a soil layer with values of  $a_i$  up to 4. These solutions are for the soil layer with  $t_m/r_o = 1.0$ ,  $\nu = 0.25$ ,  $\beta_i = 0.1$ ,  $\beta_o = 0.05$ ; in one case  $G_i/G_o = 0.25$  and in another case  $G_i/G_o = 1$  (homogeneous). Note that, for the higher values of  $a_i$ , the curves for inhomogeneous layer are undulatory. It can be explained that  $\lambda_i^*$  and  $G_i^*$  are assumed to be constant in the inner zone, resulting in undulations. As a consequence of the discontinuity of material properties at the interface of the two zones, wave reflections occur at the interface.

A general solution involving variations of  $\lambda_i^*$  and  $G_i^*$  proves to be extremely difficult because of cross coupling between the radial and tangential displacements, and higher order differential equations resulted. Hence, constant  $\lambda_i^*$  and  $G_i^*$  are assumed for the case of horizontal excitation in this study. Even under this assumption it is theoretically more complicated to derive than the other cases dealt herein, such as the cases of vertical, torsional, radial and rocking vibration.



(A)



(B)

Figure 3.16: Comparison of horizontal impedance functions by different solutions,  $t_m/r_o = 0.5$ ,  $G_i/G_o = 0.25$ ,  $\beta_i = 0.1$ ,  $\beta_o = 0.05$ ,  $\nu = 0.25$ ; (A) stiffness factor  $S_{u1}$ , and (B) damping factor  $S_{u2}$ .

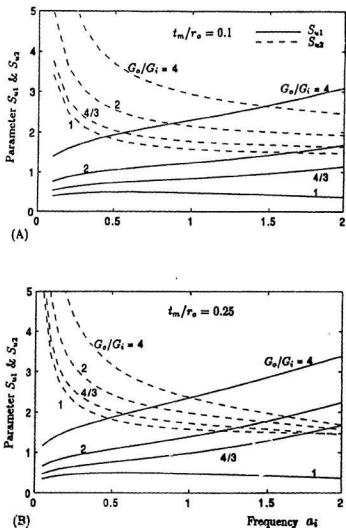


Figure 3.17: Horizontal impedances for a composite layer with material damping  $\beta_i = 0.1$ ,  $\beta_o = 0.05$ ,  $\nu = 0.25$  and different parameters: (A) for  $t_m/r_o = 0.1$ ; (B) for  $t_m/r_o = 0.25$ .

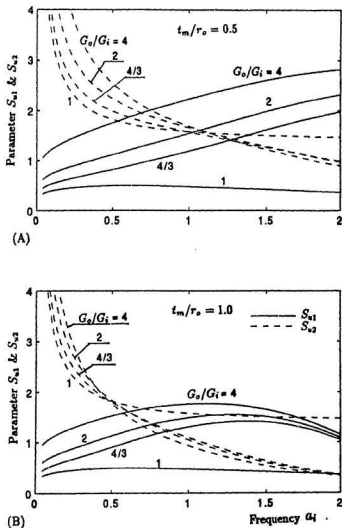
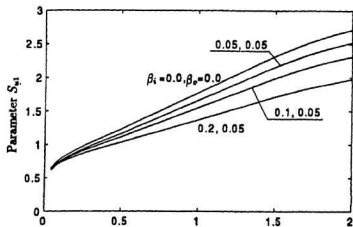
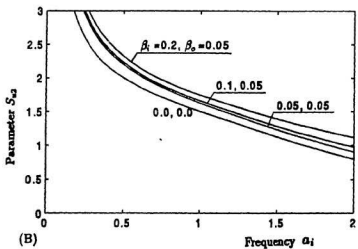


Figure 3.18: Horizontal impedances for a composite layer with material damping  $\beta_i = 0.1$ ,  $\beta_o = 0.05$ ,  $\nu = 0.25$  and different parameters: (A) for  $t_m/r_o = 0.5$ ; (B) for  $t_m/r_o = 1.0$ .

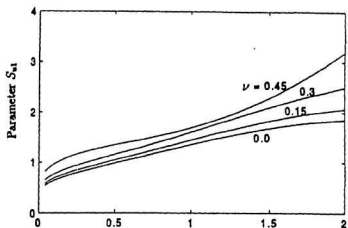


(A)

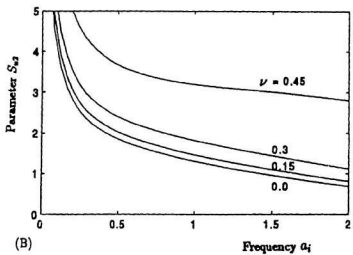


(B)

Figure 3.19: Effects of material damping on horizontal impedances of soil layer, (A) stiffness factor  $S_{u1}$ , and (B) damping factor  $S_{u2}$ .

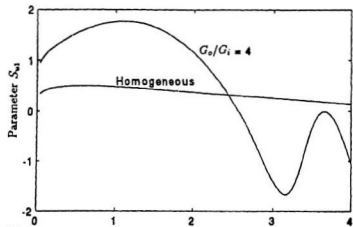


(A)

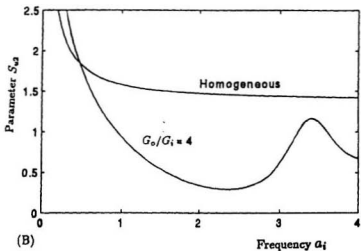


(B)

Figure 3.20: Effects of Poisson's ratio on horizontal impedances of soil layer, (A) stiffness factor  $S_{u1}$ , and (B) damping factor  $S_{u2}$ .



(A)



(B)

Figure 3.21: High-frequency behavior of horizontal impedances of a composite layer with  $t_m/r_o = 1.0$ ,  $\nu = 0.25$ ,  $\beta_i = 0.1$ ,  $\beta_o = 0.05$ ; (A) stiffness factor  $S_{u1}$ , and (B) damping factor  $S_{u2}$ .

## Chapter 4

# Stiffness and Damping of Single Piles in Layered Media

### 4.1 Introduction

The main assumptions are: The soil is composed of horizontal layers that are homogeneous, isotropic, and linearly viscoelastic with material damping of the frequency independent hysteretic type. The soil properties are constant within each layer but may be different in individual layers. To account approximately for the effects of slippage and nonlinearity, the boundary zone around the pile is assumed as described in last chapter.

The pile is vertical, linearly elastic, and of circular cross section that may vary stepwise at the interface of the layers; it is bonded to the soil. If the pile head lies above the grade or the pile is assumed to be separated from the soil, the boundary zone are modeled as void.

The soil reactions acting on a unit length of the pile are described by complex

soil stiffnesses as shown in last chapter. associated with vertical, horizontal, rocking and torsional displacements of the pile. The complex stiffness of one single pile can be written as

$$K_j = K_{j1} + i\omega C_j \quad (4.1)$$

in which  $K_{j1}$  = real stiffness of one pile,  $C_j$  = the coefficient of the equivalent viscous damping,  $i = \sqrt{-1}$ ,  $\omega$  = circular frequency and  $j$  = direction of vibration. The stiffness constant,  $K_{j1}$ , and damping constant,  $C_j$ , can be determined experimentally or theoretically. The latter approach is preferred because experiments, though very useful, are difficult to generalize. In the theoretical approaches, dynamic stiffness is generated by calculating the forces needed to produce vibration of the pile head having a sole, unit amplitude in the direction considered. These correspond to vertical vibration, horizontal vibration, and rotation in vertical plane and torsion.

## 4.2 Element Stiffness Matrices

A pile is divided into beam elements along with the soil layers and the soil below the pile is an elastic half-space, as shown in Fig. 4.1. The properties of each element are fully described by its stiffness matrix which is complex due to energy dissipation in the soil and includes the properties of both the pile and the soil. Because the pile is axisymmetrical all the stiffness are not coupled and can be described by three independent matrices.

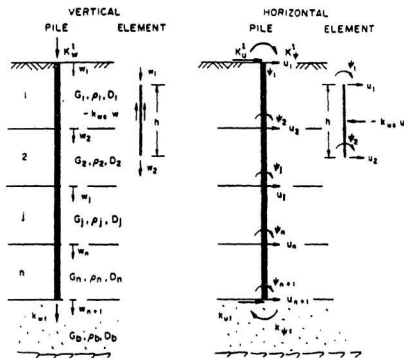


Figure 4.1: Pile embedded in layered media and node numbering

### Vertical Vibration

With the vertical impedances of the composite layer described by eq.(3.33), the differential equation of motion in the vertical direction is

$$m \frac{\partial^2 w(z,t)}{\partial t^2} + C \frac{\partial w(z,t)}{\partial t} - E_p A \frac{\partial^2 w(z,t)}{\partial z^2} + k_v w(z,t) = 0 \quad (4.2)$$

where  $m$  = mass of the pile per unit length;  $C$  = coefficient of internal damping of the pile;  $E_p$  and  $A$  = Young's modulus and the cross sectional area of the pile;  $k_v$  = vertical complex stiffness ( impedance ) of soil;  $w(z,t)$  = vertical amplitude of the

pile;  $z$  = depth of the pile; and  $t$  = time.

For harmonic motion  $w(z, t) = w(z)e^{i\omega t}$ , the complex amplitude  $w(z)$  can be determined as

$$w(z) = B_1 \cos \bar{n} \frac{z}{h} + B_2 \sin \bar{n} \frac{z}{h} \quad (4.3)$$

in which  $B_1$  and  $B_2$  = integration constants;  $h$  = height of the element of the pile; and the complex frequency parameter,  $\bar{n}$ , is

$$\bar{n} = h \sqrt{\frac{1}{E_p A} [m\omega^2 - k_v - iC\omega]} \quad (4.4)$$

The dynamic stiffnesses are defined by the boundaries  $w(0) = 1, w(h) = 0$  and  $w(0) = 0, w(h) = 1$ ; from these conditions  $B_1$  and  $B_2$  can be determined.

The amplitude of the axial force,  $N$ , is

$$N(z) = E_p A \frac{dw(z)}{dz} \quad (4.5)$$

The stiffnesses being external end forces are  $k_1 = -N(0)$  and  $k_2 = N(h)$ .

After substituting for  $w(z)$ , the element stiffness matrix in the vertical direction becomes

$$[k_v] = \frac{E_p A}{h} \bar{n} \begin{bmatrix} \cot \bar{n} & -\csc \bar{n} \\ -\csc \bar{n} & \cot \bar{n} \end{bmatrix} \quad (4.6)$$

The end forces  $N_1, N_2$  corresponding to end displacements  $w_1, w_2$  then are

$$\begin{Bmatrix} N_1 \\ N_2 \end{Bmatrix} = [k_v] \begin{Bmatrix} w_1 \\ w_2 \end{Bmatrix} \quad (4.7)$$

### Horizontal and Rotational Vibration

Horizontal vibration of a pile can be associated with both horizontal translation and rotation of the head. This horizontal vibration meet the horizontal soil reaction given by eq. (3.123) and the rotation reaction, eq. (3.97). For slender piles, the latter can be ignored and the equation of the horizontal vibration,  $u(z, t)$ , is

$$m \frac{\partial^2 u(z, t)}{\partial t^2} + C \frac{\partial u(z, t)}{\partial t} + E_p I \frac{\partial^4 u(z, t)}{\partial z^4} + N_{st} \frac{\partial^2 u(z, t)}{\partial z^2} + k_u u(z, t) = 0 \quad (4.8)$$

in which  $N_{st}$  = static axial force (load of the pile); and  $E_p I$  = bending stiffness of the pile. (The value  $N_{st}$  is positive if it acts downward.) This inclusion of  $N_{st}$  is accurate with end bearing piles; with friction piles,  $N_{st}$  varies with depth but is less important and can be neglected.

With harmonic motion  $u(z, t) = u(z)e^{i\omega t}$ , the complete solution for the amplitude,  $u(z)$ , is

$$u(z) = B_1 \cosh \bar{b} \frac{z}{h} + B_2 \sinh \bar{b} \frac{z}{h} + B_3 \cos \bar{a} \frac{z}{h} + B_4 \sin \bar{a} \frac{z}{h} \quad (4.9)$$

in which the complex frequency parameter  $\bar{a}, \bar{b}$  are

$$\bar{a}, \bar{b} = \frac{\pi}{\sqrt{2}} \left\{ \mp \frac{N_{st}}{N_E} + \sqrt{\left(\frac{N_{st}}{N_E}\right)^2 + \frac{i E_p I}{N_E^2} [m\omega^2 - k_u - iC\omega]} \right\}^{1/2} \quad (4.10)$$

in which  $N_E = \pi^2 E_p I / h^2$ .

The moment,  $M$ , and horizontal transverse force,  $H$ , are

$$\begin{cases} M(z) = -E_p I \frac{d^2 u(z)}{dz^2} \\ H(z) = -E_p I \frac{d^3 u(z)}{dz^3} - N_{st} \frac{du(z)}{dz} \end{cases} \quad (4.11)$$

The integration constants for the calculation of stiffnesses are given by end translations  $u_1 = 1, u_2 = 1$  and end rotation  $\psi_1 = 1, \psi_2 = 1$  applied one at a time. The subscripts 1 and 2 refer to the upper and lower ends of the element, respectively. Then, the element stiffness matrix for the horizontal translation and rotation is

$$[k_u] = E_p I \begin{bmatrix} \frac{1}{h^3} F_6 & \frac{1}{h^2} F_4 & \frac{1}{h^3} F_5 & -\frac{1}{h^2} F_3 \\ \frac{1}{h^2} F_4 & \frac{1}{h} F_2 & \frac{1}{h^2} F_3 & \frac{1}{h} F_1 \\ \frac{1}{h^3} F_5 & \frac{1}{h^2} F_3 & \frac{1}{h^3} F_6 & -\frac{1}{h^2} F_4 \\ -\frac{1}{h^2} F_3 & \frac{1}{h} F_1 & -\frac{1}{h^2} F_4 & \frac{1}{h} F_2 \end{bmatrix} \quad (4.12)$$

in which dimensionless functions  $F_i = F_i(\bar{a}, \bar{b})$  are

$$\begin{aligned} F_1(\bar{a}, \bar{b}) &= \frac{-1}{\phi} (\bar{a}^2 + \bar{b}^2) (\bar{a} \sinh \bar{b} - \bar{b} \sin \bar{a}) \\ F_2(\bar{a}, \bar{b}) &= \frac{-1}{\phi} (\bar{a}^2 + \bar{b}^2) (\bar{b} \cosh \bar{b} \sin \bar{a} - \bar{a} \sinh \bar{b} \cos \bar{a}) \\ F_3(\bar{a}, \bar{b}) &= \frac{-1}{\phi} \bar{a} \bar{b} (\bar{a}^2 + \bar{b}^2) (\cosh \bar{b} - \cos \bar{a}) \\ F_4(\bar{a}, \bar{b}) &= \frac{1}{\phi} \bar{a} \bar{b} [(\bar{b}^2 - \bar{a}^2) (\cosh \bar{b} \cos \bar{a} - 1) + 2\bar{a} \bar{b} \sinh \bar{b} \sin \bar{a}] \\ F_5(\bar{a}, \bar{b}) &= \frac{1}{\phi} \bar{a} \bar{b} (\bar{a}^2 + \bar{b}^2) (\bar{b} \sinh \bar{b} + \bar{a} \sin \bar{a}) \\ F_6(\bar{a}, \bar{b}) &= \frac{-1}{\phi} \bar{a} \bar{b} (\bar{a}^2 + \bar{b}^2) (\bar{a} \cosh \bar{b} \sin \bar{a} + \bar{b} \sinh \bar{b} \cos \bar{a}) \end{aligned} \quad (4.13)$$

where

$$\phi = 2\bar{a}\bar{b}(\cosh \bar{b} \cos \bar{a} - 1) + (\bar{a}^2 - \bar{b}^2) \sinh \bar{b} \sin \bar{a} \quad (4.14)$$

The soil resistance enters the element properties only through frequency parameters  $\bar{a}, \bar{b}$ .

With the stiffness matrix given by eq. (12), the element end forces and end moments due to displacements  $u_{1,2}$  and rotation  $\psi_{1,2}$  are

$$\begin{Bmatrix} H_1 \\ M_1 \\ H_2 \\ M_2 \end{Bmatrix} = [k_u] \begin{Bmatrix} u_1 \\ \psi_1 \\ u_2 \\ \psi_2 \end{Bmatrix} \quad (4.15)$$

### Tip Reactions

The reactions of soil acting on the tip can be described approximately by the viscoelastic half-space solutions. They can be written in the following form:

Vertical stiffness:

$$k_{vt} = G_b r_n [C_{v1}(a_o, \nu, D) + iC_{v2}(a_o, \nu, D)] \quad (4.16)$$

Horizontal stiffness:

$$k_{ht} = G_b r_n [C_{h1}(a_o, \nu, D) + iC_{h2}(a_o, \nu, D)] \quad (4.17)$$

Rocking Stiffness:

$$k_{\omega t} = G_b r_n^3 [C_{\omega 1}(a_o, \nu, D) + iC_{\omega 2}(a_o, \nu, D)] \quad (4.18)$$

in which  $r_n$  = pile radius at the tip;  $G_b$  = the shear modulus of the soil below the tip;  $a_o = r_n \omega / V_s$  where  $V_s$  = shear wave velocity of soil below the tip. Dimensionless parameters  $C$  can be taken from available solutions by Veletsos and Verbic (1973), Luco (1974), and others. Details of the dimensionless parameters  $C$  are given in Appendix A. The cross stiffness is less significant and can be neglected.

With eq.s 16-18 the stiffness matrix of the soil (element) underlying the pile tip is

$$[k_t] = \begin{bmatrix} k_{vt} & 0 & 0 \\ 0 & k_{ht} & 0 \\ 0 & 0 & k_{\omega t} \end{bmatrix} \quad (1.19)$$

### 4.3 Complex Stiffnesses of Pile

The complex stiffnesses (impedance functions) of the whole embedded pile are defined as external forces that have to act at the head of the pile in order to produce just one unit vibration amplitude of the head at a time. These stiffnesses of the whole pile can be established by means of the overall (structure) stiffness matrix  $[K]$  that relates forces and displacements at all joints of the pile. The elements of the structure matrix,  $K_{ij}$ , are obtained as a sum of element (member) stiffness having the same subscripts. For a one-dimensional structure such as the pile the structure stiffness,  $K_{ij}$ , is just a sum of stiffnesses of two elements meeting at a joint. Therefore, the structure stiffness matrix is banded in addition to be symmetrical. The structure stiffness of the tip is a sum of the lowest element stiffness and the corresponding tip stiffness, eq.(19).

As the vertical and horizontal stiffnesses of the pile are not coupled they can be determined independently.

#### Vertical Stiffness of Pile

For the vertical direction, the structure stiffness matrix  $[K_v]$  is assembled from eq.s (5) and (19). Using this stiffness matrix, the complex vertical stiffness of one pile

at the head,  $K_v^1$ , is obtained from these equations

$$\begin{Bmatrix} K_v^1 \\ 0 \\ 0 \\ \vdots \\ 0 \end{Bmatrix} = [K_v] \begin{Bmatrix} w_1 = 1 \\ w_2 \\ w_3 \\ \vdots \\ w_{n+1} \end{Bmatrix} \quad (4.20)$$

in which the bandwidth of  $[K_v]$  is equal to 2.

The node numbering is indicated in Fig.4.1. In eq.(20),  $w_2$  to  $w_{n+1}$  are unknown and will be denoted as a vector of unknown displacement,  $\Delta$ . Matrix  $[K_v]$  can be partitioned with the submatrices denoted by capital letters. Then, eq.(20) can be rewritten as

$$\begin{Bmatrix} K_v^1 \\ 0 \end{Bmatrix} = \begin{bmatrix} A & : & C^T \\ C & : & B \end{bmatrix} \begin{Bmatrix} 1 \\ \Delta \end{Bmatrix} \quad (4.21)$$

From the lower equations, displacements

$$\Delta = -B^{-1}C \times 1 \quad (4.22)$$

Then, from the first equation

$$K_v^1 = A \times 1 + C^T \Delta = A \times 1 - C^T B^{-1} \times 1 \quad (4.23)$$

After evaluation of eq.(23) it is convenient to split the complex stiffness,  $K_v^1$ , into its real part (true stiffness) and imaginary part (damping) and introduce the constant of equivalent viscous damping,  $c_v^1$ . Thus, the complex vertical stiffness of one pile is also

$$K_v^1 = k_v^1 + i\omega c_v^1 \quad (4.24)$$

Introducing the dimensionless stiffness and damping parameters  $f_{r1}, f_{r2}$ , the real stiffness of one pile

$$k_v^1 = \text{real}K_v^1 = \frac{E_p A_1}{r_1} f_{r1} \quad (4.25)$$

and the constant of equivalent viscous damping

$$c_v^1 = \frac{1}{\omega} \text{imag}K_v^1 = \frac{E_p A_1}{V_n} f_{r2} \quad (4.26)$$

In these equations,  $A_1, r_1$  = the area and radius of the topmost element of the pile, respectively; and  $V_n$  = shear wave velocity of soil in the lowest layer.

### **Horizontal Stiffness of Pile**

The complex stiffness of the pile head in the horizontal direction is characterized by three constants. They are  $K_{u_u}^1$  associated with the horizontal translation of the head,  $u_1$ ;  $K_{\psi\psi}^1$  associated with the rotation of the head,  $\psi_1$ ; and  $K_{u\psi}^1 = K_{\psi u}^1$  due to coupling between the end forces and moments. These constants can be found from equations employing the structure stiffness matrix for the horizontal vibration [ $K_u$ ]. This stiffness matrix is assembled from the element stiffness matrices given by eq.(12) and the tip reaction matrix described by eq.(19).

With the structure stiffness matrix assembled, the complex stiffnesses of the pile

at the head are available from equations

$$\begin{bmatrix} K_{uu}^1 & \vdots & K_{u\psi}^1 \\ K_{\psi u}^1 & \vdots & K_{\psi\psi}^1 \\ 0 & \vdots & 0 \\ 0 & \vdots & 0 \\ \vdots & \vdots & \vdots \\ o & \vdots & 0 \end{bmatrix} = [K_u] \begin{bmatrix} u_1 = 1 & \vdots & u_1 = 0 \\ \psi_1 = 0 & \vdots & \psi_1 = 1 \\ u_2 & \vdots & u_2 \\ \psi_2 & \vdots & \psi_2 \\ \vdots & \vdots & \vdots \\ \psi_{n+1} & \vdots & \psi_{n+1} \end{bmatrix} \quad (4.27)$$

in which the vertical dashed lines separate the two loading conditions, required to generate the desired stiffnesses. The bandwidth of  $[K_u]$  is 4. In this approach, explicit mass and damping matrices need not be formulated as is the case with the standard finite element method. The mass and damping of both the pile and soil are contained in the stiffness matrices  $[K_u], [K_v]$ , which are, therefore, complex and frequency variable.

The matrices in eq.(27) can again be partitioned into submatrices denoted by capital letters to facilitate the solution. Then

$$\begin{bmatrix} K_{uu}^1 & \vdots & K_{u\psi}^1 \\ K_{\psi u}^1 & \vdots & K_{\psi\psi}^1 \\ 0 & \vdots & 0 \end{bmatrix} = \begin{bmatrix} A & \vdots & C^T \\ & \vdots & \\ C & \vdots & B \end{bmatrix} \begin{bmatrix} 1 & \vdots & 0 \\ 0 & \vdots & 1 \\ \Delta_1 & \vdots & \Delta_2 \end{bmatrix} \quad (4.28)$$

This time the submatrix A is  $2 \times 2$ ,  $C_T$  is  $2 \times 2n$ , and C is  $2n \times 2$ . The solution of eq.(28) for the sought for stiffness,  $K^1$ , follows the same pattern as in the case of vertical vibration, i.e., vector  $\Delta_1, \Delta_2$  are determined first from the lower equation and, then, stiffness  $K^1$  are calculated from the upper two equations.

After evaluation of the complex stiffnesses,  $K^1$ , these can be rewritten analogously to eq.(24). Thus, the horizontal stiffness

$$K_{uu}^1 = k_{uu}^1 + i\omega c_{uu}^1 \quad (4.29)$$

in which the true horizontal stiffness

$$k_{uu}^1 = \text{real}K_{uu}^1 = \frac{E_p I_1}{r_1^3} f_{u1} \quad (4.30)$$

and the constant of equivalent viscous damping

$$c_{uu}^1 = \frac{1}{\omega} \text{imag}K_{uu}^1 = \frac{E_p I_1}{r_1^3 V_n} f_{u2} \quad (4.31)$$

The rotatory stiffness

$$K_{\psi\psi}^1 = k_{\psi\psi}^1 + i\omega c_{\psi\psi}^1 \quad (4.32)$$

in which the true rotatory stiffness

$$k_{\psi\psi}^1 = \text{real}K_{\psi\psi}^1 = \frac{E_p I_1}{r_1} f_{\psi 1} \quad (4.33)$$

and damping constant

$$c_{\psi\psi}^1 = \frac{1}{\omega} \text{imag}K_{\psi\psi}^1 = \frac{E_p I_1}{V_n} f_{\psi 2} \quad (4.34)$$

The cross-stiffness

$$K_{u\psi}^1 = K_{\psi u}^1 = k_{u\psi}^1 + i\omega c_{u\psi}^1 \quad (4.35)$$

in which the true cross-stiffness

$$k_{u\psi}^1 = \text{real}K_{u\psi}^1 = \frac{E_p I_1}{r_1^2} f_{c1} \quad (4.36)$$

and the cross-damping constant

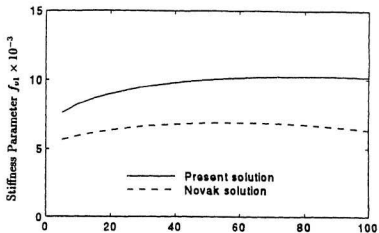
$$c_{u\psi}^1 = \frac{1}{\omega} \text{imag}K_{u\psi}^1 = \frac{E_p I_1}{r_1 V_n} f_{c2} \quad (4.37)$$

Finally,  $k_{v\psi}^1 = k_{v\psi}^1$  and  $c_{v\psi}^1 = c_{v\psi}^1$ .

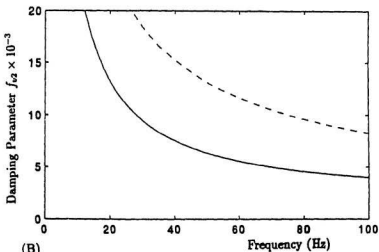
The dimensionless parameters  $f$  are suitable for parametric studies. With one homogeneous layer, they are also advantageous for presentation of pile properties.

With several different layers, a general presentation of dimensionless data is not practicable and a direct calculation of  $k^1$  and  $c^1$  using a computer appears preferable for any particular situation.

In this chapter, an example of the calculation of the dimensionless parameters  $f$  is given based on a particular case. The pile was a steel pipe with a diameter of 133 mm and a length of 3.38 m, embedded in loose sand. The distribution of shear modulus in sand is parabolic with depth, and the shear wave velocity of the sand at the pile tip is 93m/s. The detail of the soil and the pile will be described in next chapter. For this single pile, the dimensionless parameters,  $f_{v1}, f_{v2}$ , for vertical vibration and  $f_{u1}, f_{u2}$ , for horizontal vibration are computed as shown in Fig. 4.2 and Fig. 4.3, respectively. A boundary zone around the pile is assumed, with  $t_m/r_o = 0.5, G_i/G_o = 0.25, \beta_i = 0.1, \beta_o = 0.05$  and  $\nu = 0.4$ . For comparison, the parameters are also computed based on Novak's solution. From Fig. 4.2 it can be noted that the present solutions give higher stiffness parameter  $f_{v1}$  and lower  $f_{v2}$  than Novak's solution does. As described in last chapter, a non-reflective interface is included in the boundary zone for the present solution and non-mass is assumed for Novak's solution. From Fig. 4.3 it can be noted that the horizontal parameters  $f_{u1}, f_{u2}$  for present solution come close to those for Novak's solution.

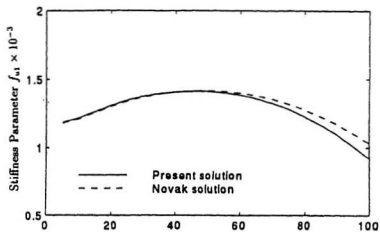


(A)

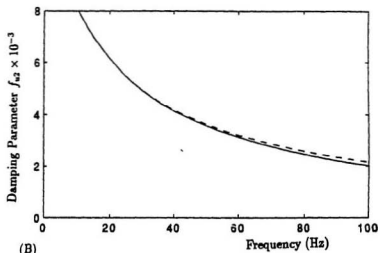


(B)

Figure 4.2: Frequency variations of vertical parameters for the steel pile in loose sand with boundary zone of  $t_m/r_o = 0.5$ ,  $G_i/G_o = 0.25$ ,  $\beta_i = 0.1$ ,  $\beta_o = 0.05$ ,  $\nu = 0.4$



(A)



(B)

Figure 4.3: Frequency variations of horizontal parameters for the steel pile in loose sand with boundary zone of  $t_m/r_o = 0.5$ ,  $G_i/G_o = 0.25$ ,  $\beta_i = 0.1$ ,  $\beta_o = 0.05$ ,  $\nu = 0.4$

## Chapter 5

# Dynamic Experiments of Single Pile

Although there have been a large number of analytical studies on the dynamic response, the published record of experimental data is rather scarce. In this study, dynamic experiments on large-scale model piles with strong horizontal and vertical vibration are described. The objective is to determine whether the basically linear theory can reproduce the behaviour of piles under strong excitation if suitable adjustments of the input parameters are made. To this end, frequency response curves and deflection curves of piles were experimentally established in the field for different intensities of excitation and contact conditions between the pile cap and the soil surface and compared with those calculated using the theories described in chapter 3 and chapter 4.

Type	Steel Pipe
Outer Diameter	133mm
Inner Diameter	121mm
Moment of Inertia	$4.84 \times 10^6 \text{mm}^4$
Area of Section	$2390 \text{mm}^2$
Length	3380mm
Young's Modulus	$2.06 \times 10^5 \text{N/mm}^2$
Poisson's Ratio	0.25
Damping Ratio	0.01
Specific Weight	$7.65 \times 7.65 \times 10^{-5} \text{N/mm}^3$

Table 5.1: Pile Properties

## 5.1 Experimental Setup

The field tests of the single pile subjected to strong harmonic excitation were conducted at the Institute of Engineering Mechanics, Harbin, China, as described by Han and Novak (1998).

The pile was a steel pipe with a diameter of 133 mm and a length of 3.38 m. The pile properties are given in Table 5.1. The pile was first placed in a pit approximately 3.6 m deep and 1.5 m in diameter. The pile cap was a concrete block 200 mm thick, 770 mm long, and 690 mm wide with a mass of 250 kg. The exciter was fixed on the cap; its mass was 120 kg. The center of gravity of the cap-exciter system was 3 mm below the cap surface.

The washed medium sand was then placed in the pit in 200 mm lifts after the pile had been positioned in the centre of the pit. The sand was compacted in place with a mechanical vibrator. Density and water content measurement were taken for

each lift. In this way good contact between the pile and soil was secured.

Soil properties that are basic in dynamic analysis are the bulk density and the shear wave velocity. Several types of static and dynamic tests were run in the laboratory and in situ on the washed medium sand and the undisturbed natural deposit around the pit. The static tests included specific gravity, density, and water content, while the dynamic tests were triaxial and seismic cross-hole tests. The samples of sand taken from the pit were tested under dynamic triaxial conditions in the laboratory. The Young's modulus variation with strain and effective stress  $\bar{\sigma}_o$  are shown in Fig. 5.1. At a dynamic strain of  $\epsilon = 10^{-3}$ , the shear modulus at the pile tip was  $G_t = 14.7MPa$ . With the mass density of sand  $\rho_s = 1700kg/m^3$ , the shear wave velocity was  $V_t = \sqrt{G_t/\rho_s} = 93m/s$ .

The density and water content of the medium sand were uniform in every lift. The properties of the backfill soil are given in Table 5.2. It is assumed that the distribution of shear modulus in the sand is parabolic with depth.

The soil profile around the pit was established from ground surface to a depth of 20 m. The soil is homogeneous sandy clay, with yellow and brown coloring. The shear wave velocity of the undisturbed natural deposit was measured using seismic cross-hole tests. The properties of the natural deposit are given in Table 5.3.

Type	Medium Sand
Bulk Density	16.7 $KN/m^3$
Dry Density	15.7 $KN/m^3$
Void Ratio	0.67
Moisture Content	0.07
Shear Wave Velocity	93 $m/s$

Table 5.2: Properties of Backfill Soil

Depth (m)	Unit Weight ( $KN/m^3$ )	Void Ratio $e$	Shear Wave Velocity ( $m/s$ )
0.0 - 2.0	18.5	0.78	185
2.0 - 5.0	16.8	0.95	179
5.0 - 12.0	19.1	0.68	256

Table 5.3: Properties of Natural Deposit

The shear wave velocity of the clay outside the pit is about twice that of the sand backfill and therefore the effect of the interface between the two soil media has to be assessed. To approximate this effect the pile dynamic deflections were evaluated for two cases: a horizontally homogeneous medium comprising only the sand and a composite medium comprising the inner zone of sand in the pit and the outer zone of clay. For low dimensionless frequencies  $a_0$ , typical of pile response, the difference in the deflections were quite small. However, it is possible that the geometric damping of the pile tested was smaller than it would have been in a horizontally homogeneous medium. This question is discussed in more detail in the last part of this chapter.

Displacement pickups, strain gauges, and compressive stress transducers were

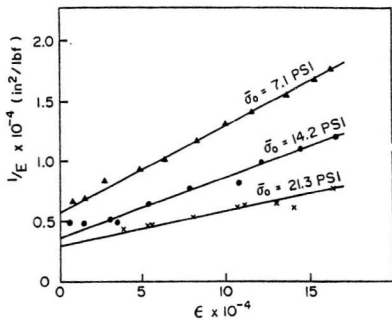


Figure 5.1: Inverse value of sand Young's modulus vs strain

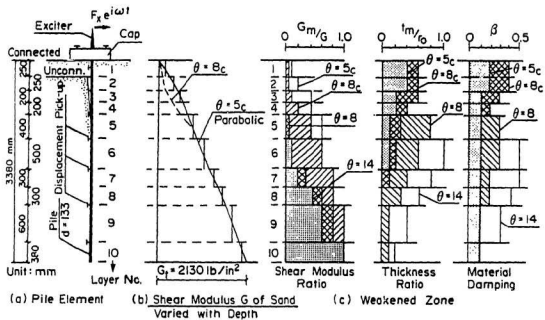


Figure 5.2: Properties of pile and soil used in analysis

Angle of Eccentric Masses, $\theta$	5	8	14
Exciting Force ( N )	$2.39f^2$	$3.79f^2$	$6.75f^2$

Table 5.4: Magnitude of Horizontal Exciting Force

fixed along the pile shaft. Displacement and acceleration pickups were mounted on the pile cap. A diagrammatic sketch of the pile and the arrangement of the instruments are shown in Fig. 5.2a.

An exciter with two counterrotating eccentric masses was used to produce the harmonic excitation. The magnitude of the exciting forces was changed by adjusting the angle of the eccentric masses,  $\theta$ . Several magnitudes of the exciting force were selected in the experiment as shown in Table 5.4 (  $f$  in the table is frequency of the exciting force in hertz).

In the experiments, two types of contact conditions between the pile cap and the soil surface were considered. In the first case, the pile cap rested directly on the soil surface ( connected situation ) and two different excitation intensities were applied,  $\theta = 5$  and 8 ( the symbols  $\theta = 5_c$  and  $8_c$  are used to identify this case later in this chapter ). In the second case, the pile cap was situated 0.20 m above the soil surface ( unconnected situation ) and the excitation intensities were  $\theta = 5, 8,$  and  $14$ .

Because of the nonlinearity of the soil-pile system, the magnitude of exciting force and the sequence of loading would affect the dynamic characteristics of the system. The steady-state response of the pile to harmonic forces was measured with increasing excitation intensities and different frequencies.

## 5.2 Pile Response under Horizontal Excitation

### Experimental Horizontal Response

Using the equipment and technique described, response to horizontal excitation was measured.

Three frequency response curves obtained with  $\theta = 5, 8$  and  $14$  for the unconnected case are shown in Fig. 5.3 and denoted by the angle  $\theta$  of the exciter. The horizontal displacements of the pile cap vary with frequency and indicate a sharp resonance peak in all cases. The maximum displacement measured on the top of the cap amounts to 2-3 mm, the maximum acceleration amounts to 0.8-0.9 g. For steady-state vibration this represents very intense motion.

In a linear system the resonance peaks occur at one frequency, no matter what the excitation intensities is. However, Fig. 5.3 shows that with increasing excitation intensity, the measured resonance peak shifts from about 7.6 to 4.7 Hz. This indicates a reduction of stiffness -proportional to  $f^2$ -to almost one-third of the highest value associated with the lowest excitation intensity. Also, the vibration amplitudes are not proportional to excitation intensity at all frequencies. These are typical features of nonlinear vibrations. However, the individual response curves observed intersected each other and are not centered around a joint backbone curve, *Omega*, as is inherent to a system whose properties are defined by one nonlinear characteristic of the restoring force and one nonlinear characteristic of nonlinear damping.

An example of such theoretical response curves is shown in Fig. 5.4. This response curve was calculated for one softening characteristic of the restoring force and nonlinear damping proportional to the  $n$ th power of vibration velocity with  $n < 1$ , that is, with damping decreasing with vibration amplitudes, using the technique described in Novak (1971). Such nonlinear characteristics of the restoring force and damping are, in general, indicated by Fig. 5.3. The amplitude increments grow with excitation intensity, and are comparable to the amplitude increments of the theoretical system (Fig. 5.4) at the frequency of the linear system,  $\omega_0$ . The presence of the response curve intersections in Fig. 5.3 and their absence in Fig. 5.4 suggest that the restoring forces of the real system do not follow one nonlinear characteristic. Rather, it seems that with increasing excitation intensity the restoring force characteristic stabilized after many cycles of load application and to a high degree linearizes within a range of peak amplitudes,  $A$ ; with a further increase in excitation intensity the restoring force again stabilizes but on a lower level of stiffness. These notions are further supported by observations made with horizontal repeated loading and by the analysis of the vertical response later herein. The features of the response observed suggest that a linear theory might reproduce the main nonlinear features of the steady-state response if the input parameters are suitably adjusted. This possibility is explored in the next paragraphs.

#### Comparison of Experimental Horizontal Response with Theoretical Predictions

With the stiffness and damping constants of the pile established in last chapter, the response of a pile-supported footing (cap) to dynamic loading can be predicted, as described by Han (1989). Under horizontal excitation the coupled horizontal trans-

lation and rotation are produced on the cap. The boundary zone around the pile included in the theoretical model gives the analysis considerable versatility.

The shear modulus distribution of the sand backfill is assumed to be parabolic along the pile shaft, which is consistent with the effect of confining pressure apparent in Fig. 5.1, and the soil below the pile tip is assumed to be homogeneous. For different excitation intensities, the soil properties in the boundary zone and at the top of the sand backfill are adjusted so that the theoretical response curves approach the measured data. It should be explained that the theoretical response curves are back-calculated results, but not the "predicted" results because there is no way to predict the parameters needed for the boundary zone model. From the comparison with the back-calculated results, engineers can understand how soil properties vary with different excitation intensities. In practice when the back-calculated parameter values are not available it is still possible to calculate upper and lower bounds on the nonlinear response. The characteristics of the pile and soil used in the calculations are given in Fig. 5.2. The material damping of the weak zone is of less important than the thickness of the weak zone and its shear modulus. The comparison of experimental results with theoretical response curves is shown in Fig. 5.3 and 5.5.

From Fig. 5.2 it can be seen that the soil properties in the weak zone and at the top of the backfill varied with the intensity of excitation and the change of the contact condition between the pile cap and the soil surface. As the excitation intensity increases, the shear modulus ratio,  $G_i/G_o$ , is reduced, whereas the thickness ratio,  $t_m/r_o$ , and the material damping are increased ( $G_i$  and  $t_m$  are the shear modulus

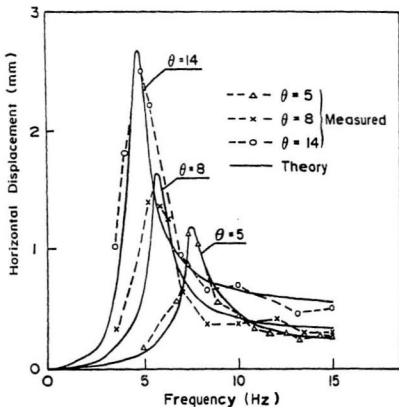


Figure 5.3: Theoretical and experimental horizontal response of pile cap for different excitation intensities (pile cap separated from soil)

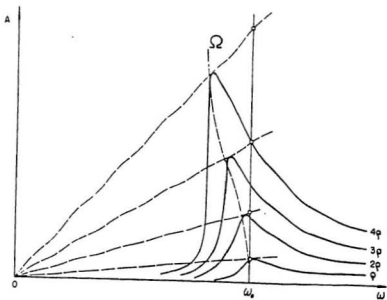


Figure 5.4: Theoretical response curves of a system with nonlinear restoring force and nonlinear damping ( $n < 1$ ) for increasing excitation intensity ( $\rho =$  excitation moment/mass =  $m_e t/m$ )

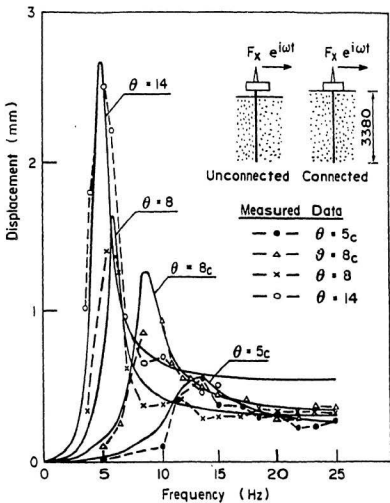


Figure 5.5: Theoretical and experimental response curves with different excitation intensity and contact between cap and soil

and thickness of the weak zone, respectively). For the connected situation ( $\theta = 5_c$  and  $8_c$ ), the soil shear modulus at the top of the backfill is reduced with the increase in excitation intensity. When the connected situation changes to the unconnected situation (from  $\theta = 8_c$  to  $\theta = 8$ ,  $G_i/G_o$  decreases,  $t_m/r_o$  increases, and material damping increases.//

Using the ratio  $G_i/G_o = 0$  in the topmost layer, the separation between the pile and the soil is accounted for. For the unconnected situation, the separation was caused by strong excitation. The depth of the anticipated separation,  $e_o$ , ranges from  $6.8d$  for  $\theta = 8$  to  $9.8d$  for  $\theta = 14$ , where  $d$  is pile diameter.

From Figs 5.3 to 5.5 it can be seen that as the excitation intensity increases, from  $\theta = 5$  to 14, the resonant frequency of the pile decrease and the resonant displacement increases. Meanwhile, for the same magnitude of exciting forces, the resonant frequency of the unconnected situation is markedly lower than that of the connected situation. Apparently, for the single pile tested, the cap contributed to the stiffness and damping of the pile, as was also found by Novak and Grigg (1976); however, in practice this observation should be applied with caution because the sand under the cap may settle more than the piles, particularly with end bearing piles. For embedded caps the soil reactions acting on the vertical sides can generate a significant amount of damping and be quite beneficial.

#### Pile Stiffness and Damping

The theoretical stiffness and damping coefficients of the pile for the horizontal and rocking directions are shown in Fig. 5.6 and 5.7, respectively. The subscript  $u$  indicates horizontal translation while  $\phi$  stands for pile head rotation (rocking).

The stiffness is almost frequency independent, as would be expected, because of low dimensionless frequencies the pile dynamic stiffness is known to be close to the static one. Fig. 5.6 and 5.7 also show the pile damping coefficients. These rapidly increase as frequency decreases. This is primarily due to the conversion of frequency-independent soil material damping to equivalent viscous damping coefficient  $c = 2\beta/\omega$ .

To provide a dimensionless measure of pile damping, the damping ratio can be evaluated from the stiffness and damping coefficients as  $c\omega/(2k)$ . These damping ratios are shown in Fig. 5.8 and 5.9. The damping ratios increase with frequency but the rate of increase is lowest for the strongest excitation. It can also be seen from Figs 5.6 to 5.9 that the damping coefficients and damping ratio mostly decrease with excitation intensity and thus with vibration amplitudes for frequencies higher than the lowest resonance frequency observed (4.7 Hz). This is further illustrated by Table 5.5. In soils, an increase in damping with strain is usually assumed. This apparent discrepancy suggests a growth in pile separation with vibration amplitudes and the weakening of the soil around the pile, as reflected in the necessary reduction in the shear modulus in the weak zone.

### Pile Deflections

The measured deflections of the pile varied with frequency and excitation intensity. A comparison of the measured data with the theoretical curves is shown in Fig. 5.10 and 5.11 for  $\theta = 8$  and 14, respectively. The theoretical characteris-

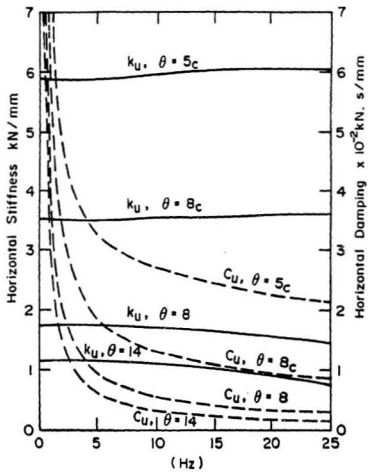


Figure 5.6: Pile horizontal stiffness and damping coefficient

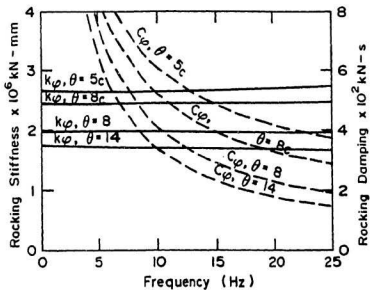


Figure 5.7: Pile rocking stiffness and damping coefficient

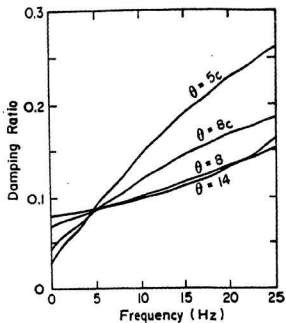


Figure 5.8: Pile horizontal damping ratio

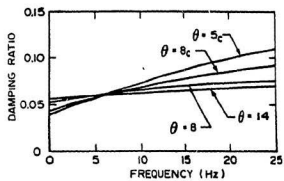


Figure 5.9: Pile rocking damping ratio

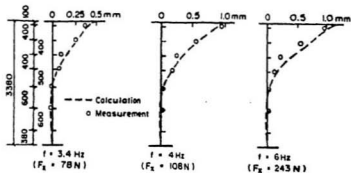


Figure 5.10: Comparison of theoretical curves and measured deflections along pile shaft (excitation  $\theta = 14$ )

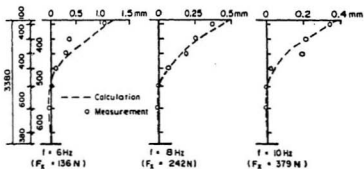


Figure 5.11: Comparison of theoretical curves and measured deflections along pile shaft (excitation  $\theta = 8$ )

Excitation Test	$\theta = 5_c$	$\theta = 8_c$	$\theta = 8$	$\theta = 14$
Resonance Frequency (Hz)	12.2	8.5	5.6	4.7
Damping Ratio	Horizontal	0.163	0.110	0.090
	Rocking	0.080	0.070	0.063

Table 5.5: Damping Parameters of the Pile

tics of the pile and soil used are the same as those used in the response analysis. It can be seen that the measured data agree well with the theoretical deflection curves.

Comparing the dynamic deflection with the static deflection of the pile, it appears that the effective pile length is about  $13.5d$  under strong horizontal excitation, and about  $11.0d$  for static loading. That is, the effective pile length for dynamic loading is slightly longer than for static loading, although the horizontal displacements along the pile length caused by dynamic loading may be larger than those due to static loading.

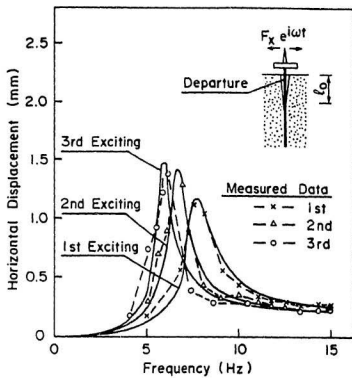


Figure 5.12: Theoretical and experimental response curves for repeated loading ( $\theta = 5$ , cap separated)

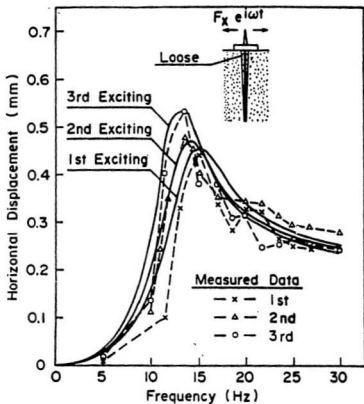


Figure 5.13: Theoretical and experimental response curves for repeated loading ( $\theta = 5_e$ , cap in contact with soil)

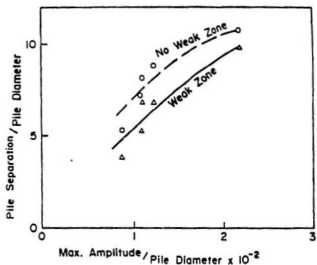


Figure 5.14: Theoretical pile separation vs dimensionless amplitude

### Effect of Repeated Loading

The soil around the pile softens and separates under repeated loading. Accordingly, the stiffness, damping, and dynamic response of the pile vary with repeated loading. To obtain data on these effects, dynamic experiments on a single pile under repeated loading were also conducted. Another pile was embedded in another sand pit, with the properties of the pile and soil, as well as the test conditions, being the same as before. The contact condition between the pile cap and the soil surface was of the two types, that is, connected and unconnected. For each case, the pile was excited three times, from low to high frequency, with the excitation intensity kept the same in all runs. The comparison of measured data with theoretical response curves for the connected and unconnected cases is shown in Fig. 5.12 and 5.13, respectively. The measured resonance peaks shift to lower frequencies and become sharper with loading repetition, indicating reduction in both stiffness and damping. With judicious choice of input data, the theoretical response curves agree with the experimental results quite well. The reduction in theoretical stiffness and damping with load repetition can be seen from Table 5.6. Because of the gap around the pile deeper, soil nonlinearity, and possibly slippage under the pile cap, the pile stiffness is reduced in the connected condition also.

The difficulty with the inclusion of the weak zone in the analysis is that its parameters are difficult to assess beforehand. Thus the question arises of whether a correction for pile separation in the form of a pile free length would not be sufficient to account for the reduction in pile stiffness and damping observed in the experiments. The need for a free length was already observed by other investigators, for example, Novak and Aboul-Ella (1978), Novak and El-Sharnouby (1984), and Roes-

Connection		Connected			Unconnected		
Order of Excitation		1st	2nd	3rd	1st	2nd	3rd
Resonant Frequency (Hz)		13.8	12.6	12.2	7.6	6.5	5.7
Stiffness	Horizontal $K_x(KN/mm)$	7.43	6.50	5.89	3.04	2.15	1.78
	Rocking $K_\psi 10^6(K.N - mm)$	2.75	2.64	2.59	2.29	2.08	1.96
Damping Ratio	Horizontal	0.193	0.185	0.162	0.081	0.064	0.060
	Rocking	0.081	0.080	0.078	0.060	0.054	0.052

Table 5.6: Dynamic parameters of pile under Repeated Loading

set et al. (1986).

For the unconnected cap, the theoretical separation between the pile and soil is  $e_o = 3.8d$  for the first excitation,  $e_o = 5.3d$  for the second, and  $e_o = 6.8d$  for the third. The separation lengths required in the analysis to provide a good fit with the experimental data for the different resonant amplitudes measured are plotted in Fig. 5.14. Analyses both with and without the weak zone were employed and gave satisfactory results, although the weak zone allows finer tuning. The separation lengths needed increase with displacement amplitude and are greater if no weak zone is considered. The maximum separation is about 10 pile diameters. The separation is given in terms of diameter but, in general, the absolute depth must be a basic parameter because it controls the confining pressure. With the pile diameter of 133 mm the maximum separation length was thus 1.33 m.

## 5.3 Pile Response under Vertical Excitation

### Experimental Vertical Response

After the testing of the pile under horizontal excitation, vertical excitation was applied, with all the other experimental conditions remaining the same.

The excitation intensity was increased stepwise and three frequency response curves, shown in Fig. 5.15, were obtained. Sharp intersecting resonance peaks are indicated like the ones shown in Fig. 5.5. The maximum displacement measured on the top of the cap is about 1.4 mm and the maximum acceleration reaches about 1.3 g. Markedly nonlinear features are again manifested particularly by the drop in the resonant frequency with the increase in excitation intensity ( $\theta$ ), but this drop is less than it was under horizontal excitation.

In the case of vertical excitation, the nonlinear features of the measured response curves can be studied more easily because this response can be treated in one degree of freedom (S.D.O.F.) and is, therefore, quite amenable to linear analysis. Such analysis is employed in the next section.

### Evaluation of the Vertical Response

#### (1) Nonlinear S.D.O.F. analysis

To identify the parameters of the soil-pile system from the measured response displaying nonlinear features, the inverse problem of nonlinear vibration has to be approached. This means that the system mass, stiffness, and damping have to be established from the experimental response. To this end, the methodology formu-

lated in Novak (1971) is employed. This procedure assumes that system stiffness is independent of frequency; this is also usually assumed for slender piles in medium soil in practical applications.

Assuming that the restoring force is nonlinear but the damping force is linear (viscous), the backbone curve, which defines the undamped natural frequencies  $\Omega$ , can be determined to a given response curve using the simple relation

$$\Omega = \sqrt{\omega_1 \omega_2} \quad (5.1)$$

in which,  $\omega_1$  and  $\omega_2$  are the frequencies corresponding to the points of intersection between the response curve and a line passing through the origin of coordinates (see Fig. 5.15). Intersecting the response curve by a trace of such lines, the backbone curve  $\Omega(A)$  can be constructed to each response curve. These backbone curves are plotted in Fig. 5.15. It can be seen that each response curve has its own backbone curve, unlike the theoretical response curves shown in Fig. 5.4. This indicates that the stiffness characteristic of the system varies with the overall level of vibration intensity rather than being unique. This is confirmed by establishing the stiffness characteristics corresponding to the individual backbone curves.

The stiffness characteristic can be assumed to be of two types: A truly nonlinear characteristic that is followed for all amplitudes  $A$  and a characteristic,  $F(A)$ , that is nonlinear but for every steady-state amplitude  $A$  linearized to give the equivalent linear stiffness depending on amplitude  $A$ , that is,

$$K_e(A) = F(A)/A \quad (5.2)$$

The latter assumption appears more suitable and is adopted here. Then, for a restoring force expressed by a power series

$$F(A) = k_1 + k_3 A^3 + k_5 A^5 + \dots + k_n A^n \quad (5.3)$$

where  $k_i$  are constants, the amplitude-dependent natural frequency is given by

$$\Omega^2(A) = \frac{K_e(A)}{m} = \frac{1}{m} (k_1 A^{-1} + k_3 A^2 + k_5 A^4 + \dots + k_n A^{n-1}) \quad (5.4)$$

in which  $m$  is the system effective mass.

The effective mass and damping can be calculated exploiting the geometric properties of the response curves. The mass and damping found are given in Table 5.7. The value of the effective mass,  $m$ , is much greater than the total mass of the pile, cap, and exciter,  $M$ . The apparent additional mass can be expressed in terms of the coefficient

$$\xi_m = \frac{m - M}{M} \quad (5.5)$$

which is also given in Table 5.7. The additional mass is very substantial and decreases with increasing excitation intensity, suggesting that partial separation of the pile from soil might have occurred with higher excitation intensity. It seems that the apparent mass increase results from the assumption that pile stiffness is constant, that is, frequency independent. In the continuum approaches, no additional mass is needed because soil mass is automatically accounted for, making the pile stiffness frequency dependent. This effect can be quite strong, particularly for stiff piles vibrating vertically and will be demonstrated in the last part of this paper.

With the mass pertinent to each response curve the restoring force characteristic

Excitation	Effective Mass		Damping Ratio $\beta$	Stiffness $k(KN/mm)$
	Mass $m(kg)$	Mass Coefficient		
$\theta = 8$	1730	3.01	0.042	23.9
$\theta = 14$	1350	2.05	0.060	15.7
$\theta = 28$	993	1.24	0.075	7.39

Table 5.7: Nonlinear vibration parameters of pile in vertical direction

follows from eq. (2) and (4) as

$$F(A) = Am\Omega^2 \quad (5.6)$$

For the three response curves shown in Fig. 5.15 the corresponding restoring force characteristic, calculated by eq. (6), are plotted in Fig. 5.16. A few observations emerge: each response curve has its own characteristic, the overall stiffness markedly decreases with increasing excitation intensity ( $\theta$ ) but the nonlinearity of individual characteristics is much less pronounced than the overall nonlinearity of the whole set of the response curves. the latter observation is consistent with those made with regard to the horizontal response and supports the assumption of linearization implied in eq.(2).

The damping ratio derived from the response curves is also given in Table 5.7. The damping found is much smaller than what would be expected for a lightly loaded fully embedded pile and increases with excitation intensity. Under horizontal excitation, the damping decreased with increasing amplitudes. This indicates that the separation effect is somewhat less severe in the vertical vibration than it is in the horizontal vibration and that slippage generating friction may contribute to

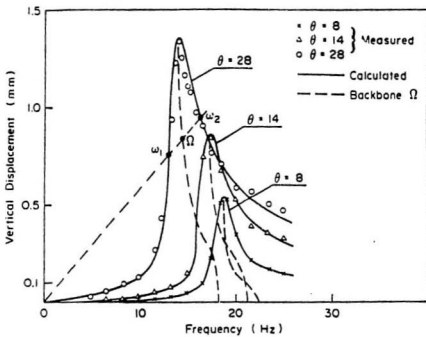


Figure 5.15: Vertical pile response measured and back-calculated for three levels of excitation intensity ( $\omega = 2\pi f$ )

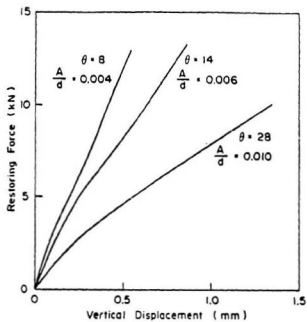


Figure 5.16: Pile restoring force characteristics vs. pile head displacement corresponding to response curves from Fig. 5.15.

the increase in the vertical damping.

With the soil-pile system mass, damping, and restoring force characteristic derived, the nonlinear response curves were back-calculated using the nonlinear theory and are plotted as solid lines in Fig. 5.15. The theoretical nonlinear response curves agree with the measured ones very well. Thus, a very good theoretical prediction can be made assuming a nonlinear restoring force characteristic and a linear, viscous damping whose constant depends on the peak amplitude.

#### (2) Linear soil-pile interaction analysis

The theoretical response curves shown in Fig. 5.15 were back-calculated using the S.D.O.F. data derived from the experiments. Another task is to predict the pile response on the basis of soil-pile interaction analysis and the properties of soil as well as the the pile, as described in chapter 3 and 4. This interaction analysis confirms that extensive pile separation must have occurred. This can be seen from Fig. 5.17 in which the large amplitude experimental response is compared with the theoretical one. When no separation is assumed (curve A) the theoretical response is heavily damped and the stiffness is very high, bring the resonance peak beyond the experimental frequency range. A large separation of 1.80 m, a weakened zone around the pile, and a true mass of the system yielded curve B and a reasonable agreement with the measured data. The discrepancy in the descendant branches of the response curves is due to the linear theory employed in this case, which cannot give a perfect agreement with the actual nonlinear response over the whole frequency range.

### Effect of Limited Size of Test Pit

Finally, it is of interest to examine the effect of the limited extent of the pit in which the tests were conducted. The pit was filled with sand whose properties differed from those of the surrounding soil. Consequently, an interface occurs between the two media from which waves may reflect back into the pit, complicating the wave pattern within the pit and creating what is known in analysis as the "box effect". To examine this effect, the vertical pile stiffness and damping were reanalyzed using the model of boundary zone in which an annular zone is allowed for around the pile with soil properties different from those of the outer soil. Because of the large extent of the pit the mass of the inner zone (sand) was accounted for. The geometry and notations for this analysis are shown in Fig. 5.18.

The dimensionless stiffness and damping parameters  $f_{v1}$  and  $f_{v2}$  defined in chapter 4 are plotted in Fig. 5.19 and 5.20. The results are shown for three pit dimensions characterized by the ratio of the zone thickness,  $t_m$ , to pile radius,  $r_o$ , and the actual soil properties of the site. Shown as solid line for comparison are the pile parameters corresponding to homogeneous soil medium, that is,  $t_m \rightarrow \infty$ . The site  $t_m/r_o$  ratio is close to 10. The presence of the interface can be seen to have only a small effect on pile stiffness (Fig. 5.19) but has a profound effect on radiation damping. At low frequencies the damping is slightly increased but at higher frequencies it is dramatically decreased compared with that of the horizontally homogeneous medium. This effect of the interface on pile damping is marked but is much less significant than pile separation, as the response curves plotted in Fig. 5.17 demonstrate.

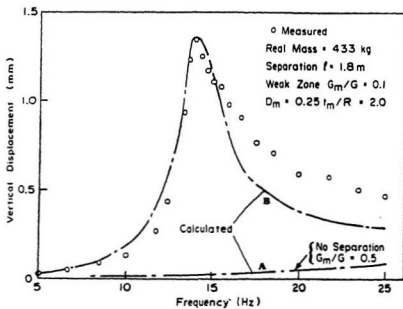


Figure 5.17: Experimental pile response in vertical direction vs. theoretical prediction ( $\theta = 28$ )

The strong variation in the stiffness parameter  $f_{v1}$  with frequency (Fig. 5.19) is also of interest. It is close to parabolic and can be interpreted as  $k_{st} - m\omega^2$  where  $k_{st}$  is the pile static stiffness and  $m$  is the effective mass. Because the pile stiffness, like  $k_{st}$ , is assumed to be frequency independent in the S.D.O.F. nonlinear analysis, the frequency variation of the actual stiffness call for the inertia term,  $m\omega^2$ , and hence for additional mass as found in Table 5.7.

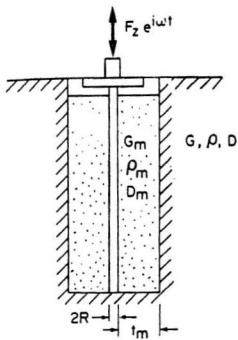


Figure 5.18: Notations and geometry for pile in test pit.

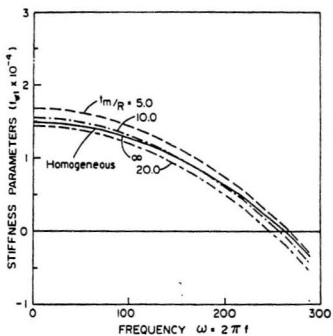


Figure 5.19: Pile stiffness parameter  $f_{v1}$  for different test pit dimensions ( $G_i/G_o = 0.25, \beta_i = \beta_o = 0.10, \rho_i = \rho_o, \nu = 0.4$ ).

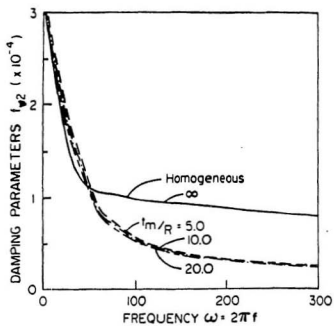


Figure 5.20: Pile damping parameter  $f_{v1}$  for different test pit dimensions ( $G_i/G_o = 0.25$ ,  $\beta_i = \beta_o = 0.10$ ,  $\rho_i = \rho_o$ ,  $\nu = 0.4$ ).

## Conclusions

Dynamic experiments with large-scale model piles subjected to strong harmonic excitation in the field were conducted. The measured response curves are compared with the theoretical curves. The comparison suggests the following conclusions:

1. Pile response at large amplitudes exhibits typical nonlinear features.
2. Consideration of a weakened zone around the pile and pile separation is necessary for piles subjected to strong vibration.
3. Good agreement can be achieved between the experimental and theoretical response curves when the characteristics of soil are suitably chosen, without resort to truly nonlinear analysis. The excitation intensity and contact conditions between the pile and soil and between the cap and soil surface change the stiffness and damping of piles.

The boundary zone model is an approximate approach rather than a rigorous nonlinear analysis for dynamic response of piles. How to select the characteristics of soil and the parameters of the boundary zone depends on the particular conditions of the soil-pile system, such as the installation of the piles, the properties of soil and piles, and the excitation intensities.

The new finding in this study are that the general recommendations can be provided as guide lines for engineering practice, such as the thickness of boundary zone and the range of  $G_i/G_o$ .

4. Under repeated loading, the stiffness and damping of single piles decrease, so that the resonant frequency decreases and resonant displacement increases.
5. The weak zone around the pile considered in the theory yields lower damping of the pile-soil system than that evaluated without a weak zone. The damping values

calculated in this way are closer to the experimental results.

6. Under dynamic horizontal deflections the effective pile length is slightly longer than it is under static loading.

7. Dynamic experiments conducted in a test pit may be affected by wave reflections from the interface between the soil in the pit and soil outside it. Damping of the test body can be more affected than its stiffness.

8. Further research is needed to develop criteria for pile separation prediction and pile nonlinear dynamic analysis.

## Chapter 6

# Stiffness and Damping of Pile Group

### 6.1 Pile-Soil-Pile Interaction

Piles are usually used in groups. The behaviour of the group depends on the distance between the piles. When the distance between the piles is large, say ten even twenty diameters or more, the pile do not affect each other and the group stiffness and damping are simple sums of contributions from the individual piles. If, however, the piles are closely spaced, they interact with each other and this pile-soil-pile interaction or group effect exerts considerable influence on the stiffness and damping of the group.

The stiffness and damping are most often evaluated using the properties of a single pile and accounting for the group effect by means of the interaction factors. The interaction factors are derived from the consideration of a group of two piles and determine the displacement of one pile due to loading of the other pile. Details of the interaction factor for the two-pile group are given in Appendix B. For static

loading, the factors were presented in the form of charts by Poulos (1979, 1980) and Butterfield (1971) and for dynamic loads by Kaynia and Kausel (1982). Dynamic group effects may vary with frequency and group stiffness, and damping can be either reduced or increased by pile-soil-pile interaction. The relationship between the displacement,  $u_G$ , of a group of  $n$  piles and the displacement,  $u$ , of a single pile carrying the same load as one pile in the group can be written as

$$u_G = u_1 \sum_{r=1}^n \alpha_r \quad (6.1)$$

in which  $\alpha_r$  = the interaction factor defined as the ratio of the settlement of the  $r$ th pile due to the settlement of the reference pile ;  $\alpha_1 = 1$  and for static loads, the other factors have absolute values smaller than unity. The sum of pile interaction factors,  $\sum \alpha_r$ , can be viewed as a group interaction factor. Stiffness of the pile group,  $K_G$ , is inversely proportional to displacement (flexibility) and, thus, for the horizontal or vertical direction can be approximately written as

$$K_G = \frac{K}{\sum \alpha_r} \quad (6.2)$$

in which  $K = \sum k$  is the group stiffness calculated without the pile interaction effect; and  $k$  = stiffness of a single (isolated) pile. For a large group of piles, loads are usually assumed to be carried equally by piles and  $\sum \alpha_r$  may be calculated for the middle pile of the outer row of the long direction taken as the reference pile. A similar but more consistent formula, which avoids the somewhat arbitrary selection of the reference pile, can be written for translations as

$$K_G = k \sum_i \sum_r \alpha_{ir} \quad (6.3)$$

in which  $\alpha_{ir}^{-1}$  = the elements of the inverted matrix,  $[\alpha_{ir}]^{-1}$ , with the  $n \times n$  matrix  $[\alpha_{ir}]$  listing all interaction factor,  $\alpha_{ir}$ , between any two piles,  $i$  and  $r$ ; the diagonal terms  $\alpha_{ii} \equiv 1$ ; and  $n$  = number of piles in the group.

The static interaction factors were derived based on Mindlin's displacement field in the elastic half-space. To extend the interaction factors approach to dynamic situation, Kaynia and Kausel (1982) presented charts for dynamic interaction. In the solution, the soil reactions acting on the piles were evaluated numerically. The dynamic interaction factor,  $\alpha_{ij}$ , is defined as

$$\alpha_{ij} = \frac{\delta_{dij}}{\delta_{sjj}} \quad (6.4)$$

where  $\delta_{dij}$  is dynamic displacement of pile  $i$  due to load on pile  $j$  and  $\delta_{sjj}$  is static displacement of pile  $j$  due to its own load. Both dynamic and static displacements are referred to the pile head.

Dynamic interaction factors are frequency dependent complex number, i.e.,  $\alpha = \alpha_1 + i\alpha_2$ , having a real part  $\alpha_1$  and an imaginary part  $\alpha_2$ . Their values depend on, among other factors,  $a_s$ ,  $E_s/E_p$ , and  $S/d$  where  $E_p$ ,  $d$  are the Young's modulus and diameter of the pile respectively,  $E_s$  is the soil Young's modulus and  $S$  is the spacing between the piles. Example of the dynamic interaction factors are shown in Fig. 6.1 for a limited range of parameters.

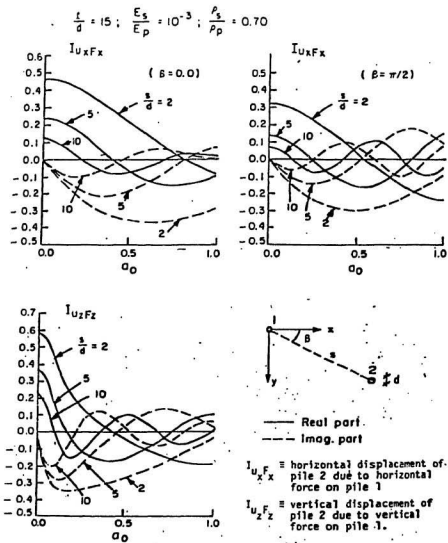


Figure 6.1: Interaction curve for horizontal and vertical displacement of pile 2 due to horizontal and vertical force on pile 1 (Kaynia and Kausel, 1982)

## 6.2 Stiffness and Damping of Pile Group

The pile group stiffness may be established either through direct analysis or by means of the superposition method. In direct analysis, all piles of the group are considered to interact at the same time. In the superposition method, the interaction between each two piles is considered separately and used to formulate the flexibility matrix of the entire group. The superposition method which is used to establish theoretical results in this study is computationally advantageous and was shown to be in good agreement with the direct analysis for the case of floating piles in a homogeneous soil. The application of superposition method is facilitated through the use of pile-soil-pile interaction factors. With rigid caps, the complex stiffness of pile group in different modes of vibration is calculated by applying the pertinent boundary conditions.

### Vertical Group Stiffness

From the definition of dynamic interaction factor in eq. (6.4), the compatibility equation can be expressed in terms of flexibility as

$$\{v\} = \bar{f}_v[\alpha]_v\{P\} \quad (6.5)$$

where  $\bar{f}_v$  is the static vertical flexibility of a single pile,  $\{P\}$  and  $\{v\}$  are the vectors of vertical forces and vertical displacements at the pile heads, respectively, and  $[\alpha]_v$

is the interaction matrix of the vertical displacements, written as

$$[\alpha]_v = \begin{bmatrix} f'_v \dots \alpha_{11} \dots \alpha_{1n} \\ \vdots \\ \alpha_{i1} \dots f'_v \dots \alpha_{in} \\ \vdots \\ \alpha_{n1} \dots \alpha_{ni} \dots f'_v \end{bmatrix} \quad (6.6)$$

in which the ratio

$$f'_v = f_v / \bar{f}_v \quad (6.7)$$

where  $f_v$  = complex vertical dynamic flexibility of a single pile and  $\alpha_{ij}$  = complex vertical interaction factors between piles  $i$  and  $j$ . The boundary conditions in this case are  $v_i = 1$  for  $i = 1, 2, \dots, n$  and yield the vertical forces on the piles

$$\{P\} = \frac{1}{f'_v} [\alpha]_v^{-1} \{1\} \quad (6.8)$$

Denoting the static stiffness of a single pile  $\bar{k}_v = 1/f_v$  and the complex elements of  $[\alpha]_v^{-1}$  by  $\epsilon_{ij}^v$ , the vertical force  $P_i$  acting on pile  $i$  is

$$P_i = \bar{k}_v \sum_{j=1}^n \epsilon_{ij}^v \quad (6.9)$$

In above equation,  $\epsilon_{ij}^v$  are to be seen as multiplied by unit displacements. The group complex stiffness is the sum of all the vertical vertical forces, i.e.,

$$K_v^G = \sum P_i = \bar{k}_v \sum_{i=1}^n \sum_{j=1}^n \epsilon_{ij}^v \quad (6.10)$$

### Horizontal Group Stiffness

For horizontal translations and rotations in either of the two vertical planes of symmetry, the compatibility equation are

$$\{\delta\} = \bar{f}_u [\alpha]_H \{P\}_H \quad (6.11)$$

where  $\bar{f}_u$  is the horizontal static flexibility of a single free-head pile,  $\{P\}_H$  is the vector of horizontal forces  $H_i$  and moments  $M_i$  at the pile head, i.e.,

$$\{P\}_H = [H_1, M_1 \dots H_n, M_n]^T \quad (6.12)$$

The vector  $\{\delta\}$  lists the horizontal translations and rotations at the pile heads, i.e.,

$$\{\delta\} = [u_1, \psi_1 \dots u_n, \psi_n]^T \quad (6.13)$$

Finally,  $[\alpha]_H$  is the matrix of interaction coefficients for the horizontal translations and rotations. For a group of  $n$  piles, the matrix  $[\alpha]_H$  has  $n \times n$  submatrices and is

$$[\alpha]_H = \begin{bmatrix} B_{11} & \dots & B_{1i} & \dots & B_{1n} \\ \vdots & & \vdots & & \vdots \\ B_{i1} & \dots & B_{ii} & \dots & B_{in} \\ \vdots & & \vdots & & \vdots \\ B_{n1} & \dots & B_{ni} & \dots & B_{nn} \end{bmatrix} \quad (6.14)$$

where each of the submatrices is  $2 \times 2$ ,

$$B_{ii} = \begin{bmatrix} f'_u & f'_c \\ f'_c & f'_\psi \end{bmatrix} \quad (6.15)$$

$$B_{ij} = \begin{bmatrix} \beta_{ij}^u & \beta_{ij}^c \\ \beta_{ij}^c & \beta_{ij}^\psi \end{bmatrix} \quad (6.16)$$

where

$$\begin{cases} f'_r = f_r / \bar{f}_u \\ \beta_{ij}^r = (\bar{f}_r / \bar{f}_u) \alpha_{ij}^r, \quad i \neq j \end{cases} \quad (6.17)$$

In above,  $f_r$  are single pile dynamic flexibility coefficients and  $r$  stands for  $u, \psi$  or  $c$  and indicates the horizontal translation, rocking or coupling directions, respectively.

For horizontal stiffnesses, the boundary conditions are  $u_i = 1$  and  $\psi_i = 0$  for  $i = 1, 2, \dots, n$  and the horizontal force on pile  $i$  follows from eq.(6.11) as

$$H_i = \bar{k}_u \sum_{j=1}^n \varepsilon_{2i-1,2j-1}^H \quad (6.18)$$

where  $\bar{k}_u = 1/f'_u$  and  $\varepsilon^H$  are the complex elements of  $[\alpha]_H^{-1}$ . The complex horizontal group stiffness being the sum of all these forces becomes

$$K_u^G = \bar{k}_u \sum_{i=1}^n \sum_{j=1}^n \varepsilon_{2i-1,2j-1}^H \quad (6.19)$$

The summation extends only over those elements of  $[\alpha]_H^{-1}$  that correspond to the horizontal forces associated with horizontal displacements, i.e., elements with positions  $2i - 1, 2j - 1$ . In eq.(6.19),  $\bar{k}_u$  is static horizontal stiffness of a free-head (pinned-head) pile but the group stiffness  $K_u^G$  is obtained for fixed-head piles. Alternatively, the group horizontal stiffness can be calculated for both pinned-head and fixed-head piles from eq.(6.10) with pertinent values of  $\bar{k}_u, f'_u$  and  $[\alpha]_H$  substituted for either pinned-head or fixed-head piles.

### Rocking Stiffness

Rocking group stiffness derived from two components: the moments required to produce unit rotations at the pile heads and the moments resulting from the vertical pile forces. The moments required to produce unit rotations at the pile heads are obtained by applying the boundary conditions  $\psi_i = 1, u_i = 0 (i = 1, 2, \dots, n)$  to eq. (6.11). This yields the moment on pile  $i$

$$M_{i(1)} = \bar{k}_u \sum_{j=1}^n \varepsilon_{2i,2j}^H \quad (6.20)$$

The vertical pile forces associated with cap rotation are obtained by applying the boundary condition  $v_i = 1 \times x_i (i = 1, 2, \dots, n)$  to eq.(6.5) giving

$$P_i = \bar{k}_v \sum_{j=1}^n \varepsilon_{ij}^v x_j \quad (6.21)$$

In above,  $x_i$  and  $x_j$  are pile distances from the rotational axes. These forces produce a moment on each pile

$$M_{i(2)} = \bar{k}_u x_i \sum_{j=1}^n \varepsilon_{ij}^v x_j \quad (6.22)$$

The rocking group stiffness is the sum of both moments shown in eq.(6.20) and (6.22) over all pile heads, i.e.,

$$K_\psi^G = \bar{k}_u \sum_{i=1}^n \sum_{j=1}^n \varepsilon_{2i,2j}^H + \bar{k}_v \sum_{i=1}^n \sum_{j=1}^n \varepsilon_{ij}^v x_i x_j \quad (6.23)$$

### Cross Stiffness

This stiffness is obtained by applying the same boundary conditions, pertaining to the horizontal translations and rotations, as in the previous case to eq.(6.11) and evaluating the resulting horizontal pile forces. these become:

$$H_i = \bar{k}_u \sum_{j=1}^n \varepsilon_{2i-1,2j}^H \quad (6.24)$$

The group cross stiffness is the sum of all horizontal force on the pile heads and hence

$$K_{uv}^G = \bar{k}_u \sum_{i=1}^n \sum_{j=1}^n \varepsilon_{2i-1,2j}^H \quad (6.25)$$

and

$$K_{vu}^G = K_{uv}^G \quad (6.26)$$

The effects of pile-soil-pile interaction on the stiffness and damping of pile group with a rigid cap are best illustrated by the group efficiency ratio (GER) defined as

for stiffness

$$GER = \frac{K^G}{n \times k} \quad (6.27)$$

and for damping

$$GER = \frac{C^G}{n \times c} \quad (6.28)$$

In above,  $K^G, C^G$  are stiffness and damping of group, respectively;  $k, c$  are stiffness and damping of a single pile, respectively;  $n$  is the number of piles in the group.

## Chapter 7

# Dynamic Experiments of Pile Group

Because of the complicated nature of dynamic pile-soil-pile interaction, experimental research is needed to verify the applicability of different theories. Although there are a number of methods available for analyzing the dynamic response of pile groups, very little information is available on the field validation of these techniques. The lack of calibrated parameters makes it rather difficult to perform reliable analysis of practical projects using the relevant models.

Most of the previous work involving dynamic response of pile group has been limited to small-amplitude vibration or linear vibration. A problem that is of more practical interest, however, is the nonlinear response of pile group involving soil yielding, pile slippage, or even partial separation of the piles from the adjoining soil (gap development) as they may occur under a reasonably strong earthquake event.

Since the nature of pile-soil-pile interaction depends on the actual confining pres-

sure and the contact situation between the piles and soil, full-scale tests on piles are considered to provide valuable data for practical applications.

A comprehensive study involving both theoretical analysis and full-scale testing of a pile group is described in this chapter. To investigate the dynamic behaviour of pile group, the experiments on the full-scale pile group were carried out under different conditions: linear vibration and nonlinear vibration. In the cold region, the ground surface may be covered by a frozen soil layer. In order to investigate the influence of frozen soil layer on dynamic behaviour of the piles, the experiments were conducted first during the winter time when the surface was covered by a frozen soil layer and then during the summer time when the frozen soil had completely thawed out. In the next year, the nonlinear vibration tests on the pile group subjected to strong excitation were done. For comparison, the dynamic experiments were also carried out on two single piles which had the same properties and size as those in the group and were placed in the same test site.

## **7.1 Experimental Setup**

### Subsurface Conditions

Field tests involving a full-scale pile group, comprising six piles, were carried out at a site within the grounds of the Institute of Engineering Mechanics, Harbin, China, as described by Han and Novak (1992). The subsurface investigation indicated that the test site was underlain by a relatively homogeneous layer of silty

Depth (m)	Unit Weight $\gamma$ (K.N/m <sup>3</sup> )	Void Ratio $e$	Moisture Content $w$ (%)
2	20.2	0.58	21.8
4	18.5	0.75	23.7
6	19.7	0.60	20.5
8	20.0	0.59	20.2

Table 7.1: Soil properties

clay with occasional lenses of sandy clay mixture down to a depth of 30 meters. The ground-water table was established at 20 m below the ground surface. Both laboratory and in situ tests were performed to characterize the dynamic and static properties of the soil. Laboratory tests were performed on undisturbed samples extracted at every one meter interval. The experiments included triaxial tests to measure the variation of shear modulus and damping ratio with shear strain; specific gravity; bulk density and Atterberg Limit tests. The dynamic in situ test consisted of seismic cross-hole tests for determining the shear wave velocity of the soil. Fig. 7.1 illustrates the arrangement adopted in performing the cross-hole tests in relation to the piles. Some of the measured soil properties used in this study are listed in Table 7.1.

The variation of shear modulus and damping ratio against the shear strain are shown in Fig. 7.2, which were measured in the triaxial system. The variation of void ratio,  $e$ , degree of saturation,  $S$ , and Atterberg Limits over the length of the pile (i.e., 7.5 m) are shown in Fig. 7.3. The specific gravity,  $G_s$ , was almost constant throughout the depth, ranging between 2.66 to 2.68. The Poisson's ratio for the soil is assumed to be 0.3.

Unit Weight $\gamma (K.N/m^3)$	Moment of Inertia $I (m^4)$	Modulus $E_p (MPa)$	Poisson's Ratio, $\nu_p$	Damping Ratio, $D_p$
24.5	$5.15 \times 10^{-4}$	$1.96 \times 10^4$	0.25	0.01

Table 7.2: Pile properties

### Pile Test Setup

The pile group under study was comprised of six cast-in-place reinforced concrete piles; each pile was 7.5 m long and 0.32 m in diameter. Fig. 7.4 (a) shows the layout of the pile group; the concrete cap was 2.5 m long (X - direction), 1.6 m wide (Y - direction), and 0.5 m thick, weighing 49 kN and having a clearance of 0.25 m above the ground surface. The arrangement of the piles was different for the X - direction and Y - direction. Three piles were placed in one row in X - direction and two piles in one row in Y - direction. Fig. 7.4 (b) shows the variation of shear wave velocity and mass density of soil over the length of the pile. The properties of the piles are shown in Table 7.2. The pile slender ratio,  $L/d = 23.4$  and spacing ratio,  $s/d = 2.81$ , where  $L$  is pile length,  $s$  is pile spacing, and  $d$  is pile diameter.

An exciter with two counter-rotating eccentric mass was bolted to the pile cap to produce the harmonic excitation as shown in Fig. 7.5. The exciting force is given by

$$F(t) = m_e e \omega^2 \cos \omega t \quad (7.1)$$

where  $m_e e$  is the excitation intensity,  $\omega$  is the circular frequency, and  $t$  is the time. Different excitation intensities were used in the experiments, and the magnitude of exciting force was changed by adjusting the angle of eccentric mass. Two exciters

were used in the experiments respectively. The smaller one was used to produce linear vibration of the pile group and the larger one was used for nonlinear vibration. The detail will be described in next section.

Two horizontal displacement pick-ups ( to measure the horizontal vibration) and two vertical displacement pick-ups (to measure the rocking vibration) were mounted on the pile cap. The steady-state dynamic response of the pile group under horizontal excitation was measured under different frequencies and different excitation intensities.

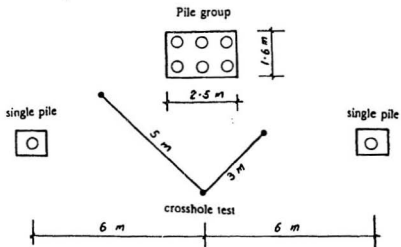


Figure 7.1: Plan view of piles and cross-hole test

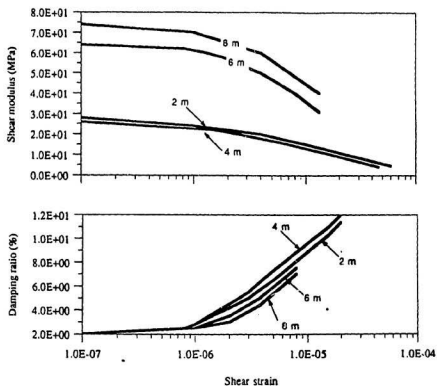


Figure 7.2: Triaxial test measured data for the soil in the test site at several different depth

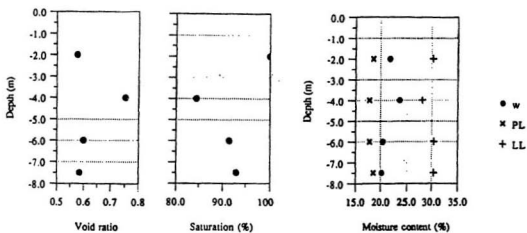


Figure 7.3: Laboratory-measured properties of the soil in the test site

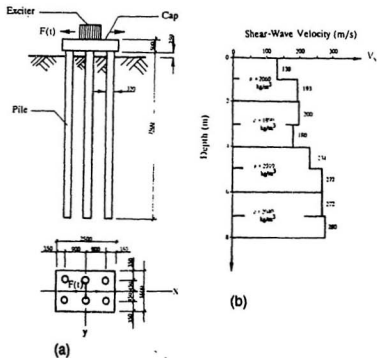


Figure 7.4: (a) Layout of the pile group and (b) the measured shear wave velocity and mass density of the soil.



Figure 7.5: Test setup for the lateral vibration of the pile cap

## 7.2 Linear Vibration of Pile Group

A smaller exciter, weighing 1.18 kN, was fixed on the pile cap by foundation bolt to produce the harmonic excitation in Y - direction only. The active component of the horizontal excitation was situated 0.2 m above the cap surface, and the center of gravity of the cap-exciter system was 0.25 m below the cap surface. The magnitude of exciting force was changed by adjusting the angle of eccentric mass,  $\theta$ . Several levels of excitation intensities,  $m_e e$ , were used in the experiments, as indicated in Table 7.3. As shown later,  $\theta$  is used to represent the excitation intensity. The maximum horizontal amplitude of the pile group was measured to be 0.104 mm at top of the pile cap; this is considered to be a small amplitude vibration, say linear vibration. Under horizontal excitation, the cap produced coupled horizontal and rocking vibration. The horizontal and rocking response curves measured on the cap of the group in different excitation intensities are shown in Fig. 7.6.

For linear vibration, the response curves of the group can be normalized. Normalized response amplitude for translation is defined as:

$$A = (m/m_e e)U \quad (7.2)$$

and for rotation by:

$$\Phi = [I/(m_e e Z_e)]\Psi \quad (7.3)$$

where  $U$  and  $\Psi$  are the real translation and rotation, respectively;  $m$  and  $I$  are the mass and mass moment of inertia for the cap;  $Z_e$  is the height of the horizontal excitation above the center of gravity.

Angle of eccentric mass $\theta$	Excitation intensity $m_e(\text{kg.mm})$
8	96
14	171
28	259

Table 7.3: Excitation scheme adopted for linear vibration

Comparison of experimental response curves with the theoretical predictions is shown in Fig. 7.7 for horizontal and rocking vibration of the group. The theoretical predictions were done in two way. In one way, the boundary zone is accounted for each pile in the group. The relevant parameters of the boundary zone are as follows:  $G_i/G_o = 0.1$ ,  $t_m/r_o = 0.5$ ,  $\beta_i = 0.07$ , and  $\beta_o = 0.035$ . Poisson's ratio of soil is assumed,  $\nu = 0.3$ . The calculated curves are shown by solid line in Fig. 7.7.

In another way, the analysis were repeated with no regard to the boundary zone effects (i.e., the boundary zone was omitted). In this case, in order to properly account for the actual soil and pile contact, allowance was made for a free pile length (equivalent separation between pile and soil) at the top of the pile. Separation of the top segment of the pile from the soil can occur because of the very low confining stress that exists in soil layer within the close proximity of the ground surface. Herein, the free pile length is taken as  $0.5d$ , where  $d$  is the diameter of pile. This is based on a specific case in an experimental site. In this depth, the sand backfill is very loose in the sand pit. The dashed lines in Fig. 7.7 represent the theoretical calculation without boundary zone. It can be seen that the solid lines (calculated with boundary zone) agree with the measured results quite well, particularly for the

horizontal vibration; the agreement with the dashed lines (without boundary zone), albeit reasonable, is not as good as the case with the boundary zone.

In order to demonstrate the influence of pile-soil-pile interaction on the dynamic response of the pile group, the dynamic response was calculated with interaction effects omitted. The comparison of horizontal and rocking vibration against measured data is shown in Fig. 7.8. It can be seen that the theoretical predictions without interaction (dashed lines in the figure) result in a higher resonant frequency and a larger displacement amplitude. It can also be noticed that another resonant peak develops around the frequency of 100 Hz; this is primarily due to the second mode of vibration for the coupled horizontal and rocking vibration of the pile cap.

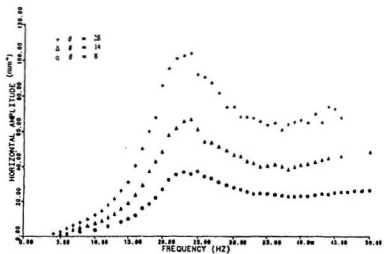
The stiffness and damping for horizontal and rocking vibration of the pile group are shown in Fig. 7.9. From this figure it can be seen that the stiffness of pile group is reduced and damping is increased by the pile-soil-pile interaction, as was noted previously. For comparison, the frequency response curves of stiffness and damping for a single pile are included in Fig. 7.9.

The group efficiency ratio, GER, for the horizontal vibration is shown in Fig. 7.10. It can be noticed that the GER for stiffness is less than 1, implying that the stiffness of the group is reduced by the pile-soil-pile interaction (by more than 50% larger than 1 for damping, implying that the damping of the pile group is increased by interaction. Furthermore, it can be noted that the GER for stiffness and damping is not constant, rather it varies with frequency. With the frequency range considered

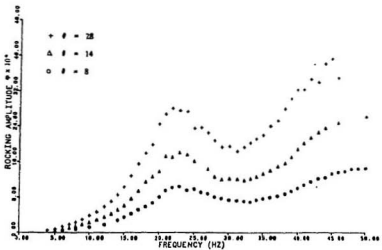
here, GER for stiffness is reduced and that for damping is increased with an increase in frequency.

### 7.3 Nonlinear Vibration of Pile Group

A larger exciter, weighing 4.9 kN, was fixed on the pile cap by foundation bolt to produce the harmonic excitation in both X - direction and Y - direction. The active component of the horizontal excitation was situated 0.2 m above the cap surface, and the center of gravity of the cap-exciter system was 0.24 m below the cap surface. Representing the number of additional eccentric masses placed in the slotted steel plate capping the exciter with  $L$ , Table 7.4 provides the range of excitation intensities,  $m_e e$ , employed in the experiments. As shown later,  $L$  is used in this section to represent the excitation intensity that were applied in the nonlinear vibration tests. The maximum horizontal amplitude of the pile group was measured to be 1.4 mm ( or  $4.4 \times 10^{-3}d$ ) at top of the pile cap, with a corresponding maximum acceleration of 1.13g; this represents a rather intense harmonic vibration, resulting in a nonlinear vibration of the pile group. Under horizontal excitation, the cap produced coupled horizontal and rocking vibration. The horizontal and rocking displacement response curves measured on the cap of the group in different excitation intensities are shown in Fig. 7.11 and 7.12 for X - direction and Y - direction, respectively. It should be explained that the results for the excitation intensity  $L = 6$  are missing from Fig. 7.11 and 7.12 because of problems encountered in measuring the rocking vibration for this case.



(a)



(b)

Figure 7.6: Measured on the cap (a) for horizontal response; (b) for rocking response

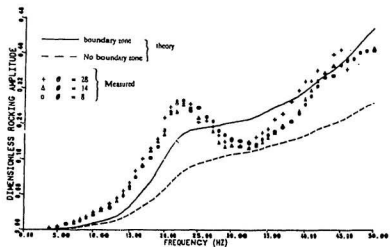
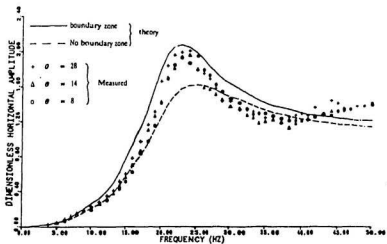


Figure 7.7: Comparison of theoretical predictions with experimental results

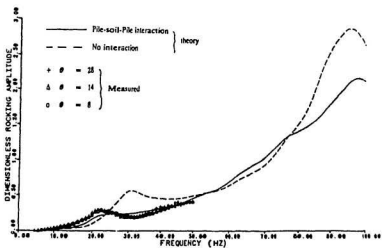
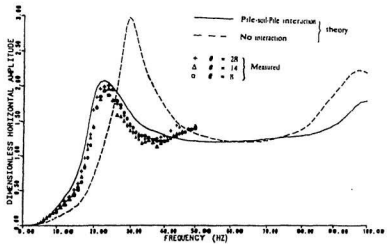


Figure 7.8: Influence of pile-soil-pile interaction on dynamic response of group

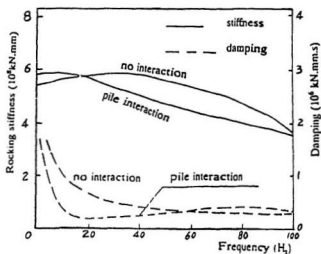
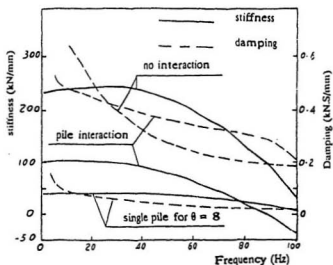


Figure 7.9: Stiffness and damping of pile group

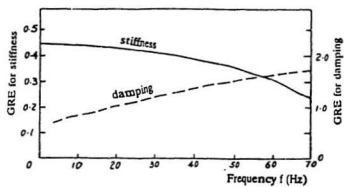


Figure 7.10: GER (group efficiency ratio) for horizontal vibration of group

No. of additional mass	Excitation intensity
$L$	$m_{ce}(kg.m.m)$
0	472
1	887
2	1360
6	3870

Table 7.4: Excitation scheme adopted for nonlinear vibration

From the measured response curves shown in Fig. 7.11 and 7.12, it can be observed that the resonance peaks reduce with increasing excitation intensity and the vibration amplitudes are not proportional to excitation intensity at all frequencies. These are typical features of nonlinear vibration. The detail nonlinear features of the group vibration will be described in the following.

To depict the nonlinear response theoretically, the boundary zone concept, which accounts for yielding of soil around the pile, was incorporated into the linear-elastic-based mathematical model. This model provides for the gradual expansion of the yield zone as the excitation level increase. Tables 7.5 and 7.6 show the parameters of boundary zone chosen for matching the theoretical results with the measured response curves for the X- and Y-direction tests, respectively.

As can be noted from Tables 7.5 and 7.6, the damping ratios of inner and outer zones remain unchanged for the cases studied as in the case of linear vibration; thickness of the boundary zone, however, varies for the cases considered. From the comparison of the parameters of boundary zone in linear vibration and in nonlinear

vibration, it can be observed that for the excitation intensity  $L = 0$  the thickness of the boundary zone is reduced from  $0.5r_0$  for the linear case to  $0.3r_0$  for the nonlinear case. It is also of interest to observe that the boundary zone behaves in a stiffer manner after having been yield during the experiments that were conducted a year earlier in testing the pile group under linear vibration conditions.

In matching the measured data, allowance had to be made for the pile separation. For instance, for the strongest excitation used ( $L = 6$ ), the separation between the pile and soil, denoted by  $l_s$ , was  $310mm(0.97d)$  and  $350mm(1.1d)$  for tests in the X- and Y- direction, respectively. It should be mentioned that the separation lengths could not be physically measured yet in the field at present; the values given here were inferred by using a trial-and-error technique of matching the theoretical and measured response curves. The separation length between the pile and soil (free pile length) depends on the vibration amplitude of the pile and the soil properties. Based on large-scale tests reported by Han and Novak (1988) involving strong vibration (nonlinear) of steel pipe piles in loose sand, curves relating separation length to vibration amplitude were empirically developed. These curves, along with those obtained from the full-scale tests in clayey soils described in this chapter are shown in Fig. 7.13.

Comparison of the experimental response curves with the theoretical predictions is shown in Fig. 7.14 for X-direction excitation and in Fig. 7.15 for Y-direction. It can be noted that the theoretical predictions agree with the measured results quite well for both horizontal and rocking vibrations. It can be concluded from these

Excitation Intensity	Modulus Ratio	Thickness Ratio	Damping Ratio	Damping Ratio	Poisson's Ratio
$L$	$G_i/G_o$	$t_m/r_o$	Inner, $D_i$	Outer, $D_o$	$\nu$
0	0.2	0.3	0.07	0.035	0.3
1	0.1	0.3	0.07	0.035	0.3
2	0.1	0.6	0.07	0.035	0.3
6	0.1	0.9	0.07	0.035	0.3

Table 7.5: Boundary zone parameters for nonlinear vibration in X-direction

Excitation Intensity	Modulus Ratio	Thickness Ratio	Damping Ratio	Damping Ratio	Poisson's Ratio
$L$	$G_i/G_o$	$t_m/r_o$	Inner, $D_i$	Outer, $D_o$	$\nu$
0	0.1	0.3	0.07	0.035	0.3
1	0.1	0.6	0.07	0.035	0.3
2	0.1	0.9	0.07	0.035	0.3
6	0.1	0.9	0.07	0.035	0.3

Table 7.6: Boundary zone parameters for nonlinear vibration in Y-direction

results that the employed mathematical model, incorporating a boundary zone, is capable of capturing the nonlinear vibration of a pile group. The results show that the resonant frequency of the pile group reduces and the resonant amplitude increases as the excitation intensity increases. For instance, when the excitation level is increased from  $L = 0$  to  $L = 6$ , the resonant frequency of the pile group reduces from 27 Hz to 16.2 Hz for the X-direction test and from 24 Hz to 15.8 Hz for the Y-direction test.

The theoretically determined horizontal and rocking stiffness of the pile group under different excitation intensities are shown in Fig. 7.16. It can be noted that for both horizontal and rocking modes of vibration, stiffness of the pile group decreases as the excitation intensity increases. The reduction in stiffness of the pile group as the excitation intensity increases is mainly due to development and growth of the yield zone of soil. These reductions are quite pronounced. For instance, horizontal stiffness of the pile group reduces by almost half, for both X-direction and Y-direction, when the excitation intensity increases from  $L = 0$  to  $L = 6$ . This reduction can principally be attributed to an increase in the thickness of the boundary zone and the soil-pile separation effects. As can be expected, there is an appreciable difference in the rocking stiffness between X- and Y-directions at all excitation levels. This difference stems from different pile arrangements in these directions (see Fig. 7.4).

Some of the salient features of the nonlinear vibration of the pile group are listed in Tables 7.7 and 7.8 for X- and Y-direction, respectively. The stiffnesses and damp-

Excitation intensity $L$	Resonant frequency (Hz)	Horizontal		Rocking	
		Stiffness ( $MN/m$ )	Damping ratio, $D_x$	Stiffness ( $10^2 MN.m$ )	Damping ratio, $D_\psi$
0	27	119	0.43	10.1	0.056
1	24	106	0.34	9.58	0.030
2	22	91	0.29	8.87	0.029
6	16.2	53.0	0.20	7.98	0.004

Table 7.7: Theoretical dynamic behaviour of the pile group in X-direction

Excitation intensity $L$	Resonant frequency (Hz)	Horizontal		Rocking	
		Stiffness ( $MN/m$ )	Damping ratio, $D_x$	Stiffness ( $10^2 MN.m$ )	Damping ratio, $D_\psi$
0	24	114	0.34	5.40	0.039
1	22	97.7	0.29	4.97	0.039
2	20	87.7	0.25	4.67	0.039
6	15.8	54.0	0.20	4.31	0.018

Table 7.8: Theoretical dynamic behaviour of the pile group in Y-direction

ing ratios shown in these tables correspond to the resonant frequency for the first mode of vibration of the pile group.

From the parameters shown in Tables 7.7 and 7.8 and the response illustrated in Figs 7.11 to 7.16, it can be concluded that the resonant frequency of the pile group reduces and the resonant amplitude increases as the excitation intensity increases. Horizontal stiffness and rocking stiffness of the pile group reduce as the excitation intensity increases. The reasons may be that increases in excitation intensity result in widening of the boundary zone and, at higher levels, separation of piles from the surrounding soil. It can be noted that the damping ratio of the group reduces for

both horizontal and rocking modes of vibration as the excitation intensity increases. This trend can be attributed to the fact that development and spread of a weakened zone of soil and a concomitant pile separation result in a reduction in the radiation damping (at higher frequencies, radiation damping is the predominant component of damping).

The range of parameters of the boundary zone is recommended as guide lines for engineering practice : the thickness of boundary zone within  $0.5r_o$  or  $1.0r_o$  and  $G_i/G_o$  within 0.5. As an example consider the experiments where excitation  $\theta = 8$ , the measured horizontal displacements were shown in Fig. 7.6. The same parameters were used as in Fig. 7.7, i.e.,  $t_m/r_o = 0.5$ ,  $\beta_i = 0.07$  and  $\beta_o = 0.035$ , but  $G_i/G_o = 0.1, 0.25$  and  $0.5$  were taken to obtain different theoretical response curves as shown in Fig. 7.17. From the comparison in Fig. 7.17, it can be seen that the response curve for  $G_i/G_o = 0.1$  is the upper bound and the curve for  $G_i/G_o = 0.5$  is the lower bound. The range for  $G_i/G_o$  is 0.1 to 0.5.

## 7.4 Summary and Conclusions

A comprehensive study involving both theoretical analysis and field testing on full-size pile group was undertaken. Field tests were performed on a pile group comprised of six cast-in-place reinforced concrete piles, embedded in a relatively homogeneous silty clay formation. The theoretical calculations for matching the observed field data were made using the approach of dynamic interaction factors. To properly account for soil yielding under strong vibrations, provisions were made for the in-

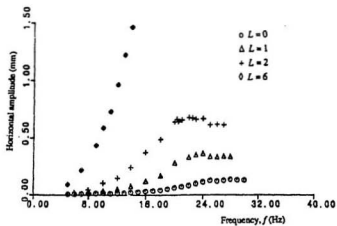
clusion of a weakened zone in the theoretical model. Reasonably good agreement was obtained between the theoretical predictions and the field-measured data. The findings from this study have provided some insight into the influence of pile-soil-pile interaction on the dynamic response of pile groups. These findings include the following:

(1) Dynamic response of the pile group under strong lateral excitation exhibits typical nonlinear features; for both horizontal and rocking modes of vibration, stiffness and damping ratio of the pile group reduce as the excitation intensity increases. This in turn results in a reduction of the resonant frequency and an increase in the resonant amplitude. For the case studied horizontal stiffness of the pile group under the strongest excitation intensity was found to be reduced to almost half of that arising from the lowest excitation intensity; this observation indicates that the pile group response in a nonlinear manner.

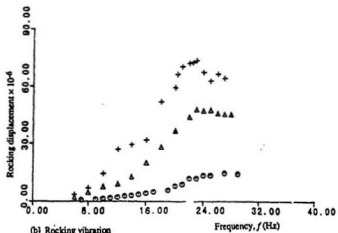
(2) Horizontal stiffness was found not to be appreciably affected by the pile group configuration. As to be expected, rocking stiffness was found to be strongly dependent upon pile group configuration. For the case studied, rocking stiffness in the X-direction (comprised of three piles in each row) was almost twice that in the Y-direction (comprised of two piles).

(3) Over the frequency range employed, the pile-soil-pile interaction results in a reduction in the stiffness and an increase in the damping of the pile group.

(4) From comparison of the theoretical predictions with the field-measured results it was deduced that, under moderate levels of excitation, both pile-soil-pile interaction effects and soil yielding play a significant role in the overall dynamic response of pile groups. Inclusion of the mathematical aspects related to these effects are, therefore, recommended in numerical models used for analyzing such problems.

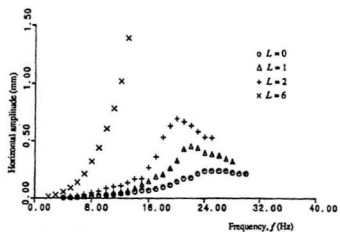


(a) Horizontal vibration

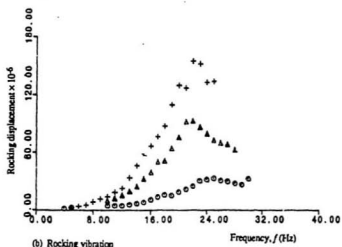


(b) Rocking vibration

Figure 7.11: Measured displacement response of the pile group in X-direction, (a) horizontal vibration, (b) rocking vibration.



(a) Horizontal vibration



(b) Rocking vibration

Figure 7.12: Measured displacement response of the pile group in Y-direction, (a) horizontal vibration, (b) rocking vibration.

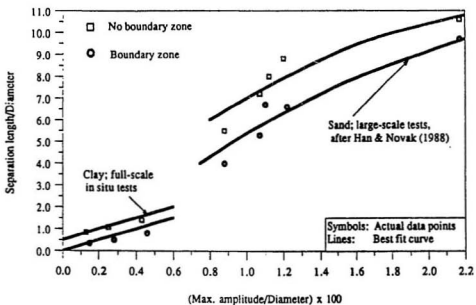
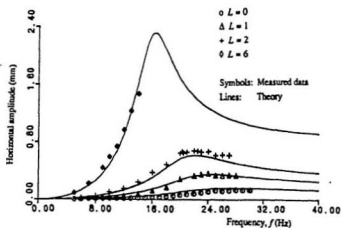
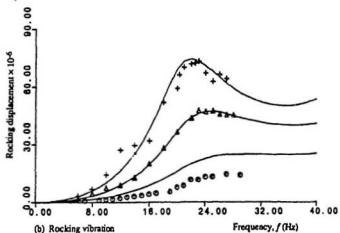


Figure 7.13: Theoretical-deduced relationships between pile separation and maximum vibration amplitude

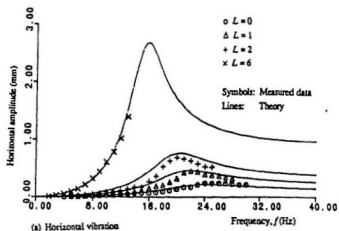


(a) Horizontal vibration

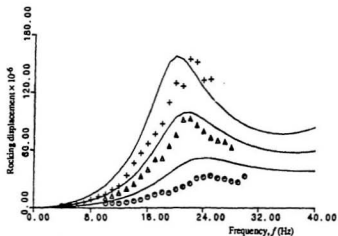


(b) Rocking vibration

Figure 7.14: Comparison of theoretical and measured response of the group in X-direction, (a) horizontal vibration, (b) rocking vibration.

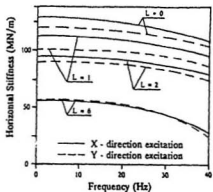


(a) Horizontal vibration

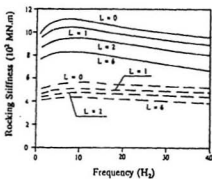


(b) Rocking vibration

Figure 7.15: Comparison of theoretical and measured response of the group in Y-direction, (a) horizontal vibration, (b) rocking vibration.



(a) Horizontal Vibration



(b) Rocking Vibration

Figure 7.16: Stiffness of the pile group under different excitation intensities (a) horizontal vibration, (b) rocking vibration.

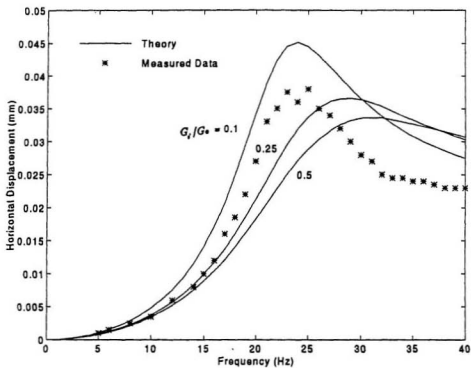


Fig. 7.17 Comparison of measured response for  $\theta = 8$  with theoretical predictions in different parameters of boundary zone.

## Chapter 8

# Influence of Frozen Soil on Piles

Partially frozen subsoil conditions, such as the frozen of a 0.5 m thick layer just below the surface, can be encountered in large regions of the world, particularly in most of Canada during the winter months. Geotechnical engineers are sometimes confronted with problems concerning the design and construction of structures on sites underlain by permafrost, ice or simply frozen soil layers. The general practice under these conditions is to use pile foundations for the support of above-grade heated structures. Although a considerable body of analysis and field observations is now available to support some of the techniques that have been proposed for the static design of piles in frozen soils (e.g., Nixon, 1978, 1984; Nixon and McRoberts, 1976; Morgenstern et al., 1980 and Crowther, 1990), no field measurements are available for the dynamic response of piles in frozen soil.

### 8.1 Pile Group

To study the influence of a frozen soil layer on the dynamic response of a pile group, a similar set of experiments as described in the last chapter was performed during

the winter months when the ground surface was covered by a layer of frozen soil, 0.35 m thick. The shear wave velocity of the frozen soil layer was established by employing the surface wave method, and the measured shear wave velocity of the layer was 540 m/s which, incidentally, is about four times greater than the unfrozen portion just beneath it.

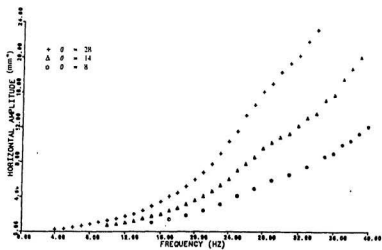
The smaller exciter was used in Y-direction only, and the excitation intensities were the same as in linear vibration tests as shown in Table 7.3. In this case, due to the increased soil resistance resulting from soil freezing, the maximum horizontal displacement that could be achieved (with the employed exciter system) was only 0.023 mm. For such small displacements and hence strains, it was considered inappropriate to allow for either soil separation or yielding in the frozen soil layer for the analysis. The measured horizontal and rocking displacement response curves of the pile group for different excitation intensities are shown in Fig. 8.1.

The comparison of experimental response curves with the theoretical predictions (approach of dynamic interaction factor) is shown in Fig. 8.2 for horizontal and rocking vibration of the pile group. Because of the much higher resonant frequency and the limitation of the exciter, the resonant peak could not be obtained. However, the results, at least over the portion for which data were available, show a satisfactory agreement with the measured response.

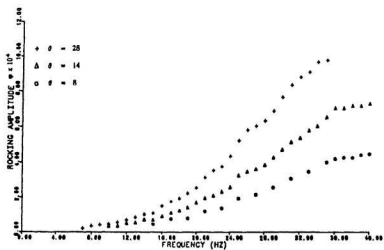
In order to assess where the resonant frequency for the pile group with a layer of frozen soil would occur, the theoretical calculations were extended to a frequency

of 100 Hz. These results are shown in Fig. 8.3 for the horizontal and rocking vibration. For comparison, the results for the case without frozen layer as described in preceding section are also plotted along with the measured data. From this figure it can be seen that the resonant frequency for the group with frozen soil layer is much higher than that without the frozen soil.

The stiffness and damping of the group with and without the frozen layer is shown in Fig. 8.4. From this figure it can be seen that the stiffness and damping of the pile group with the frozen soil layer are much higher than those without the frozen soil. For instance, the horizontal stiffness of the pile group is increased by a factor of eight as compared to the case without frozen soil. From these observations it can be concluded that the presence of even a thin layer of frozen soil (in the order of  $1/20$  of the pile length) can have a profound influence on the response of pile group, as was demonstrated by a significant reduction in displacements and an increase in the resonant frequency.



(a)



(b)

Figure 8.1: Measured displacement response of pile group with frozen layer (a) horizontal vibration, (b) rocking vibration

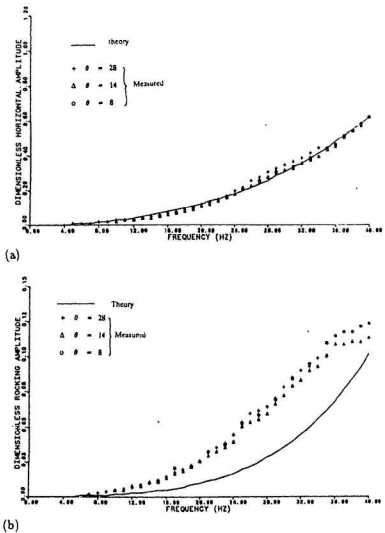


Figure 8.2: Comparison of theoretical predictions with measured response of pile group with frozen layer (a) horizontal vibration, (b) rocking vibration

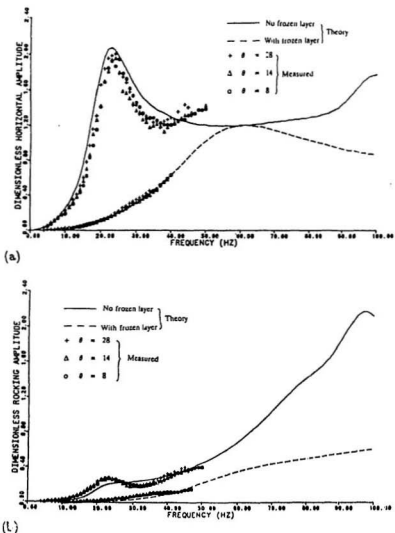
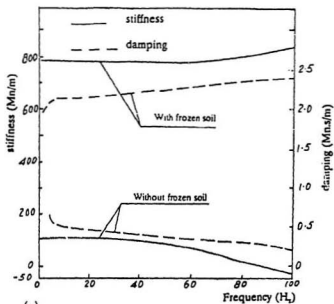
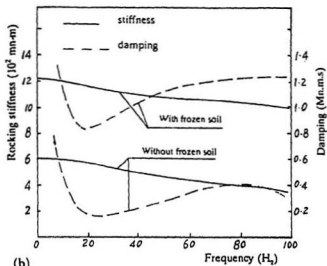


Figure 8.3: Effect of frozen soil on dynamic response of pile group (a) horizontal vibration, (b) rocking vibration



(a)



(b)

Figure 8.4: Effect of frozen soil on stiffness and damping of pile group (a) horizontal vibration, (b) rocking vibration

## 8.2 Single Piles

For comparison with the pile group, the dynamic experiments were also conducted on single piles which have the same properties and the same size as those in the pile group, and placed in the same site as shown in Fig. 7.1. The cast-in-place reinforced concrete pile was 7.5 m long and 0.32 m in diameter, capped by a 0.3 m thick concrete block with 1.1 m long by 0.9 m wide. The pile cap had a clearance of 0.02 m and 0.1 m above the ground surface under frozen ground and thawed conditions, respectively, weighing 7.25 kN. The smaller exciter, as shown in Table 7.3, was fixed on the cap by foundation bolts, and the centre of gravity of the cap-exciter system was 0.1 m below the cap surface. The active component of the horizontal excitation was situated about 0.2 m above the cap surface. The steady-state dynamic response of the single pile under horizontal excitation was measured under the condition with frozen soil layer and without frozen soil, respectively. In the case with frozen soil, the thickness of frozen soil layer was 0.4 m and its shear wave velocity was measured to be 540 m/s.

The horizontal response curves for the single pile without the frozen soil were measured and shown in Fig. 8.5, under excitation intensities corresponding to  $\theta = 8, 14$  and 28. The maximum displacement amplitude and acceleration on top of the pile cap were measured to be 1.25 mm and 1.2  $g$ , respectively. From the measured response curves shown in Fig. 8.5, it can be seen that the resonant peaks reduced with the increase of excitation intensities, indicated that nonlinear response occurred. The nonlinearity of dynamic response of the single pile will be discussed

later in this section. The horizontal response curves for the pile in the presence of a frozen soil layer under two excitation levels corresponding to  $\theta = 8$  and 28 were measured and shown in Fig. 8.6. The maximum horizontal displacement measured on the cap was only 0.051 mm. Because of the much higher resonant frequency and the limitation of the exciter employed, the resonant peaks could not be obtained in the case with frozen soil.

For the case without frozen soil, two approaches are employed for analysis of dynamic response of the single pile. In one approach, the boundary zone around the pile is accounted for. The weakened zone is assumed with  $G_i/G_o = 0.1$ ,  $t_m/r_o = 0.5$ ,  $\beta_i = 0.04$  and  $\beta_o = 0.02$ . Since nonlinear response occurred, it was considered reasonable to allow for pile separation in the analysis. Using a trial-and-error technique, different separation lengths were chosen for each excitation intensity until the optimum match between the theoretical and experimental results was obtained. In this way, the separation lengths,  $l_s$ , are 0.15 m, 0.19 m and 0.27 m corresponding to  $\theta = 8, 14$  and 28, respectively. Comparison between the measured and theoretical calculations, as seen in Fig. 8.7, shows a close agreement at all excitation levels.

As another approach, the weakened zone is not accounted for. In the absence of the yielded zone, a much larger pile separation (relative to the previous case) has to be required to provide a close match with the observed data. In this way, the separation lengths,  $l_s$ , should be 0.32 m, 0.36 m and 0.44 m corresponding to  $\theta = 8, 14$  and 28, respectively. Fig. 8.8 illustrates the comparison between the calculated and observed data for the three levels of intensity. It can be seen that the measured

results agree with the calculated response curves with the larger pile separations employed in analysis.

In the case with frozen soil, the maximum measured displacement was only 0.051 mm. For such small displacements and hence strains, it was considered inappropriate to allow for either soil separation or yielding in the analysis. Fig. 8.9 depicts the comparison between computed and measured response of the pile. The results, at least over the portion for which data were available, appear to satisfy the measured response quite well. In order to assess where the resonant frequency for the soil system underlain by a layer of frozen soil would occur, the theoretical calculations were extended to a frequency of 100 Hz. These results, for excitation levels corresponding to  $\theta = 8$  and 28 are shown in Fig. 8.10 and 8.11, respectively. For comparison, the calculated response curves for the case with no frozen layer also plotted along with the measured data. It can be seen from these figures that the resonant frequency for the pile with frozen soil layer is much higher than that without the frozen soil layer. The theoretical results also indicate that a secondary mode of vibration develops at approximately 100 Hz for the case with no frozen soil, which is primarily due to the coupled horizontal and rocking vibration of the pile cap.

The theoretical horizontal stiffness and damping coefficient of the pile for both cases with frozen soil layer and without frozen soil are shown in Fig. 8.12. It can be noted that the pile stiffness in the case with frozen soil layer is much higher than that without frozen soil. In the case without frozen soil, pile stiffness decreases with increasing excitation intensity; however, with the frozen layer, stiffness remains al-

Case	Excitation intensity,	Resonant frequency (Hz)	Soil-pile system, Horizontal response		Pile separation/pile diameter ( $l_p/d_p$ )	
			Stiffness, $K$ (MN/m)	Damping ratio, $D$	With boundary zone	Without boundary zone
With frozen soil layer	$\theta = 8$	59.0	587	0.149	N/A	N/A
	$\theta = 28$					
Without frozen soil	$\theta = 8$	17.6	40.5	0.108	0.47	1.00
	$\theta = 14$	16.8	38.1	0.103	0.59	1.13
	$\theta = 28$	15.6	33.8	0.096	0.84	1.38

Table 8.1: Theoretical dynamic behaviour of the pile with and without the frozen soil layer

most constant over the range of applied excitation (i.e.,  $\theta = 8$  and 28). This stems from the fact that with the frozen soil layer the pile response is almost linear and its theoretical resonant frequency, as shown in Fig. 8.10 and 8.11, remains unchanged (59 Hz) at the two different intensities tested. Some of the salient features of the pile response, with and without the frozen layer, are shown in Table 8.1. It should be noted that the stiffness and damping ratio in the table are those corresponding to the resonant frequency of the pile.

From the figures and Table 8.1, it can be concluded that the presence of frozen soil, even in a relatively thin layer, can significantly affect the dynamic behaviour of piles. Although the thickness of the frozen layer was about 1/19 of the pile length, its presence increased the horizontal stiffness of the pile by 15 times and its res-

onant frequency by about 3.5 times. Furthermore, the frozen soil layer, over the excitation range tested, largely removed the nonlinearity in the vibration which was manifested in the case without the frozen soil by a shift in the resonance frequency (from 17.6 Hz to 15.6 Hz) and a reduction in stiffness (from 40.5 to 33.8  $M \cdot s^{-2} \cdot m$ ) as the excitation level was increased from  $\theta = 8$  to  $\theta = 28$ .

The experiments described in chapter 5, 7 and 8 were conducted before the Ph.D. program. The measured results were used in this study to verify the new theory, boundary zone model with non-reflective interface. The dimensionless frequency,  $a_o = \omega r_o / V_s$ , in the experiments is  $a_o = 0.2$  to  $0.3$ . From Fig. 3.16, it can be seen that the new theory is identical with the old theory (Novak's theory) in the lower frequency range. However, in some other case,  $a_o \leq 0.5$ , the results from the theory will be different with those ones from the old theory. It should also be remembered that the mass was ignored in the boundary zone for Novak's model, which is unrealistic. Therefore, the new theory presented in the thesis is reasonable for applications.

The new theory is verified by means of comparison with the experimental results. In the lower frequency range, the results from the new theory are identical with those previously published by Han and others.

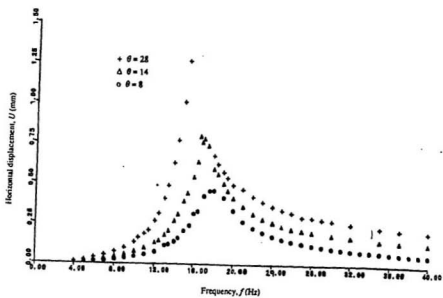


Figure 8.5: Measured horizontal displacement response of the pile with no frozen soil

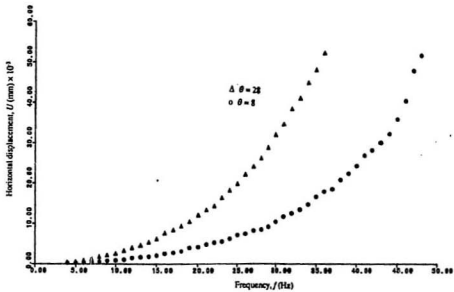


Figure 8.6: Measured horizontal displacement response of the pile with frozen soil layer

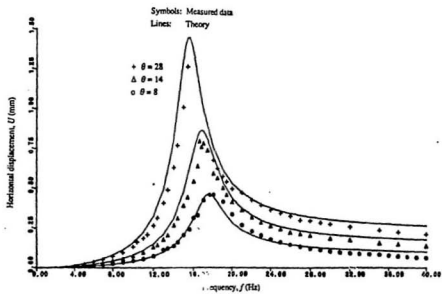


Figure 8.7: Measured and theoretical response of the pile with boundary zone in the case without frozen soil

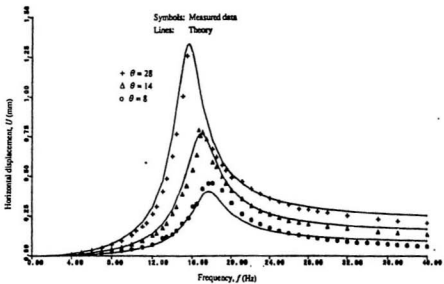


Figure 8.8: Measured and theoretical response of the pile with no boundary zone in the case without frozen soil

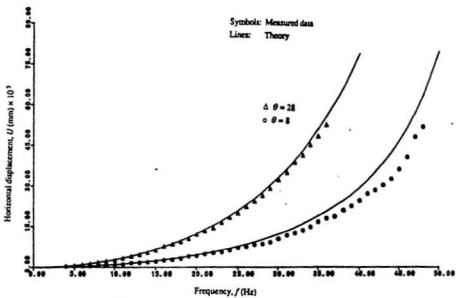


Figure 8.9: Measured and theoretical response of the pile in the case with a frozen soil layer

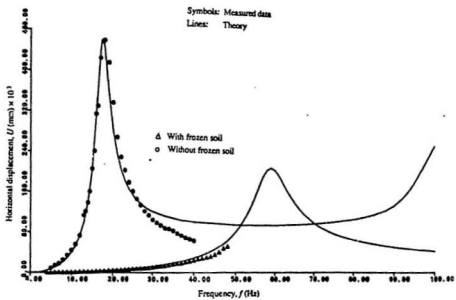


Figure 8.10: Relative influence of a frozen soil layer on the pile response at  $\theta = 8$

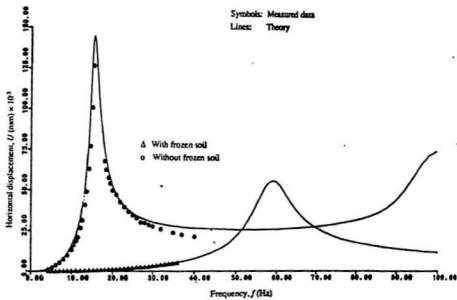


Figure 8.11: Relative influence of a frozen soil layer on the pile response at  $\theta = 28$

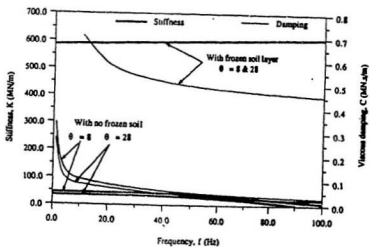


Figure 8.12: Influence of a frozen soil layer on the stiffness and damping of a single pile

## Chapter 9

# Summary, Conclusions and Recommendations

A systematic study is presented for dynamic behaviour of pile foundations under harmonic excitations. In this thesis we have accomplished the following:

(1) The impedances for a composite soil layer are formulated based on a new model of the boundary zone with non-reflective interface. A parabolic variation of the medium properties is assumed, so that the boundary zone has properties smoothly approaching those of the outer zone to alleviate wave reflections from the interface. The impedances of the soil layer are presented for different modes of vibration, included vertical, torsional, radial, rocking and horizontal vibration.

(2) With the impedances of the soil layer formulated, the stiffness and damping of single piles in layered media are derived using the finite element method. The vertical, horizontal and rocking impedances of single pile are presented. To determine whether the basically linear theory can reproduce the behaviour of piles under

strong excitation, dynamic experiments on large-scale model piles, steel pipe piles with a diameter of 133 mm and a length of 3.38 m, were conducted with strong horizontal and vertical vibration. The frequency response curves and deflection curves of the piles were experimentally established in the field for different intensities of excitation and contact conditions between the pile cap and the soil surface.

(3) Using the properties of the single pile and accounting for the group effect, pile-soil-pile interaction, the group stiffness and damping are evaluated by means of the interaction factor approach. To investigate the dynamic behaviour of pile group, the experiments on a full scale pile group, comprised of six cast-in-place reinforced concrete piles with 7.5 m long and 0.32 m in diameter, were carried out in the field under different conditions: linear vibration and nonlinear vibration. In order to investigate the influence of frozen soil layer on dynamic behaviour of piles, the experiments were also conducted during the winter time when the surface was covered by a frozen soil layer.

The following conclusions may be drawn:

(1) The impedances of the soil layer are evaluated over wide range of the parameters involved and compared with those obtained from Novak's and Veletsos's model, which are the leading models at present, as well as compared with those for a homogeneous layer. The results from the present analysis are smooth curves over a wide range, which indicates that the wave reflections from the interface are removed because it embodies a continuous variation in soil properties in the boundary zone

with smooth transition ( continuous derivatives ) into the outer zone. Thus, the impedances ( soil stiffness and damping ) presented in this study are considered to be more suitable to practical applications than previous ones.

(2) Since the pile response at large amplitude exhibits typical nonlinear features, consideration of a weakened zone ( boundary zone ) around the pile and pile separation is necessary. Good agreement can be achieved between the experimental and theoretical response curves when the characteristics of soil are suitable chosen, without resort the truly nonlinear analysis. The nonlinearity of the soil-pile system is accounted for approximately by means of the model of boundary zone.

How to select suitable characteristics of soil depends on the specific conditions in the field, such as the installation of the piles, the properties of soil and piles and the excitation intensity. Under different excitation, the range of the thickness of boundary zone within  $0.5r_0$  or  $1.0r_0$ , and  $G_i/G_0$  within 0.5.

(3) The excitation intensity and contact conditions between the pile and soil and between the cap and soil surface change the stiffness and damping of piles. Under repeated loading, the stiffness and damping of single piles decrease, so that the resonant frequency decreases and resonant displacement increases.

(4) Dynamic response of the pile group under strong lateral excitation also exhibits typical nonlinear features; stiffness and damping ratio of the pile group reduce as the excitation intensity increases for both horizontal and rocking mode of vibra-

tion. This in turn results in a reduction of the resonant frequency and an increase in the resonant amplitude.

(5) The pile-soil-pile interaction results in a reduction in the stiffness and an increase in the damping of the group. Both pile-soil-pile interaction and soil yielding around the piles (boundary zone) play a significant role in the overall dynamic response of pile group, even under moderate levels of excitation.

(6) The presence of frozen soil, even in a relatively thin layer, can significantly affect the dynamic behaviour of piles. In this study, the thickness of the frozen layer was about 1/19 of the pile length, its presence increased the horizontal stiffness of the pile by 15 times and its resonant frequency by about 3.5 times.

### **Suggestions for Further Research**

(1) In the case of horizontal excitation, a general solution involving variations of soil properties in the boundary zone proves to be extremely difficult because of cross coupling between the radial and tangential displacements. Hence, constant  $\lambda_i^*$  and  $G_i^*$  are assumed for horizontal excitation in this study. In the lower frequency region the undulations of the impedance functions caused by wave reflections from the interface can not be observed, but wave reflections occur in higher frequency region. If the demand for higher frequency rises in applications, further research should be done for the case of horizontal excitation.

(2) Since the properties of the pile foundation are established, they can be incorporated into the examination of pile-structure interaction using the substructure approach just as with other type of foundation. With the better understanding of the behaviour of piles, the dynamic analysis of structures supported with pile foundations can be conducted, such as the soil-pile-structure interaction under wave loading in offshore engineering or seismic response of buildings supported with piles. Further research should be done in both theory and experiment in order to apply the advanced theory of pile dynamics to engineering practice.

(3) Dynamic measurements on bearing capacity of piles, integrity testing and pile driving are often employed in constructions, using Wave Equation Analysis of Piles (WEAP) or Pile Driving Analysis (PDA). One of the more important problem in matching the predications with the measured data is how to simulate the soil-pile interaction. The subject of soil-pile interaction is investigated comprehensively in both theory and experiments in this study. Further research of model tests on centrifuge facilities and full-scale tests in the field are needed.

## References

- Abramowitz, M. and Segun, I.A. (1968). "Handbook of mathematical functions", Dover Publications, Inc., New York, p1046.
- American Petroleum Institute (1986). "Recommended practice for planning, designing and constructing fixed offshore platforms", (16th edition). Dallas, TX.
- Baba, K. (1991). "Dynamic analysis of soil-pile interaction system under earthquake type loading", proc. of 2nd. Int. Conf. on Recent Advances in Geotech. Earthq. Eng. and Soil Dyn. St. Louis, Missouri.
- Banerjee, P.K. (1978). "Analysis of axially and laterally loaded pile groups", Chapter 9 in Developments in Soil Mechanics, Ed. C.R.Scott, Appl. Sci. Pub., London, 317-346.
- Banerjee, P.K. and Sen, R. (1987). "Dynamic behaviour of axially and laterally loaded piles and pile groups", Chapter 3 in Dynamic Behaviour of Foundations and Buried Structures, Ed., P.K.Banerjee, Elsevier App.Sc., London. 95-133.
- Blaney, G.W., Kausel, E. and Roesset, J.M. (1976). "Dynamic stiffness of piles", Proc., 2nd Int. Conf. on Num. Methods in Geomech., Blacksburg, Virginia, 1001-1012.
- Butterfield, R. and Banerjee, P.K. (1971). "The elastic analysis of compressible piles and pile groups", Geotechnique, Vol.21, 43-60.
- Clough, R.W. and Penzien, J. (1975). "Dynamics of structures", McGraw-Hill Inc.
- Clough, R.W. (1992). "A structural engineer's view of soil-structure interaction", Developments in Dynamic Soil-Structure Interaction, Kemer, Antalya, Turkey, July 8-16, 91-109.
- Crouse, C.B. and Chang, L. (1987). "Dynamic testing and analysis of pile-group foundations", Geotech. Special Pub., ASCE, No.11, 79-98.
- Crowther, G.S. (1990). "Analysis of laterally loaded piles embedded in layered frozen soil", J. of Geotech. Engrg., ASCE, 116(7), 1137-1152.
- De Beer, E. et al. (Eds.) (1977). "The effects of horizontal loads on piles due to surcharge or seismic effects", Proc. of Specialty Session 10, 9th ICSMFE, TOKYO, July 14, 200p.

- Dobry, R., Vincente, E., O'Rourke, M.J. and Roesset, J.M. (1982). "Horizontal stiffness and damping of single piles", *J. Geotech. Eng. Div., ASCE*, Vol. 108, No. GT3, 439-459.
- Dobry, R. and Gazetas, G. (1988). "Simple method for dynamic stiffness and damping of floating pile groups", *Geotechnique*, Vol.38, No.4, 557-574.
- Dotson, K.W. and Veletsos, A.S. (1990). "Vertical and torsional impedances of radially inhomogeneous viscoelastic soil layers", *Soil Dyn. and Earthq. Eng.*, Vol.9, No.3, 110-119.
- El-Hifnawy, L. and Novak, M. (1986). "Uplift in seismic response of pile supported buildings", *J. Earthq. Eng. and Struct. Dyn.*, Vol.14, 573-593.
- El-Hifnawy, L. and Novak, M. (1987). "Seismic response of buildings with pile uplift", *Proc. 5th Canadian Conf. on Earthq. Eng.*, Ottawa, July, 181-190.
- El-Marsafawi, H., Han, Y.C. and Novak, M. (1992). "Dynamic experiments on two pile groups", *J. Geotech. Eng., ASCE*, 118(4), 576-592.
- El-Sharnouby, B. and Novak, M. (1985). "Static and low frequency response of pile groups", *Canadian Geotech. J.*, Vol.22, No.1, 79-94.
- El-Sharnouby, B. and Novak, M. (1986). "Flexibility coefficients and interaction factors for pile group analysis", *Canadian Geotech. J.*, Vol.23, 441-450.
- El-Sharnouby, B. and Novak, M. (1990). "Stiffness constants and interaction factors for vertical response of pile groups", *Canadian Geotech. J.*, Vol. 27, NO.6, 813-822.
- Finn, W.D.L. and Gohl, W.B. (1987). "Centrifuge model studies of piles under simulated earthquake loading", *Geotech. Special Pub., ASCE*, No.11, 21-38.
- Gazetas, G. and Makris, N. (1991). "Dynamic pile-soil-pile interaction, I: Analysis of axial vibration", *J. Earthq. Eng. and Struct. Dyn.*, Vol.20, No.2.
- Hadjian, A.H., Falgren, R.B. and Lou, L. (1990). "Imperial county services building revisited: a reevaluation with pile-soil-structure interaction", *Proc. 4th US. Nat. Conf. on Earthq. Eng.*, Palm Springs, Cal., Vol.3, 835-844.
- Han, Y.C. (1989). "Coupled vibration of embedded foundation", *J. Geotech. Eng. Div., ASCE*, Vol.115, No.9, 1227-1238.
- Han, Y.C. (1989a). "Dynamic analysis for single piles under horizontal load", *Earthq. Eng. and Eng. Vibration*, Vol.9, No.2, 97-106.
- Han, Y.C. (1989b). "Available method for nonlinear vibration analysis of single piles", *China Civil Eng. J.*, Vol.22, No.3, 39-47.

- Han, Y.C. (1992). "Dynamic behaviour of pile group with pile -soil-pile interaction", China Civil Eng.J., Vol.25, No.5, 24-33.
- Han, Y.C. and Novak, M. (1988a). "Dynamic behaviour of single piles under strong harmonic excitation", Canadian Geotech. J., Vol. 25, No. 3, 523-534.
- Han, Y.C. and Novak, M. (1988b). "Nonlinear vibration of single pile under vertical harmonic excitation". Proc. 3rd Int. Conf. on Appl. Stress-Wave Theory to Piles, Ottawa, 399-408.
- Han, Y.C., and Novak, M. (1992). "Dynamic behaviour of pile group", China Civil Engrg. Journal, Vol.25, No. 5, 24-33.
- Han, Y.C., Vaziri, H. and Hubble, D. (1991). "Dynamic response of pile foundation in forzen soils", 44th Canadian Geotech. Conf., Calgary, Alberta.
- Han, Y.C. and Vaziri, H. (1992). "Dynamic response of pile groups under lateral loading", Soil Dyn. and Earthq. Eng., Vol.11, No.2, 87-99.
- Kaynia, A.M.(1982). "Dynamic stiffness and seismic response of pile groups", MIT Res.Rep. R82-03, Cambridge, MA.
- Kaynia, A.M. and Kausel, E. (1982). "Dynamic behaviour of pile groups", 2nd Int. Conf. on Num. Methods in offshore piling, Austin, TX, 509-532.
- Kaynia, A.M. and Kausel, E. (1990). "Dynamic of piles and pile groups in layered soil media", Int. J. Soil Dyn. and Earthq. Eng.
- Kobori, T., Nakazawa, M., Hijikata, K., Kobayashi, Y., Miura, K., Miyamoto, Y. and Moroi, T. (1991). "Study on dynamic characteristics of a pile group foundation", Proc. of 2nd Int. Conf. on Recent Advances in Geotech. Earthq. Eng. and Soil Dyn., St.Louis, Missouri.
- Kuhlemeyer, R.L. (1979a). "Vertical vibration of piles", J. Geotech. Eng. Div., ASCE, Vol.105, 273-287.
- Kuhlemeyer, R.L. (1979b). "Static and dynamic laterally loaded floating piles", J.Geotech.Eng.Div., ASCE, Vol.105, 289-304.
- Lakshmanan, N. and Minai, R. (1981). "Dynamic soil reaction in radially non-homogeneous soil media", Bul. Disaster Prevention Res. Inst., Kyoto Univ., Vol.31, 79-114.
- Luco, J.E. (1974). "Impedance functions for a rigid foundation on a layered media", Nuclear Engineering and design. Vol.31, 204-217.
- Luco, J.E. (1982). "Linear soil-structure interaction: A Review", Applied Mech. Div., Vol.53, ASME, 41-57.

- Makris, N., Gazetas, G. and Fan, K. (1989). "Analytical results for pile-soil-pile interaction in vertical harmonic motion", ERCAD Conf., Berlin.
- Mamnoon, S.M. and Banerjee, P.K. (1990). "Response of piles and pile groups to traveling SH-waves", J. of Earthq. Eng. and Struct. Dyn., Vol.19, No.4, 597-610.
- Masuda, K., Saseki, F., Urao, K., Veno, K. and Miyamoto, Y. (1986). "Simulation analysis of forced vibration test of actual pile foundation by thin layer method", Proc. Annual Meeting of Archit. Inst. of Japan.
- Matlock, H., Foo, H.C. and Bryant, L.M. (1978). "Simulation of lateral pile behaviour under earthquake motion", Proc. Am. Soc. Civ. Engrg., Specialty Conf. on Earthq. Eng. and Soil Dyn., Pasadena, CA, 2, 600-619.
- Matlock, H. and Foo, H.C. (1980). "Axial analysis of piles using a hysteretic degrading soil model", Proc. Int. Symp. Numer. Methods on Offshore Piling, Institute of Civil Engrg., London, 127-133.
- Merritt, R.G. and Housner, G.W. (1954). "Effect of foundation compliance on earthquake stresses in a multistory building", Bulletin of the Seismological Society of America (BSSA).
- Meyerhof, G.G. (1976). "Bearing capacity and settlement of pile foundations", J. of Geotech. Eng., ASCE, Vol. 102, No. GT3, 195-228.
- Mitwally, H. and Novak, M. (1988). "Pile driving analysis using shaft models and FEM", Proc. 3rd Int. Conf. on Appl. of Stress-Wave Theory to Piles, Ottawa, 455-466.
- Mitwally, H. and Novak, M. (1987). "Response of offshore towers with pile interaction", J. Engrg. Mech., ASCE, 113(7), 1065-1084.
- Mizuhata, K. and Kusakabe, K. (1984). "Comparison of experimental and analytical results of vibration of a full scale pile", Proc. 8th WCEE, San Francisco, Vol.3, 633-640.
- Morgenstern, N.R., Roggensack, W.D., and Weaver, J.S. (1980). "The behaviour of friction piles in ice and ice-rich soils", Can. Geotech. J., 17, 405-415.
- Nixon, J.K. (1978). "Foundation design approaches in permafrost areas", Can. Geotech. J., 15, 96-112.
- Nixon, J.K. (1984). "Laterally loaded piles in permafrost", Can. Geotech. J., 21, 431-438.
- Nixon, J.K., and McRoberts, E.C. (1976). "A design approach for pile foundations in permafrost", Can. Geotech. J. 13, 40-57.

- Nogami, T. (1985). "Flexural response of grouped piles under dynamic loading". *Earthq. Eng. and Struct. Dyn.*, Vol.13, 321-336.
- Nogami, T.(Ed.) (1987). "Dynamic response of pile foundations - Experiment, Analysis and Observation", ASCE, Geotech. Spec. Publication, No.11, 186p.
- Nogami, T., Janes, H.W. and Mosher, R.L. (1991). "Seismic response analysis of pile supported structures assessment of commonly used approximations", Proc. of 2nd Int. Conf. on Recent Advances in Geotech. Earthq. Eng. and Soil Dyn., St.Louis, Missouri.
- Nogami, T. and Konagai, K. (1987). "Dynamic response of vertically loaded nonlinear pile foundations", *J. Geotech. Eng.*, ASCE, 113(2), 147-160.
- Nogami, T. and Konagai, K. (1988). "Time domain flexural response of dynamically loaded single piles", *J. Eng. Mech. Div.*, ASCE, 114(9), 1512-1525.
- Nogami, T., Konagai, K. and Otani, J. (1988). "Nonlinear pile foundation model for time-domain dynamic response analysis", 9th WCEE, Tokyo, Vol.3, 593-598.
- Nogami, T. and Novak, M. (1976). "Soil-pile interaction in vertical vibration", *Earthq. Eng. Struct. Dyn.*, Vol.4, 277-293.
- Novak, M. (1971). "Data reduction from nonlinear response curves", ASCE, *J. of Engineering Mechanics*, 97(EM4):1187-1204.
- Novak, M. (1974). "Dynamic stiffness and damping of piles", *Canadian Geotech. J.*, Vol.11, No.4, 574-598.
- Novak, M. (1977). "Vertical vibration of floating piles", *J. Eng. Mech. Div.*, ASCE, Feb., Vol. 103, No. EM1, 153-168.
- Novak, M. (1991). "Piles under dynamic loads", Proc. of 2nd Int. Conf. on Recent Advances in Geotechnical Earthquake Engineering and Soil Dynamics, Vol.3, St.Louis, Missouri, 250-273.
- Novak, M. and Aboul-Ella, F. (1978a). "Impedance functions of piles in layered media", *J. Eng. Mech. Div.*, ASCE, June, Vol.104, No.EM3, 643-661.
- Novak, M. and Aboul-Ella, F. (1978b). "Stiffness and damping of piles in layered media", Proc. Earthq. Eng. Soil Dyn., ASCE, Special Conf., Pasadena, CA, June 19-21, 704-719.
- Novak, M. and El-Sharnouby, B. (1983). "Stiffness constants of single piles", *J. Geotech. Eng. Div.*, ASCE, Vol. 109, No. 7, 961-974.
- Novak, M. and El-Sharnouby, B. (1984). "Evaluation of dynamic experiments on pile groups", *J. Geotech. Eng.*, ASCE, Vol.110, No.6, 738-756.

- Novak, M. and Han, Y.C. (1990). "Impedances of soil layer with boundary zone", *J. Geotech. Eng.*, ASCE, June, 116(6), 1008-1014.
- Novak, M. and Howell, J.F. (1977). "Torsional vibration of pile foundations", *J. geotech. Eng. Div.*, ASCE, April, Vol.103, No.GT4, 271-285.
- Novak, M. and Howell, J.F. (1978). "Dynamic response of pile foundation in torsion", *J. Geotech. Eng. Div.*, ASCE, Vol.104, No.GT5, 535-552.
- Novak, M. and Nogami, T. (1977). "Soil pile interaction in horizontal vibration", *Earthq. Eng. Struct. Dyn.*, Vol.5, 263-282.
- Novak, M. and Mitwally, H. (1990). "Random response of offshore tower with pile-soil-pile interaction", *J. Offshore Mech. and Arctic Engrg.*, Feb., Vol.112, 35-41.
- Novak, M. and Sheta, M. (1980). "Approximate approach to contact problems of piles", *Proc. Geotech. Eng. Div.*, ASCE National Convention "Dynamic Response of Pile Foundations: Analytical Aspects", Florida, Oct.30, 53-79.
- O'Neill, M.W. (1983) "Group action in offshore piles", *Geotechnical Practice in Offshore Engineering*, ASCE, New York, N.Y.
- O'Neil, M.W. and Dobry, R.(Eds.) (1980). "Dynamic response of pile foundations: Analytical Aspects", ASCE, 112P.
- Otani, J., Nogami, T. and Konagai, K. (1991) "Nonlinear time domain numerical model for pile group under transient dynamic forces", *Proc. of 2nd Int. Conf. on Recent Advances in Geotech. Earthq. Eng. and Soil Dyn.*, St. Louis, Missouri.
- Pak, R.Y. and Jennings, P.C. (1987). "Elastodynamic response of pile under transverse excitations", *J. Eng. Mech. Div.*, ASCE, Vol.113, 1101-1116.
- Parmelee, R.A., Penzien, J., Scheffey, C.F., Seed, H.B. and Thiers, G.R. (1964). "Seismic effects on structures supported on piles extending through deep sensitive clays", *Inst. Engrg. Res.*, U.of California, Berkeley, Rep. SESM 64-2.
- Penzien, J. (1970). "Soil-pile foundation interaction", in *Earthquake Engineering*, Ed. R.L. Wiegel, Prentice-Hall, Englewood Cliffs, New Jersey, 349-381.
- Poulos, H.G. (1968). "Analysis of settlement of pile groups", *Geotechnique*, Vol.18, 449-471.
- Poulos, H.G. (1971). "Behaviour of laterally loaded piles, II-pile groups", *J. Soil Mech. Foundations Div.*, ASCE, Vol.97, No.SM5, 733-751.
- Poulos, H.G. (1979). "Group factors for pile-deflection estimation", *J. Geotech. Eng. Div.*, ASCE, No.GT12, 1489-1509.

- Poulos, H.G. and Davis, E.H. (1980). "Pile foundations analysis and design", John Wiley and Sons, 397p.
- Prakash, S. and Sharma, H.D. (1990). "Pile foundations in engineering practice", Wiley, Chap.7.
- Rajapakse, R.K.N.D. and Shah, A.H. (1987a). "On the longitudinal harmonic motion of an elastic bar embedded in an elastic half space", *Int. J. Solids Structures*, Vol.23, 267-285.
- Rajapakse, R.K.N.D. and Shah, A.H. (1987b). "On the lateral harmonic motion of an elastic bar embedded in an elastic half-space", *Int. J. Solids Structure*, Vol.23, 287-303.
- Rajapakse, R.K.N.D. and Shah, A.H. (1989). "Impedance curves for an elastic pile", *Soil Dyn. and Earthq. Eng.*, Vol.3, No.3, 145-152.
- Roeset, J.M. (1980). "Stiffness and damping coefficients of foundations", *Proc. of Session on Dyn. Response of Pile Foundation: Analytical Aspects*, ASCE, Florida, Oct., 1-30.
- Roeset, J.M., Stokoe, K.H., Baka, J.E. and Kwok, S.T. (1986). "Dynamic response of vertically loaded small-scale piles in sand", *Proc. 8th European Conf. Earthq. Eng.*, Lisbon, Vol.2, 5.6/65-72.
- Roeset, J.M. and Tassoulas, J.L. (1982). "Nonlinear soil structure interaction: an overview", *Applied Mech. Div.*, Vol.53, ASME, 59-76.
- Roeset, J.M., Whitman, R.V. and Dobry, R. (1973). "Modal analysis for structure with foundation interaction", *J. Struct. Div.*, ASCE, 99, 399-416.
- Sanchez-Salinero, I. (1982). "Static and dynamic stiffnesses of single piles", *Geotech. Eng. Rep. GR82-31*, Civil Eng. Dept., U. of Texas at Austin, August, 225p.
- Sarrazin, M., Roeset, J.M. and Whitman, R.V. (1972). "Dynamic soil-structure interaction", *J. Struct. Div.*, ASCE, 98, 1525-1544.
- Sen, R., Davies, T.G. and Banerjee, P.K. (1985). "Dynamic analysis of piles and pile groups embedded in homogeneous soil", *Earthq. Eng. Struct. Dyn.*, Vol.13, 53-65.
- Sen, R., Kausel, E. and Banerjee, P.K. (1985). "Dynamic analysis of piles and pile groups in non-homogeneous soil", *Int. J. Num. and Anal. Mech. in Geomech.*, Vol.9, 507-524.
- Sheta, M. and Novak, M. (1982). "Vertical vibration of pile groups", *J. Geotech. Eng. Div.*, ASCE, Vol.108, No.GT4, 570-590.
- Shimizu, N., Yamamoto, S. and Koori, Y. (1977). "Three-dimensional dynamic analysis of soil-structure system by thin layer element method", *Trans. Archit. Inst. of Japan*, No.253, 31-41.

- Sokolnikoff, I.S. (1956). "Mathematical theory of elasticity", McGraw-Hill Book Company, Inc. P.476.
- Stanton, J.F., Banerjee, S. and Hasayan, I. (1988). "Shaking table tests on piles", Final Report, Washington State, Dept. of Trans.
- Tajimi, H. (1969). "Dynamic analysis of a structure embedded in an elastic stratum", proc. 4th WCEE, Chile.
- Tajimi, H. (1977). "Seismic effects on piles", Proc. of Specialty Session 10, State-of-The-Art rep., 9th ICSMFE, TOKYO, 15-26.
- Terzaghi, K. and Peck, R.B. (1967). "Soil mechanics in engineering practice", 2nd Ed., New York: Wiley.
- Veletos, A.S. and Dotson, K.W. (1986). "Impedances of soil layer with disturbed boundary zone", J. Geotech. Eng., ASCE, 112(3), 363-368.
- Veletos, A.S. and Dotson, K.W. (1988). "Vertical and torsional vibration of foundation in inhomogeneous media", J. Geotech. Eng., ASCE, 114(9), 1002-1021.
- Veletos, A.S. and Verbic, B., (1973). "Vibration of Viscoelastic Foundations", Earthquake Engineering and Structural Dynamics, Vol.2, No.1, 87-102.
- Wass, G. and Hartmann, H.G. (1981). "Pile foundations subjected to dynamic horizontal loads", European Simulation Meeting "Modelling and simulation of large scale structural systems", Capri, Italy, Sept.
- Wass, G. and Hartmann, H.G. (1984). "Seismic analysis of pile foundations including pile-soil-pile interaction", Proc. 8th WCEE, San Francisco, Vol.5, 55-62.
- Wolf, J.P. (1985). "Dynamic soil-structure interaction", Englewood Cliffs, NJ: Prentice-Hall, 466p.
- Wolf, J.P. (1988). "Soil-structure interaction analysis in time domain", Englewood Cliffs, NJ: Prentice-Hall, 446p.
- Wolf, J.P. and Von Arx, G.A. (1978). "Impedance functions of a group of vertical piles", Proc., ASCE Specialty Conf. on Earthq. Eng. and Soil Dyn., Pasadena, CA, Vol.2, 1024-1041.
- Woods, R.D. (1984). "Lateral interaction between soil and pile", Proc. Int. Symp. on Dyn. Soil-Structure Interaction, Minneapolis, MN, Sept., 47-54.
- Yan, L. and Byrne, P.M. (1989). "Application of hydraulic gradient similitude method to small-scale footing tests on sand", Can. Geotech. J., 26(2), 246-259.

## Appendix A

# Impedance Functions of Viscoelastic Halfspace

A rigid disk of infinitesimal thickness and weight is supported at the surface of a linear viscoelastic halfspace, which is idealized either as a standard Voigt solid or as a constant hysteretic solid. The harmonic exciting forces investigated include a horizontal force  $He^{i\omega t}$ , a vertical force  $Pe^{i\omega t}$  and an overturning moment  $Me^{i\omega t}$ , where  $\omega$  is the circular frequency of the excitation,  $t$  is the time and  $i = \sqrt{-1}$ .

Let  $u, v$  and  $\psi$  be, respectively, the amplitudes of the horizontal, vertical and angular displacements of the disk. Neglecting the small coupling between the horizontal and rocking motions, the relationship between the force amplitudes and displacement amplitudes may be stated as

$$\begin{cases} H = k_{u i} u \\ P = k_{v i} v \\ M = k_{\psi i} \psi \end{cases} \quad (\text{A.1})$$

where  $k_{j i}$  are complex-valued stiffness or impedance functions of the form

$$k_{j i} = K_j [\hat{C}_{j1}(a_0, \nu, D) + i a_0 \hat{C}_{j2}(a_0, \nu, D)] \quad (\text{A.2})$$

in which the subscript  $j$  is used in a generalized sense to denote  $u, v$  or  $\psi$ ;  $a_0$  is the dimensionless frequency parameter,  $\nu$  is Poisson's ratio,  $D = \tan \delta$  is hysteretic material damping of the viscoelastic medium and  $\delta$  is loss angle.

The symbol  $K_j$  in eq. (A.2) represents the static stiffness of the disk in the  $j$  direction, defined as

$$\begin{cases} K_u = \frac{8Gr_0}{2-\nu} \\ K_\psi = \frac{8Gr_0^3}{3(1-\nu)} \\ K_v = \frac{4Gr_0}{1-\nu} \end{cases} \quad (\text{A.3})$$

where  $G$  is the shear modulus of the viscoelastic medium and  $r_0$  is the radius of the disk.

In eq. (A.2)  $\tilde{C}_{j1}$  and  $\tilde{C}_{j2}$  are real valued function of  $a_0, \nu$  and  $D$ . For the horizontally excited disk,  $j = u$ , the following expressions are obtained for  $\tilde{C}_{u1}$  and  $\tilde{C}_{u2}$

$$\begin{cases} \tilde{C}_{u1} = 1 - \sqrt{0.5(R-1)}\alpha_1 a_0 \\ \tilde{C}_{u2} = \sqrt{0.5(R+1)}\alpha_1 + \frac{D}{a_0} \end{cases} \quad (\text{A.4})$$

where

$$R = \sqrt{1+D^2} = \sqrt{1+\tan^2 \delta} \quad (\text{A.5})$$

For the disk in rocking motion,  $j = \psi$ , the corresponding expressions are

$$\begin{cases} \tilde{C}_{\psi 1} = 1 - \chi_\psi - \beta_3 a_0^2 \\ \tilde{C}_{\psi 2} = \varphi_\psi + \frac{D}{a_0} \end{cases} \quad (\text{A.6})$$

where

$$\begin{cases} \chi_\psi = \frac{3_1[R + \sqrt{0.5(R-1)}\beta_2 a_o](\beta_2 a_o)^2}{R + 2\sqrt{0.5(R-1)}(\beta_2 a_o) + (\beta_2 a_o)^2} \\ \varphi_\psi = \frac{\beta_1 \beta_2 \sqrt{0.5(R+1)}(\beta_2 a_o)^2}{R + 2\sqrt{0.5(R-1)}(\beta_2 a_o) + (\beta_2 a_o)^2} \end{cases} \quad (\text{A.7})$$

For the disk in vertical motion,  $j = v$ , the corresponding expressions are

$$\begin{cases} \bar{C}_{v1} = 1 - \chi_v - \sqrt{0.5(R-1)}\gamma_4 a_o - \gamma_3 a_o^2 \\ \bar{C}_{v2} = \sqrt{0.5(R+1)}\gamma_4 + \varphi_v + \frac{D}{a_o} \end{cases} \quad (\text{A.8})$$

where

$$\begin{cases} \chi_v = \frac{\gamma_1[R + \sqrt{0.5(R-1)}(\gamma_2 a_o)](\gamma_2 a_o)^2}{R + 2\sqrt{0.5(R-1)}(\gamma_2 a_o) + (\gamma_2 a_o)^2} \\ \varphi_v = \frac{\gamma_1 \gamma_2 \sqrt{0.5(R+1)}(\gamma_2 a_o)^2}{R + 2\sqrt{0.5(R-1)}(\gamma_2 a_o) + (\gamma_2 a_o)^2} \end{cases} \quad (\text{A.9})$$

In above equations,  $\alpha_1, \beta_i$  and  $\gamma_i$  are numerical coefficients which depend on Poisson's ratio,  $\nu$ .

Substituting eq.(A.3) into eq.(A.2), the impedance functions can be expressed in the following form:

$$\begin{cases} k_{vt} = Gr_o[C_{v1}(a_o, \nu, D) + iC_{v2}(a_o, \nu, D)] \\ k_{ut} = Gr_o[C_{u1}(a_o, \nu, D) + iC_{u2}(a_o, \nu, D)] \\ k_{\psi t} = Gr_o^2[C_{\psi 1}(a_o, \nu, D) + iC_{\psi 2}(a_o, \nu, D)] \end{cases} \quad (\text{A.10})$$

## Appendix B

### Interaction Factor of Two-Pile Group

A group of two identical, equally-loaded piles is considered, as shown in Fig. B.1, each pile is divided into  $n$  cylindrical elements and a uniformly-loaded circular base. If conditions remain purely elastic within the soil and no slip or yield occurs at the pile-soil interface, the pile and soil displacements at the center of each element may be equated. The equation for the pile displacement are identical with those for the single pile. The soil displacements for a floating pile may be written as follows:

$$\{v\} = \frac{d}{E_s} [I_{11} + I_{22}] \{P\} \quad (\text{B.1})$$

in which  $d$  is diameter of the pile;  $E_s$  is Young's modulus of the soil;  $\{v\}$  is vector of soil displacement;  $\{P\}$  is vector of shear stresses;  $[I_{11} + I_{22}]$  is  $(n+1) \times (n+1)$  matrix of displacement-influence factor, containing elements  $I_{1ij} + I_{2ij}$ , where  $I_{1ij}$ ,  $I_{2ij}$  are displacement-influence factors at element  $i$  on pile 1 caused by shear stress on element  $j$  of pile 1 and pile 2, respectively.

The soil displacements thus obtained may be equated to the pile displacements

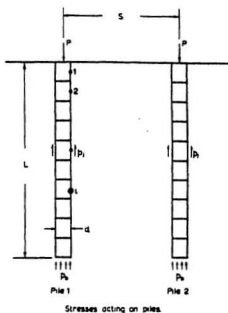


Figure B.1: Group of two floating piles

and the resulting system of equations solved, to obtain the unknown shear-stresses and displacements along the piles. The analysis of a two-pile group is therefore identical with that of a single pile, except that the soil-displacement-influence matrix includes contributions from the second pile. The results of the above analysis may be conveniently expressed in terms of an "interaction factor"  $\alpha$ , where

$$\alpha = \frac{\delta_{ij}}{\delta_{ii}} \quad (\text{B.2})$$

where  $\delta_{ij}$  is the additional settlement caused by adjacent pile  $j$ , and  $\delta_{ii}$  is the settlement of pile  $i$  under its own load. The pile  $i$  and the adjacent pile  $j$  carry the same load.

The value of  $I_{1ij}$  and  $I_{2ij}$  may be obtained by integration of the Mindlin equation. The geometry of a typical cylindrical pile element is shown in Fig. B.2. For a general point  $i$  in the soil mass, the value of  $I_{ij}$  is

$$I_{ij} = 2 \int_{(j-1)\delta}^{j\delta} \int_0^{\pi/2} I_p d\theta dc \quad (\text{B.3})$$

where  $I_p$  is influence factor for vertical displacement due to a vertical point load, and  $\delta$  is the length of element.

From Mindlin's equation,  $I_p$  is given by

$$I_p = \frac{1 + \nu}{8\pi(1 - \nu)} \left( \frac{z_1^2}{R_1^3} + \frac{3 - 4\nu}{R_1} + \frac{5 - 12\nu + 8\nu^2}{R_2} + \frac{(3 - 4\nu)z^2 - 2cz + 2c^2}{R_2^3} + \frac{6cz^2(z - c)}{R_2^5} \right) \quad (\text{B.4})$$

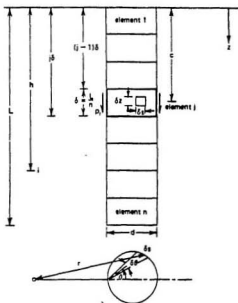


Figure B.2: Single pile-basis geometry

where

$$\begin{cases} z = h + c \\ z_1 = h - c \\ R_2^2 = d^2/4 + x^2 - xd \cos \theta + z^2 \\ R_1^2 = d^2/4 + x^2 - xd \cos \theta + z_1^2 \end{cases} \quad (\text{B.5})$$

The integral with respect to  $c$  in eq. (B.3) can be evaluated analytically to give

$$\begin{aligned} \int I_p dc = & \frac{1+\nu}{8\pi(1-\nu)} \left[ \frac{z_1}{D_1} - 4(1-\nu) \ln(z_1 + D_1) + 8(1-2\nu + \nu^2) \ln(z + D) \right. \\ & \left. + \frac{2h^2z/r^2 - 4h - (3-4\nu)z}{D} + \frac{2(hr^2 - h^2z^3/r^2)}{D^3} \right] \end{aligned} \quad (\text{B.6})$$

where  $h$  and  $r$  are defined in Fig. B2,

$$D_1 = (r^2 + z_1^2)^{1/2}$$

$$D = (r^2 + z^2)^{1/2}$$

and the limits of integration in eq. (B.6) are

$$z_1 \text{ from } h - (j-1)\delta \text{ to } h - j\delta$$

and

$$z \text{ from } h + (j-1)\delta \text{ to } h + j\delta$$

The integral with respect to  $\theta$  is, however, only conveniently evaluated numerically.

The geometry of the pile base is shown in Fig. B.3. To allow for an enlarged base, a base radius  $r_b (= d_b/2)$  different from the pile shaft radius is considered. For a general point  $i$  in the soil mass,

$$I_{ib} = \frac{1}{d} \int_0^{2\pi} \int_0^{r_b} I_p r dr d\theta \quad (\text{B.7})$$

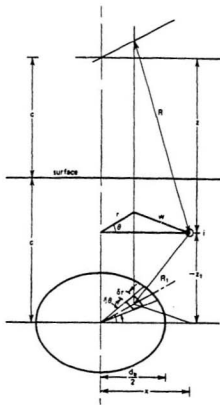


Figure B.3: Geometry for integration over circular area

where  $I_p$  is given in eq. (B.4), and for this case,

$$\begin{cases} c = n\delta = L \\ R_2^2 = z^2 + x^2 + r^2 - 2rx \cos \theta \\ R_1^2 = z_1^2 + x^2 + r^2 - 2rx \cos \theta \\ z = z_1 + 2c \end{cases} \quad (\text{B.8})$$

The integration with respect to  $r$  can be done analytically and yields

$$\begin{aligned} \int I_p r dr &= \frac{1 + \nu}{8\pi(1 - \nu)} \left\{ \frac{z_1^2(rA - R_2^2)}{(R_2^2 - A^2)\sqrt{X_0}} + (3 - 4\nu)[\sqrt{X_0} + A \ln(2\sqrt{X_0} \right. \\ &\quad \left. + 2r - 2A)] + (5 - 12\nu + 8\nu^2)[\sqrt{X_1} + A \ln(2\sqrt{X_1} \right. \\ &\quad \left. + 2r - 2A)] + [(3 - 4\nu)z^2 - 2cz + 2c^2] \frac{Ar - B}{(B - A^2)\sqrt{X_1}} + \right. \\ &\quad \left. 6cz^2(z - c) \left[ \frac{-1}{3\sqrt{X_1^3}} + \frac{A(r - A)}{3(B - A^2)\sqrt{X_1}} \left( \frac{1}{X_1} + \frac{2}{B - A^2} \right) \right] \right\} \quad (\text{B.9}) \end{aligned}$$

where

$$\begin{cases} R_0^2 = z_1^2 + x^2 \\ A = x \cos \theta \\ X_0 = r^2 - 2Ar + R_0^2 \\ X_1 = r^2 - 2Ar + B \\ B = R_0^2 + 4c^2 + 4cz_1 \\ z = z_1 + 2c \end{cases} \quad (\text{B.10})$$

The integration with respect to  $\theta$  is again evaluated most readily by numerical means.







